

# **Mineral Chemistry and Structural Relationships of Inclusions in Diamond Samples**

Dissertation  
zur Erlangung des Grades  
„Doktor der Naturwissenschaften“

am Fachbereich Chemie, Pharmazie und Geowissenschaften  
der Johannes Gutenberg-Universität Mainz

Somruedee Satitkune  
geb. in Bangkok, Thailand

Mainz, 2009

Dekan:

1. Berichterstatter:

2. Berichterstatter:

Tag der mündlichen Prüfung:

## ZUSAMMENFASSUNG

Diamant ist das härteste Mineral – und dazu ein Edelstein -, das unter höchstem Druck und hohen Temperaturen in tiefen kontinentalen Regionen der Erde kristallisiert. Die Mineraleinschlüsse in Diamanten werden durch die physikalische Stabilität und chemische Beständigkeit der umgebenden – eigentlich metastabilen - Diamant-Phase geschützt. Aufgrund der koexistierenden Phasenkombination ermöglichen sie, die Mineral-Entwicklung zu studieren, während deren der Einschlüssen und die Diamanten kristallisierten.

Die Phasenkombinationen von Diamant und Chrom-Pyrop, Chrom-Diopsid, Chromit, Olivin, Graphit und Enstatit nebeneinander (teilweise in Berührungsexistenz) mit Chrom-Pyrop Einschlüssen wurden von neunundzwanzig Diamant-Proben von sechs Standorten in Südafrika (Premier, Koffiefontein, De Beers Pool, Finsch, Venetia und Koingnaas Minen) und Udachnaya (Sibirien/Russland) identifiziert und charakterisiert. Die Mineraleinschlüsse weisen z.T. kubo-oktaedrische Form auf, die unabhängig von ihren eigenen Kristallsystemen ausgebildet werden können. Das bedeutet, dass sie syngenetische Einschlüsse sind, die durch die sehr hohe Formenergie des umgebenden Diamanten morphologisch unter Zwang stehen. Aus zweidiemnsionalen Messungen der ersten Ordnung von charakteristischen Raman-Banden lassen sich relative Restdrucke in Diamanten zwischen Diamant und Einschlussmineral gewinnen; sie haben charakteristische Werte von ca. 0,4 bis 0,9 GPa um Chrom-Pyrop-Einschlüsse, 0,6 bis 2,0 GPa um Chrom-Diopsid-Einschlüsse, 0,3 bis 1,2 GPa um Olivin-Einschlüsse, 0,2 bis 1,0 GPa um Chromit-Einschlüsse, beziehungsweise 0,5 GPa um Graphit Einschlüsse.

Die kristallstrukturellen Beziehung von Diamanten und ihren monomineralischen Einschlüssen wurden mit Hilfe der Quantifizierung der Winkelkorrelationen zwischen der [111] Richtung von Diamanten und spezifisch ausgewählten Richtungen ihrer mineralischen Einschlüsse untersucht. Die Winkelkorrelationen zwischen Diamant [111] und Chrom-Pyrop [111] oder Chromit [111] zeigen die kleinsten Verzerrungen von 2,2° bis zu 3,4°. Die Chrom-Diopsid- und

Olivin-Einschlüsse zeigen die Missorientierungswerte mit Diamant [111] bis zu  $10,2^\circ$  und  $12,9^\circ$  von Chrom-Diopsid [010] beziehungsweise Olivin [100].

Die chemische Zusammensetzung von neun herausgearbeiteten (orientiertes Anschleifen) Einschlüssen (drei Chrom-Pyrop-Einschlüsse von Koffiefontein-, Finsch- und Venetia-Mine (zwei von drei koexistieren nebeneinander mit Enstatit), ein Chromit von Udachnaya (Sibirien/Russland), drei Chrom-Diopside von Koffiefontein, Koingnaas und Udachnaya (Sibirien/Russland) und zwei Olivin Einschlüsse von De Beers Pool und Koingnaas) wurden mit Hilfe EPMA und LA-ICP-MS analysiert. Auf der Grundlage der chemischen Zusammensetzung können die Mineraleinschlüsse in Diamanten in dieser Arbeit der peridotitischen Suite zugeordnet werden.

Die Geothermobarometrie-Untersuchungen waren aufgrund der berührenden Koexistenz von Chrom-Pyrop- und Enstatit in einzelnen Diamanten möglich. Durchschnittliche Temperaturen und Drücke der Bildung sind mit ca.  $1087 (\pm 15)^\circ\text{C}$ ,  $5,2 (\pm 0,1) \text{ GPa}$  für Diamant DHK6.2 von der Koffiefontein Mine beziehungsweise ca.  $1041 (\pm 5)^\circ\text{C}$ ,  $5,0 (\pm 0,1) \text{ GPa}$  für Diamant DHF10.2 von der Finsch Mine zu interpretieren.

## ABSTRACT

Diamond is known as the hardest (gem) mineral, which originates in the deep continental region of the earth under very high pressures and temperatures crystallizing over long periods of time. The mineral inclusions occurring in diamonds are protected by the durability and stable chemical properties of their diamond hosts, which enable the study the evolution during which the inclusions and diamonds had formed.

The chrome-pyrope, chrome-diopside, chromite, olivine, graphite and enstatite coexisting (touching) with chrome-pyrope inclusions were identified from twenty nine diamond samples from six localities in South Africa (Premier, Koffiefontein, De Beers Pool, Finsch, Venetia mine and Koingnaas (alluvial deposit)) and Udachnaya (Russia/Siberia). Some mineral inclusions show the cubo-octahedral form, which is irrespective of their crystal systems and have no visible fractures reaching into the diamonds. This implies that they are syngenetic inclusions and the actual crystal forms of inclusions were controlled by their individual diamond hosts. The relative residual pressures in diamonds derived from the shift of first-order Raman diamond spectra derived by two dimensional mapping techniques range approximately from 0.4 to 0.9 GPa. around chrome-pyrope inclusions, from 0.6 to 2.0 GPa. around chrome-diopside inclusions, from 0.3 to 1.2 GPa. around olivine inclusions, from 0.2 to 1.0 GPa. around chromite inclusions and 0.5 GPa. around graphite inclusion, respectively.

The structural relationship of diamonds and their inclusions were studied by calculating the angle correlation between the [111] direction of diamonds and specifically selected directions of their distinct mineral inclusions. The angle correlations between diamond [111] and chrome-pyrope [111] or chromite [111] show relatively small misalignments up to  $2.2^\circ$  and  $3.4^\circ$  between the chrome-pyrope and chromite inclusions, respectively. The chrome-diopside and olivine inclusions, however, showed a degree of miss-orientation between diamond [111] and chrome-

diposide [010], olivine [100] up to 10.2° and 12.9° for chrome-diopside and olivine, respectively.

The chemical compositions of nine exposed inclusions (three chrome-pyrope inclusions from Koffiefontein, Finsch and Venetia mines (two from three coexisting with enstatite), one chromite from Udachnaya (Siberia/Russia), three chrome-diopside from Koffiefontein, Koingnaas and Udachnaya (Siberia/Russia) and two olivine inclusions from De Beers Pool and Koingnaas) were analysed by EPMA and LA-ICP-MS. On the basis of chemical composition, mineral inclusions in diamonds in this study can usually be assigned to the peridotite suite.

The genetically interpretation on the base of geothermobarometry proved by inclusions was investigated by the partitioning of Fe and Mg between touching inclusions (chrome-pyrope + enstatite) in individual diamonds. Average temperatures and pressures are estimated for 1087 ( $\pm 15$ ) °C, 5.2 ( $\pm 0.1$ ) GPa for diamond DHK6.2 from Koffiefontein mine and 1041 ( $\pm 5$ ) °C, 5.0 ( $\pm 0.1$ ) GPa for diamond DHF10.2 from Finsch mine, respectively.



# CONTENTS

ZUSAMMENFASSUNG .....	i
ABSTRACT .....	iii
CONTENTS .....	vi
INDEX OF FIGURES .....	viii
INDEX OF TABLES .....	xiii
1. INTRODUCTION .....	1
1.1 Diamond .....	1
1.2 Origin of Diamond .....	3
1.3 Diamond Deposits .....	4
1.4 Mineral Inclusions in Diamonds .....	5
2. DESCRIPTION OF DIAMOND SAMPLES ACCORDING TO EXTERNAL CHARACTERISTICS .....	9
2.1 Sample Localities .....	9
2.2 Sample Description .....	13
2.3 Surfaces Features .....	20
3. CHARACTERIZATION OF DIAMOND SAMPLES RELATED TO INTERNAL PROPERTIES .....	22
3.1 Optical or Colour Centres due to Nitrogen Impurities .....	22
3.2 Fourier Transform Infrared Spectrophotometer (FTIR) .....	24
3.3 UV-Vis Spectrophotometer .....	26
3.4 Internal Growth Features .....	28
4. MINERAL INCLUSIONS IN DIAMOND SAMPLES .....	33
4.1 Raman Spectroscopy .....	33
4.2 Mineral Inclusions Identification .....	33
4.3 Pressure Differences between Diamond Host Crystals and Their Guest Inclusions .....	44
5. ORIENTATION OF CRYSTAL INCLUSIONS IN DIAMONDS .....	48
5.1 The Structural Relationships of Inclusions in Diamonds .....	51
5.2 The Twin Law Approach to Mineral Inclusions in Diamonds .....	60
6. MINERAL CHEMISTRY OF INCLUSIONS IN DIAMONDS .....	66
6.1 Electron Probe Micro-Analysis (EPMA) .....	67
6.2 Laser Ablation Inductively Coupled Plasma Mass Spectrometry (LA-ICP-MS) .....	68
6.3 Geothermobarometry .....	87
7. CONCLUSIONS .....	90



---

8. REFERENCES .....	95
APPENDIX .....	106

## INDEX OF FIGURES

Figure 1.1	(a) Diamond crystal structure showing a continuous network of carbon atoms and (b) cubic unit cell of diamond .....	1
Figure 1.2	Crystal structure of graphite .....	2
Figure 1.3	Pressure – temperature phase diagram for carbon. The blue dashed line separates the stability fields of graphite from diamond. Diamonds can form at depths below 150 kilometers beneath the continental region, whereas underneath oceans, diamonds can form at depths of at least 200 kilometers. (modified after Matthes, 1987; Bundy et al., 1996; Kirkley, 1998 and Stachel, 2007) .....	4
Figure 2.1	A map of South Africa showing locations of the diamond samples used in this study .....	9
Figure 2.2	Udachnaya open-pit mine in Russia (www.allaboutgemstones.com) .....	12
Figure 2.3	Diamond samples crystallized in octahedral form (a) DHU2.2 from Udachnaya (Siberia/Russia) and (b) DHF11 with rounded edges from Finsch mine in South Africa .....	17
Figure 2.4	A rhombic dodecahedral shape crystal .....	17
Figure 2.5	Octahedron with dodecahedral faces in sample DHF7 shows curved faces and round edges .....	17
Figure 2.6	Diamond sample DHP5.3: octahedron pretends a flat tabular form .....	18
Figure 2.7	Asymmetric deviation of octahedral habit resulting in An elongated crystal (DHP4.3) .....	18
Figure 2.8	(a) Flat triangular or macle shaped diamond (DHV12.2); (b) two prominent {111} faces divided by a twin plane parallel (spinel-twin-law) .....	19
Figure 2.9	Twining in diamond (a) contact twin (D10) and (b) the complex crystal caused by twinning over only part of the growing surface (DHV12.1) .....	19
Figure 2.10	Diamond crystal (DHU3.1) showing stacked growth layers on its octahedral face .....	20
Figure 2.11	Groups of negative trigons on octahedral faces of diamonds (a) DHU2.1 and (b) DHV12.2 .....	21
Figure 2.12	Surface features in diamond (a) hillocks on diamond surfaces (DHU2.1) and (b) edge abrasion (DHP5.3) .....	21
Figure 3.1	Typical infrared spectrum of an IaAB diamond including a narrow peak at $1364\text{ cm}^{-1}$ due to the presence of nitrogen platelets .....	25
Figure 3.2	Typical infrared spectrum of an IaA diamond .....	25
Figure 3.3	UV-Vis absorption spectrum of diamond in which A centres are the predominant impurities .....	26

Figure 3.4	UV-Vis absorption spectrum of a diamond in which N3 centres contribute to the absorption .....	27
Figure 3.5	Catholuminescence images of diamonds showing blue colour: (a) DHU1.1 and (b) DHK6.1 .....	29
Figure 3.6	Catholuminescence images of diamonds showing yellow-blue oscillation on their surfaces: (a) DHP4.2, (b) DHP4.3, (c) DHP5.1 and (d) D10 .....	29
Figure 3.7	Cathodoluminescence image of DHK13, polished along {110} faces, showing blue colour luminescence parallel to internal zones .....	30
Figure 3.8	Cathodoluminescence image of DHK14, polished along {110} faces, showing the yellow luminescence internal structure with rounded corner .....	31
Figure 3.9	Internal structure of diamond (DHU3.1) and its inclusions. Cathodoluminescence images of polished faces on {110} diamond face .....	31
Figure 3.10	Cathodoluminescence image of DHF10.2, polished along the {110} face, showing the brighter luminescence around the chrome-pyropite + enstatite inclusion .....	32
Figure 4.1	The octahedral form of mineral inclusions in diamonds: (a) chrome-pyropite inclusion in diamond DHU2.1 and (b) olivine inclusion in diamond DHP5.3 .....	35
Figure 4.2	Co-existing inclusions within individual diamonds: (a) graphite (black) and chrome-pyropite (purplish red) inclusions in diamond DHP4.1 and (b) chrome-diopside (green) and olivine (colourless) inclusions trapped in DHK14 .....	36
Figure 4.3	Intergrowths of two mineral inclusions (chrome-pyropite + enstatite) trapped in single host (a) DHK6.2 and (b) DHF 10.2 .....	36
Figure 4.4	Chrome-diopside inclusions in diamonds: (a) DHU1.2 observed under stereo-microscope and (b) chrome-diopside crystal inclusion in DHF11 with stepping of octahedral faces .....	37
Figure 4.5	In situ Raman spectrum of a chrome-diopside inclusion in diamond DUH1.1 .....	38
Figure 4.6	The common crystal morphologies of garnet: (a) a twelve-faced rhombic-dodecahedron ( <a href="http://www.healingcrystal.com">www.healingcrystal.com</a> ) and (b) twenty-four-faced trapezohedron ( <a href="http://skywalker.cochise.edu">skywalker.cochise.edu</a> ) .....	38
Figure 4.7	Chrome-pyropite inclusions embedded in diamonds: (a) DHU2.2 and (b) DHF10.1 .....	39
Figure 4.8	In situ Raman spectrum of a chrome-pyropite inclusion in diamond DHF10.2 .....	39
Figure 4.9	Chromite inclusions in diamonds: (a) DHU3.1 and (b) DHU3.2 .....	40
Figure 4.10	In situ Raman spectrum of a chromite inclusion in diamond DHU3.1 .....	40

Figure 4.11	Olivine inclusions in diamonds: (a) DHU1.3 and (b) DHP5.3 .....	41
Figure 4.12	In situ Raman spectrum of an olivine inclusion in diamond DHK13 .....	41
Figure 4.13	Graphite inclusions in diamonds: (a) DHU1.3 and (b) DHP4.1 .....	42
Figure 4.14	In situ Raman spectrum of a graphite inclusion in diamond DHP4.1 .....	43
Figure 4.15	Raman spectrum of an enstatite inclusion in diamond DHF10.2 .....	44
Figure 4.16	(a) Chrome-diopside inclusion in diamond DHU1.2, (b) Raman map of diamond DHU1.2 (view through {111}) around the chrome-diopside inclusion. The colour-code represents the shift of the first-order Raman band of diamond. The relative pressure between diamond and chrome-diopside inclusion is 1.13 GPa .....	45
Figure 4.17	(a) Strain birefringence around a chrome-diopside inclusion in the adjacent diamond DHU1.3. (b) The first-order Raman peak of diamond DHU1.3 on {111} direction which splits into a spectral doublet .....	47
Figure 5.1	Octahedral diamonds from Udachnaya (Siberia/Russia), showing the octahedrally shaped inclusions which are imposed by the diamonds: (a) chrome-diopside inclusion in diamond DHU1.2 and (b) chrome-pyrope inclusion in diamond sample DHU2.1 .....	50
Figure 5.2	Octahedral shape inclusions in octahedral diamond DHP5.3 from Premier Mine, showing the octahedron face of olivine inclusion, which are imposed by the diamond host .....	50
Figure 5.3	(a) Diamond sample DHU2.1 with chrome-pyrope inclusion (view along [111] perpendicular through the octahedral face), (b) the directions of diamond crystallographic axes, (c) the directions of the two sets of axes show the orientation of diamond lattice and chrome-pyrope inclusion .....	54
Figure 5.4	Plot of angle correlations between [111] directions of diamond and [111] of chrome-pyrope, chromite [111], chrome-diopside [010] and olivine [100] inclusions from various mines in this study .....	57
Figure 5.5	Plot of angle correlation between [111] directions of diamond and chrome-pyrope inclusions [111] from various mines .....	57
Figure 5.6	Plot of angle correlation between [111] directions of diamond and chromite inclusions [111] from Udachnaya (Siberia/Russia) .....	58
Figure 5.7	Plot of angle correlation between [111] directions of diamond and chrome-diopside inclusions [010] from various mines .....	58
Figure 5.8	Plot of angle correlation between [111] directions of diamond and olivine inclusions [100] from various mines .....	59

Figure 5.9	Plot of rotation angles for inclusions and diamonds from Udachnaya (Siberia/Russia) and various mines in South Africa .....	63
Figure 5.10	Plot of twinning rotation angles for chrome-pyrope inclusions in diamonds from various mines .....	63
Figure 5.11	Plot of twinning rotation angles for chromite inclusions in diamonds from Udachanaya (Siberia/Russia) .....	64
Figure 5.12	Plot of twinning rotation angles for chrome-diopside inclusions in diamonds from various mines .....	64
Figure 5.13	Plot of twinning rotation angles for olivine inclusions in diamonds from various mines .....	65
Figure 6.1	Chrome-pyrope inclusion in diamond DHV12.3 .....	69
Figure 6.2	Chrome-pyrope inclusions in diamonds DHK6.2, DHF10.2, and DHV12.3, plotted in terms of four major oxides. The chrome-pyrope inclusions lie in the peridotitic fields. The outlines of the peridotitic and eclogitic fields are taken from Meyer (1987) .....	72
Figure 6.3	Plot of Cr <sub>2</sub> O <sub>3</sub> versus CaO (wt%) for garnets from diamond samples DHK6.2, DHF10.2 and DHV12.3. The chrome-pyrope inclusions lie in the harzburgite fields. The compositional field for lherzolite field is taken from Sobolev et al. (1973) .....	73
Figure 6.4	REE concentration diagram for the three chrome-pyrope inclusions in diamonds from three different mines. The grey dot line is average compositions of harzburgitic garnet inclusions from worldwide sources (Stachel et al., 2004). All elements are normalized to the C1-chondrite composition given by McDonough and Sun (1995) .....	74
Figure 6.5	Touching inclusions of chrome-pyrope and enstatite in diamonds (a) DHK6.2 and (b) DHF10.2 .....	76
Figure 6.6	Chondrite normalized trace elements concentration diagram for the two enstatite inclusions in diamonds from two different mines. All elements are normalized to the C1-chondrite composition given by McDonough and Sun (1995) .....	77
Figure 6.7	Two parts of chromite inclusions exposed on the surface of diamond DHU3.1 .....	78
Figure 6.8	(a) FFM ratio vs. Cr <sub>2</sub> O <sub>3</sub> and (b) FFM ratio vs. SiO <sub>2</sub> plots for chromite inclusions in diamond DHU3.1 from Udachnaya (Siberia/Russia). The chromite inclusions lie in the world-wide peridotitic chromite fields. The outline of the world-wide peridotitic chromite inclusion field is modified from Stachel and Harris (1997a) .....	80
Figure 6.9	Chrome-diopside inclusions (a) DHK7 and (b) DHK14 .....	80
Figure 6.10	REE concentrations in chrome-diopside inclusions in diamonds from three different mines normalized to the composition of C1-chondrites (McDonough and Sun, 1995) .....	83
Figure 6.11	Olivine inclusions (a) DHD8.2 and (b) DHK13 .....	85

---

Figure 6.12	NiO vs. Fo (forsterite contents) in olivine inclusions in diamonds from De Beers Pool and Koingnaas (alluvial) in South Africa. Plot of olivine inclusions fall in the field for olivines from diamonds world-wide as published by Sobolev et al. (2004) .....	86
Figure 6.13	Chondrite normalized trace elements concentration diagram for the two olivine inclusions in diamonds from two different mines. All elements are normalized to the C1-chondrite composition published by McDonough and Sun (1995) .....	86

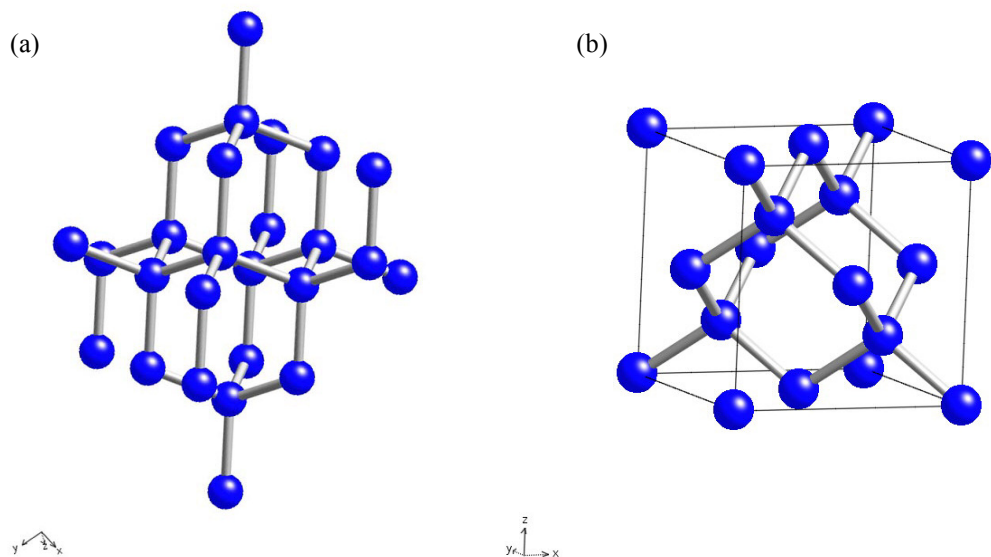
## INDEX OF TABLES

Table 1.1	Mineral inclusions in diamonds (after Meyer, 1985, 1987 and Harris, 1993) .....	7
Table 2.1	Sample description .....	13
Table 3.1	Diamond types, optical absorption and cathodoluminescence effects .....	27
Table 4.1	Mineral inclusions in diamonds from Russia and South Africa .....	35
Table 4.2	Relative pressure differences between host diamond crystals and their guest inclusions .....	46
Table 5.1	Crystallographic cell parameters of chrome-pyropo inclusions in diamonds .....	51
Table 5.2	Crystallographic cell parameters of chromite inclusions in diamonds .....	51
Table 5.3	Crystallographic cell parameters of chrome-diopside inclusions in diamonds .....	52
Table 5.4	Crystallographic cell parameters of olivine inclusions in diamonds .....	52
Table 5.5	The angle and deviation between the [111] direction of diamonds and their inclusions .....	55
Table 5.6	The rotation angle for twinning of lattices and the deviation angles between diamonds and their inclusions .....	60
Table 6.1	Mineral inclusions exposed from diamond samples .....	67
Table 6.2	Chemical analyses of chrome-pyropo inclusions in diamond DHV12.3 .....	70
Table 6.3	Chemical analyses of chrome-pyropo inclusions from the Cr-Prp + En pairs in diamonds DHK6.2 and DHF10.2 .....	71
Table 6.4	Chemical analyses of enstatite inclusions from the Cr-Prp + En pairs in diamonds DHK6.2 and DHF10.2 .....	76
Table 6.5	Chemical analyses of chromite from diamond sample DHU3.1 .....	78
Table 6.6	Chemical analyses of chrome-diopside from diamond sample DHU1.1, DHK7 and DHK14 .....	81
Table 6.7	Chemical analyses of olivine inclusions from DHD8.2 and DHK13 .....	84
Table 6.8	Estimated equilibration temperatures and pressures for coexisting peridotitic mineral inclusions in individual diamonds .....	88

# 1. INTRODUCTION

## 1.1 Diamond

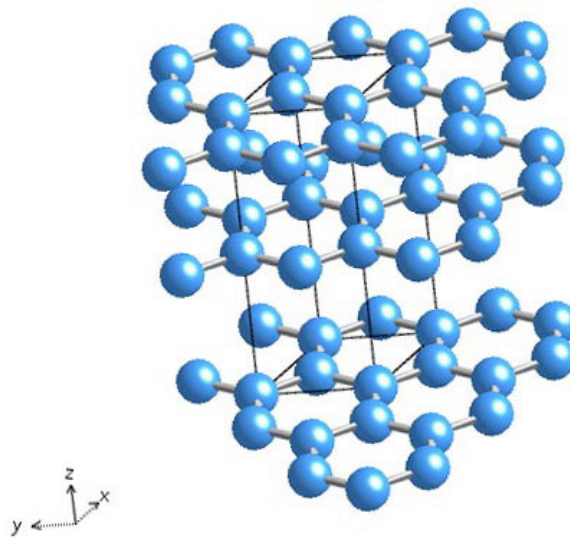
Diamond, the hardest known mineral, consists of carbon (C) atoms, which are linked together forming a continuous three dimensional network of carbon atoms in the cubic crystal system. Each carbon atom bonds to four neighboring carbon atoms in tetrahedral coordination, a repeating geometry that creates a highly symmetrical and uniform framework (Figure 1.). In this way, electron sharing causes a tightly rigid covalent bonding, which leads to the great hardness of 10 by Mohs' scale, combined with a high melting point.



**Figure 1.1** (a) Diamond crystal structure showing a continuous network of carbon atoms and (b) cubic unit cell of diamond.



Another prominent and under ambient parameters stable crystalline form of carbon is graphite. Here each carbon atom has three nearest neighboring carbon atoms. Three of the four valence electrons in each carbon atom take part in covalent bonds. The resulting structure of these bonds is a flat sheet of hexagonal rings (Figure 1.). The atoms are closely linked with stronger atomic bonds, even stronger than in the diamond arrangement, but the forces between the layers are weak, which give the perfect basal cleavage and easy gliding of sheets parallel to the layer.



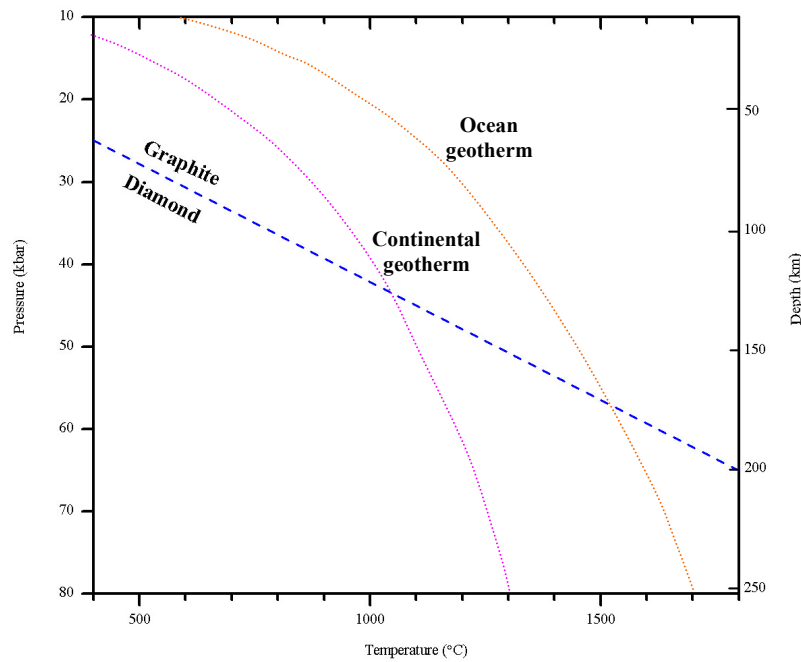
**Figure 1.2** Crystal structure of graphite.

***Crystal Data of Diamond***

Composition:	Carbon (C)
Crystal system:	Cubic
Space group:	<i>Fd3m</i>
Lattice parameter:	$a = 3.567 \text{ \AA}$ ; $Z = 8$
Common forms:	octahedron {111}, cube {100}, dodecahedron {110}, rounded variations
Cleavage:	perfect parallel to octahedral {111} faces
Density:	$3.52 \pm 0.01 \text{ g/cm}^3$
Appearance and luster:	colourless to yellow or various other colours; adamantine
Refractive index:	2.42 (monochromatic yellow light source; 589 nm)
Dispersion (CF):	0.025

**1.2 Origin of Diamond**

Diamond originates in the deep continental regions of the earth under very high pressures and temperatures covering a long period of time. Natural diamonds usually have formed at depths below 150 km under diamond-stable conditions defined by the graphite-diamond equilibrium boundary of the carbon system (Meyer and Boyd, 1972; Mitchell and Giardini, 1977) (Figure 1.). At low pressures or temperatures it is unstable with respect to graphite and may be converted to graphite at moderate temperatures; but usually it is metastable and the transformation to graphite is energetically prohibited. Rocks consisting of diamond and various accompanying minerals, possibly cogenetic to diamond, were driven upwards by explosive pressures of gas-rich magmas from great depths, to penetrate the Earth's crust and to solidify in fissures and pipes (Bruton, 1970).



**Figure 1.3** Pressure – temperature phase diagram for carbon. The blue dashed line separates the stability fields of graphite from diamond. Diamonds can form at depths below 150 kilometers beneath the continental region, whereas underneath oceans, diamonds can form at depths of at least 200 kilometers. (modified after Matthes, 1987; Bundy et al., 1996; Kirkley, 1998 and Stachel, 2007).

### 1.3 Diamond Deposits

Primary diamond deposits are in general hosted in volcanic pipes (e.g. kimberlites and lamproites), and secondary deposits may be the results from erosion of primary deposits and redeposition of diamonds in heavy mineral concentrates in rivers and along oceanic coast lines (Stachel and Harris, 2005; Stachel, 2007). The growth of diamonds is not related to their kimberlite or lamproite host rocks. The relationship of diamonds to their volcanic host rocks is that they are the transporting medium by which diamond ascends to the Earth's surface (Mayer, 1985).

Kimberlites and lamproites are products of continental intra-plate alkaline magmatism, which are a primary source of diamonds, carry a variety of upper mantle-derived xenoliths and are apparently generated at deeper levels in the mantle than most other magmatic products (Mitchell, 1989).

Kimberlite as volcanic pipes or dikes, tend to occur in groups, sills are relatively rare. On the surface, most are of an irregular oval contour, more or less level with the surface (which may be a product of weathering). The composition of kimberlite varies from pipe to pipe and even within the same pipe (Bruton, 1970). Mineralogically, kimberlite is a volatile rich, potassic, ultrabasic rock consisting in principle of olivine and several of the following minerals i.e. phlogopite, carbonate (commonly calcite), serpentine, clinopyroxene (commonly diopside). Other high pressure, mantle-derived minerals that may be present include chromite, ilmenite, pyrope-garnet and magnetite (Mitchell, 1989; Keller, 1990).

Lamproites are stock of potassium-rich mafic to ultramafic alkaline rocks that may be plutonic, hypabyssal or volcanic. Lamproites are classified into groups which are named related to their dominant minerals. The major divisions are based upon the predominance of phlogopite, richterite, olivine, diopside, sanidine and leucite (Meyer, 1985; Mitchell, 1989).

Secondary deposits caused by the erosion of diamondiferous kimberlites liberate diamonds onto the land surface for redistribution by streams and rivers. The pipes must have been upstream of the river beds where diamonds are found. Alluvial diamond occurs in five main types of deposit i.e. fluvial, marine, wind deflation, lacustrine and glacial. The degree of diamond concentration varies considerably in different deposits of any one category; the most economically significant deposit type is the marine, followed by the fluvial. The concentration in glacial deposits is very small, remain a matter of academic interest only (Bruton, 1970; Marshall and Baxter-Brown, 1995).

#### **1.4 Mineral Inclusions in Diamonds**

Diamond genesis and growth occurs principally on the base of chemical compositions in peridotitic and eclogitic environments. A third minor websteritic paragenesis is involved occasionally (Meyer, 1987; Harris, 1993). Mineral inclusion assemblages parallel the mineralogy of the two most important categories of xenolithic inclusions in the upper mantle rock types with which diamond is associated (Richardson

et al., 1984). Mineral inclusions occurring in three groups are presented in Table 1.1. The mineral inclusions may occur in more than one group. Members of one group do not coexist in the same diamond with minerals of the other group, but diamonds containing both occur together in some kimberlite pipes (Meyer, 1985; Boyd and Gurney, 1986).

Mineral inclusions in diamond were originally divided according to their genetic relationship to their host crystals into three groups:

*Protogenetic minerals*: mineral inclusions which had formed before the encapsulation by the host diamond. The inclusions have irregular morphologies or morphologies consistent with the mineral's crystal structure (Meyer, 1987).

*Syngenetic minerals*: mineral inclusions which crystallized under the same physical condition as diamond. The morphological control of the habit by the diamond host is an evidence of these inclusions. Syngenetic inclusions may show a topotaxial relationship to the host diamond. (Harris and Gurney, 1979; Meyer, 1987; Taylor et al., 2003).

*Epigenetic minerals* are secondary mineral inclusions which formed subsequent to diamond formation, either whilst the diamond was still in its original petrogenetic setting or during later transportation with a kimberlite and deposition at an alluvial deposit (Harris and Gurney, 1979; Taylor et al., 2003). Epigenetic inclusions appear to be mostly alteration product of pre-existing inclusions. The alteration most likely through the agency of the kimberlitic or lamproitic fluids, has been facilitated by cracks in the host diamond (Meyer, 1987).

The majority of the mineral inclusions in diamonds are formed of minerals found in the Earth's mantle and which appear as xenoliths in the kimberlite pipe containing the diamonds (Wilks and Wilks, 1991). The mineral species most commonly found in diamonds are shown in Table 1.1.

**Table 1.1** Mineral inclusions in diamonds (after Meyer, 1985, 1987 and Harris, 1993).

Protogenetic and/or Syngenetic			Epigenetic	Uncertain Paragenesis
Peridotitic	Eclogitic	Websteritic		
Olivine* <sup>♦</sup>	Clinopyroxene* <sup>♦</sup>	Clinopyroxene <sup>♦</sup>	Serpentine	Phlogopite
Enstatite* <sup>♦</sup>	Pyrope-Almandine Garnet* <sup>♦</sup>	Enstatite <sup>♦</sup>	Calcite	Biotite
Pyrope garnet* <sup>♦</sup>	Sulphide*	Pyrope-Almandine Garnet	Graphite	Muscovite
Chromite* <sup>♦</sup>	Kyanite	Majorite	Hematite	Amphibole
Sulphides* <sup>♦</sup>	Sanidine	Magnesio-Wustite	Kaolinite	Magnetite
Cr-Diopside <sup>♦</sup>	Coesite	Moissanite	Acmite	Apatite
Cr-Spinel	Rutile		Richterite	
Mg-Ilmenite	Ruby		Perovskite	
Zircon	Ilmenite		Mn-Ilmenite	
Native Iron	Chromite		Spinel	
Cloud-like particles	Cloud-like particles		Xenotime	
Diamond	Diamond		Sellaite	
			Goethite	

\* relatively common inclusions.

<sup>♦</sup> principal mineralogical composition of the three upper mantle rock types with which diamond is commonly associated.

Meyer and Boyd (1972) suggested that olivine is the most common inclusion in diamonds from many different localities, followed by garnet, chromite, enstatite and diopside.

Inclusions captured in diamonds are protected by the durability of their diamond host and also the low diffusion coefficients for the elements in diamond, which makes it possible to study the evolution during which the inclusions and the diamonds have been formed. Many mineral inclusions have retained the chemical compositions that reflect the systems in which they have grown. Some mineral inclusions in diamonds have chemical compositions comparable to the minerals constituting the host rock.

The mineral inclusions in diamonds therefore bring scientific knowledge from the mantle to the Earth's surface. Therefore, detailed research on diamond inclusions will provide various kinds of knowledge, for example, the mineral assemblages of the diamond growth environment, the mineral chemistry of some

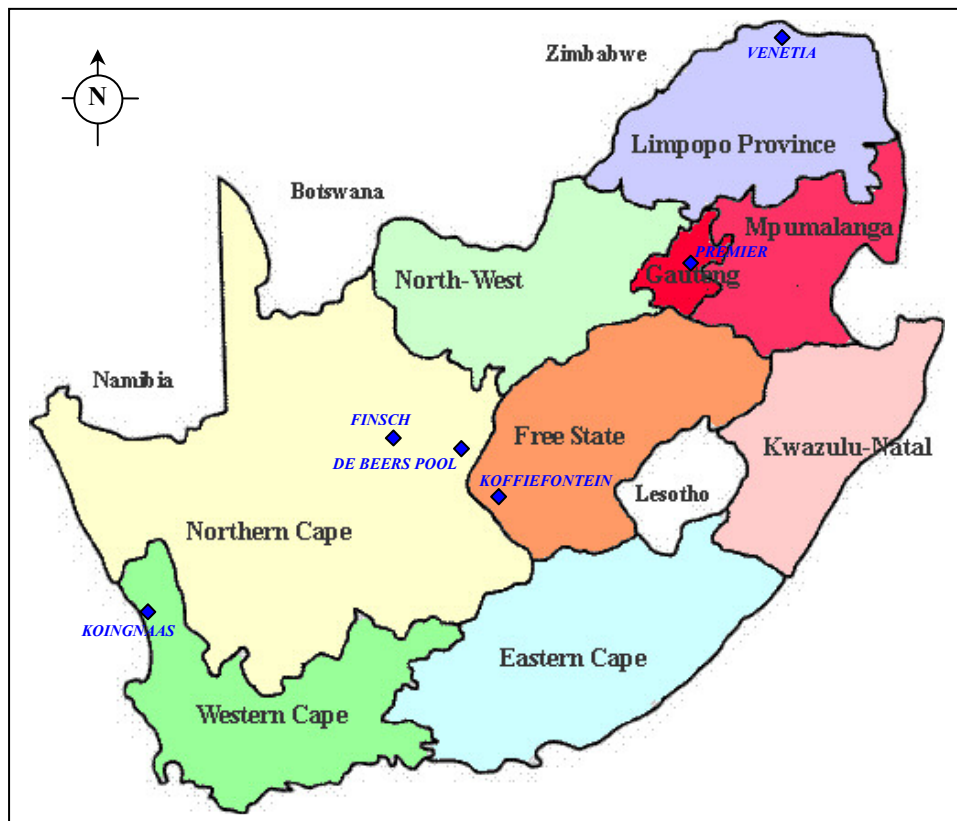
composite inclusions and, in special cases, the parameters of pressure and temperature during crystal growth.

Estimated conditions of equilibration for co-existing peridotitic suite inclusions in diamond are between 900 and 1300 °C and 45 to 65 kbar (Meyer, 1985; Boyd and Gurney, 1986).

## 2. DESCRIPTION OF DIAMOND SAMPLES ACCORDING TO EXTERNAL CHARACTERISTICS

### 2.1 Sample Localities

Diamond deposits are classified as primary (kimberlites and lamproites) or secondary (alluvial). In this study, 22 diamond samples from 6 mines in South Africa (Figure 2.1), and 7 samples from Udachnaya (Siberia/Russia) have been studied.



**Figure 2.1** A map of South Africa showing locations of the diamond samples used in this study.



### **Premier Mine**

The Premier mine (renaming the Cullinan mine celebrating its centenary in 2003) is the underground diamond mine located in the interior of the Archaean Kaapvaal Craton (Richardson, 1986), 30 km east-northeast of Pretoria. It represents the largest kimberlite occurrence in South Africa (Deines et al., 1984). Its eruption age has been reported as  $\sim 1180 \pm 30$  Ma (Harris, 1993).

### **Koffiefontein Mine**

Koffiefontein is an underground diamond mine in the southern Kaapvaal Craton (Izraeli et al., 2004). The Koffiefontein kimberlite pipe is predominantly non-micaceous, phlogopite is absent or comprises a small proportion of the groundmass minerals (Smith, 1983), which has an age of  $\sim 90$  Ma (Rickard et al., 1989; Pearson et al., 1998). The mineral inclusions in diamonds from Koffiefontein show a wide variation in composition but still fall within the range of typical diamond inclusions worldwide (Rickard et al., 1989). The peridotitic (P-type) diamonds formed at temperatures close to 1100 °C and pressures of  $\sim 5.0$  GPa at the base of the lithosphere, whereas the eclogitic (E-type) diamonds crystallized at slightly higher temperatures ( $\sim 1150$ -1250 °C).

### **De Beers Pool Mine**

The De Beers Pool pipe, one from five pipes (the De Beers Pool, Kimberley, Bultfontein, Dutoitspan and Wesselton pipes dated between 84 and 87 Ma., [www.debeersgroup.com](http://www.debeersgroup.com)) in the Kimberley mines group is located in the Kimberley region, which is significant as the site of the first diamond discovered in South Africa. The average pressure-temperature conditions (deduced from non-touching inclusion pairs) are 6.3 GPa and 1200 °C, and  $\sim 5.4$  GPa and 1080 °C, respectively (deduced from touching inclusion pairs; Phillips et al., 2004).

### **Finsch Mine**

The Finsch pipe is the second largest kimberlite pipe in South Africa (Gurney and Switzer, 1973), it is of slightly elliptical shape (535 m  $\times$  460 m). It is located in the farm Brits about 160 km west of Kimberley (Shee et al., 1982), which is

in the southwestern interior of the Archaean Kaapvaal Craton (Richardson et al., 1990). The mine was acquired by De Beers in 1965 and changed from an open-pit to an underground operation in 1990 ([www.debeersgroup.com](http://www.debeersgroup.com)). The xenoliths of peridotitic rocks are common in the Finsch kimberlite, corresponding to diamonds predominated by peridotitic suite inclusions (Meyer, 1987). A previous study of eclogitic diamonds and their inclusions from the Finsch mine (Gurney et al., 1979, cited in Appleyard et al., 2004) suggested that these diamonds are rare at Finsch compared to the common peridotitic suite. Eclogitic garnet and clinopyroxene inclusions in Finsch diamonds yield Sm-Nd isochron ages of 1580 Ma (Richardson et al., 1990). The eruption age of the kimberlite in Finsch mine is ~ 118 Ma (Harris, 1993). Geothermobarometric calculations from the diamond bearing xenoliths indicated that the xenoliths were equilibrated at ~1130 °C and pressures >5.0 GPa within the diamond stability field (Shee et al., 1982).

### **Venetia Mine**

The Venetia kimberlite cluster is 533 Ma in age and located near Alldays, Northern Province of South Africa. The Venetia kimberlites lie within the Central Zone of the Limpopo Belt (Viljoen, 2002). In an area of about 3 km<sup>2</sup>, there are twelve individual kimberlite pipes known, which are generally of irregular shapes and varying from a few tens to about 800 m in the largest cross-sectional dimension (Deines et al., 2001). Silicate inclusions in diamonds from Venetia either belong to a peridotitic (P-type), an eclogitic (E-Type) or a transitional, websteritic (W-type) paragenesis (Deines et al., 2001).

### **Koingnaas (alluvial deposits)**

The Koingnaas alluvial is located on the west coast onshore deposits in South Africa. There are two types of deposits at Koingnaas, a lower non-marine or 'channel clay' deposit, overlain by younger marine sediments preserved in broad bedrock depressions. The channel clay deposit consists of a series of steep gradients filled with basal gravels. During several transgressive and regressive post-Miocene cycles, some of the channel deposits were reworked by marine processes and the diamonds were concentrated in association with basal marine gravels in bedrock depressions ([www.debeersgroup.com](http://www.debeersgroup.com)).

### **Udachnaya Mine (Siberia/Russia)**

The Udachnaya pipe is an open-pit operation (Figure 2.), located in the north-western part of the Daldyn field of the Siberian diamondiferous province, Russia with an age of approximately 350 Ma. It consists of two adjacent bodies (east and west) that become separated at 250-270 m depth. The pipe has a complex structure, which reflects multiple events of magma injection (Kamenetsky et al., 2007). Pressures and temperatures of formation are approximately 1023 °C at 50 kb and 1300 °C at 65 kb for medium-temperature harzburgite peridotite type and high-temperature lherzolite peridotite type, respectively (Gornova et al., 2007).

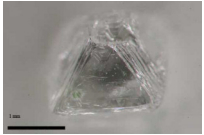
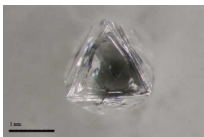
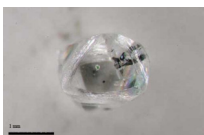
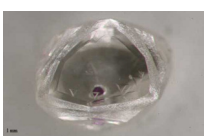





**Figure 2.2** Udachnaya open-pit mine in Russia ([www.allaboutgemstones.com](http://www.allaboutgemstones.com)).


## 2.2 Sample Description

Twenty-nine diamond samples containing prominent and visible mineral inclusions from various localities in South Africa (Premier Mine, Koffiefontein Mine, De Beers Pool, Finsch Mine, Venetia Mine and Koingnaas (alluvial deposit)) and Udachnaya Mine (Russian/Siberia) were studied (Table 2.1).

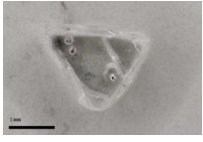
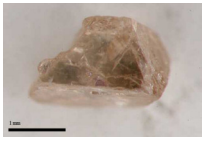
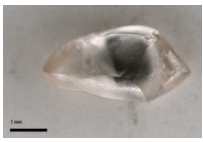
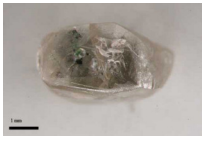

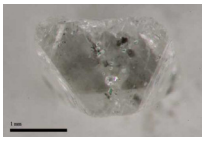

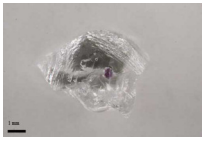
**Table 2.1** Sample description.

Samples name	Pictures	Weight (ct)	Appearances	Mineral inclusions	Localities
DHU1.1		0.06	nearly colourless, transparent, trigons, cracks, stacked growth layers	Cr-Di	Udachnaya Mine (Siberia/Russia)
DHU1.2		0.07	nearly colourless, transparent, glossy surface, cracks, stacked growth layers	Cr-Di	
DHU1.3		0.05	nearly colourless, transparent, hillocks	Cr-Di, Ol, Gr	
DHU2.1		0.06	faint yellow, transparent, trigons, hillocks, stacked growth layers	Cr-Prp, Ol	
DHU2.2		0.05	faint yellow, transparent, cracks, stacked growth layers, hillocks	Cr-Prp	
DHU3.1		0.06	faint yellow, transparent, cracks, stacked growth layers, hillocks	Chr, Ol	
DHU3.2		0.06	faint yellow, transparent, cracks, stacked growth layers, hillocks, trigons	Chr	

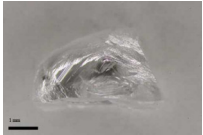
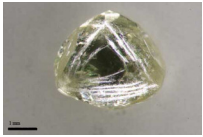
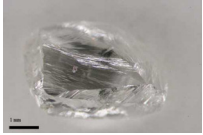
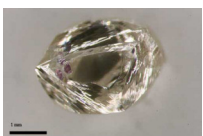
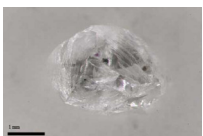




Notes: Cr-Di: chromium diopside; Cr-Prp: chromium pyrope; Chr: chromite; Gr: graphite and Ol: olivine.

: 1 mm.

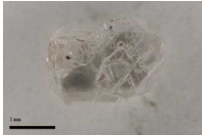
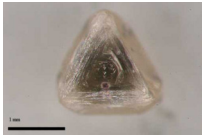
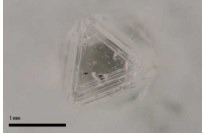


**Table 2.1** (continued).

Samples	Pictures	Weight (ct)	Appearances	Mineral inclusions	Localities
DHP4.1		0.02	faint yellow, transparent, cracks, stacked growth layers, hillocks	Cr-Prp, Gr	Premier Mine
DHP4.2		0.04	light brown, transparent, cracks, stacked growth layers, edge abrasion, percussion marks, trigons, shallow depressions, abraded surface	Cr-Prp	
DHP4.3		0.09	very light brown, semi-transparent, hillocks, edge abrasion, plastic deformation lines	Cr-Prp	
DHP5.1		0.38	very light brown, transparent, hillocks, trigons, stacked growth layers	Cr-Di	
DHP5.2		0.25	faint yellow, transparent, hillocks, trigons, shallow depressions	Cr-Di	
DHP5.3		0.06	nearly colourless, transparent, cracks, edge abrasion, shallow depressions, stacked growth layers	Cr-Di, Ol	
DHK6.1		1.08	nearly colourless, transparent, hillocks, stacked growth layers, trigons	Cr-Prp	Koffrefontein Mine
DHK6.2		0.65	nearly colourless, transparent, cracks, hillocks, trigons, hexagons	Cr-Prp	

**Table 2.1** (continued).

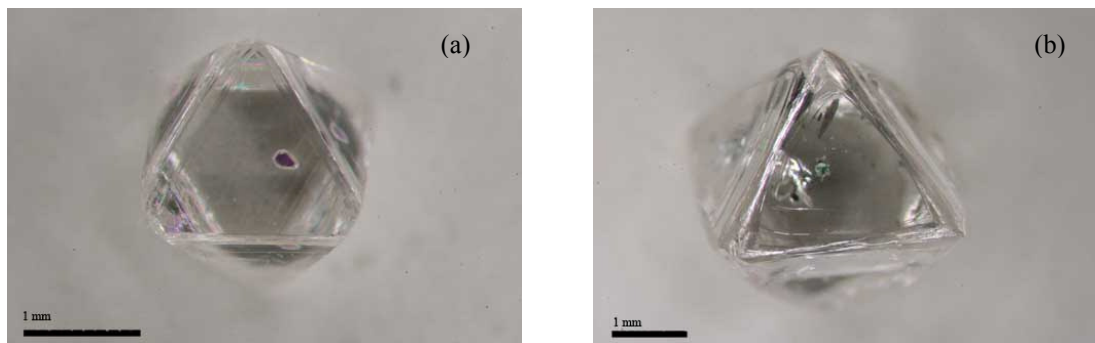
<b>Samples</b>	<b>Pictures</b>	<b>Weight (ct)</b>	<b>Appearances</b>	<b>Mineral inclusions</b>	<b>Localities</b>
<b>DHK6.3</b>		0.24	nearly colourless, transparent, cracks, hillocks, trigons, hexagons, stacked growth layers	Cr-Prp	Koffiefontein Mine
<b>DHK7</b>		0.24	light yellow, transparent, glossy surface, hillocks, stacked growth layers, trigons	Cr-Di	
<b>DHD8.1</b>		0.39	nearly colourless, transparent, hillocks, stacked growth layers	Cr-Prp	De Beers Pool
<b>DHD8.2</b>		0.22	light yellow, transparent, glossy surface, crack, hillocks, stacked growth layers	Cr-Prp	
<b>DHD8.3</b>		0.13	nearly colourless, transparent, cracks, twin, trigons, stacked growth layers	Cr-Prp	
<b>D10</b>		0.32	light brown, transparent, hillocks, cracks, stacked growth layers, trigons	Cr-Prp	Finsch Mine
<b>DHF10.1</b>		0.44	light brown, transparent, stacked growth layers, hillocks, trigons, cracks	Cr-Prp	
<b>DHF10.2</b>		0.30	faint yellow, transparent, hillocks, stacked growth layers	Cr-Prp	
<b>DHF11</b>		0.36	faint yellow, transparent, hillocks, stacked growth layers	Cr-Di	

**Table 2.1** (continued).

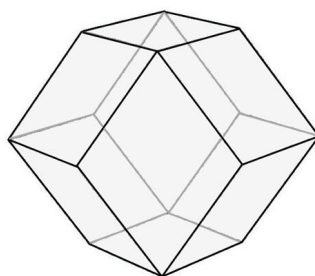
Samples	Pictures	Weight (ct)	Appearances	Mineral inclusions	Localities
DHV12.1		0.05	faint yellow, transparent, cracks, stacked growth layers, edge abrasion, shallow depressions	Cr-Prp, Ol	Venetia Mine
DHV12.2		0.04	light brown, transparent, macle, trigons, stacked growth layers, shield-shape laminae	Cr-Prp	
DHV12.3		0.05	faint yellow, transparent, cracks, stacked growth layers	Cr-Prp	
DHK13		0.21	faint yellow, transparent, macle, hillocks, percussion marks	Cr-Di, Cr-Prp, Ol	Koiingnaas (alluvial)
DHK14		0.19	light yellow, transparent, hillocks, stacked growth layers, trigons	Cr-Di, Cr-Prp	

The diamond samples in this study are nearly colourless to light yellow and light brown with glossy surface within the size range from 1.5 to 5.9 mm in diameter. Seven samples from Udachnaya (Siberia/Russia) and some samples from South Africa are mostly well octahedrally shaped (Figure 2.3a), which is a result of all eight octahedral planes (111) growing parallel to each other at a invariable growth rate which holds for all points of the face (Bulanova, 1995) even with rounded edges (Figure 2.3b) representing the morphology of crystals which received only slight dissolution (Sunagawa (1984), cited in Censier and Tourenq, 1995). However, sharp-edged octahedra are quite rare, rounded edges of octahedra are the usual shape modification. Moreover, an overall rounding of the crystal, resulting in a rounded dodecahedral habit (Figure 2.4), is very common (Lang, 1979). An Octahedron with dodecahedral faces, a sample with curved faces and rounded edges, which experienced dissolution, annealing

and plastic deformation during the transportation process by magma (Sunagawa, 1990; Stachel, 2007) is shown in Figure 2.5.



**Figure 2.3** Diamond samples crystallized in octahedral form (a) DHU2.2 from Udachnaya (Siberia/Russia) and (b) DHF11 with rounded edges from Finsch mine in South Africa.



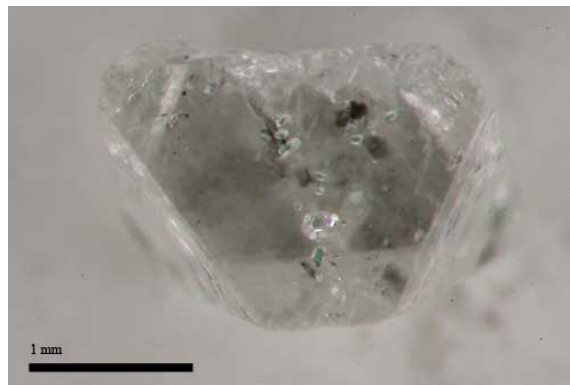
**Figure 2.4** A rhombic dodecahedral shape crystal.



**Figure 2.5** Octahedron with dodecahedral faces in sample DHF7 shows curved faces and round edges.



In general, some asymmetry of the octahedral habit, i.e. elongation or flattening, might arise from several causes. There are many variations from octahedral ideality with some of the faces having developed more than the others (Wilks and Wilks, 1991), as the octahedron in Figure 2.6, which pretends a flat tabular form. These variations are caused by asymmetric distributions of growth promoters (dislocation outcrops or growth-promoting contacts with other bodies and a growth-rate limited by diffusion in the matrix which encourages elongation (Lang, 1979) as portrayed in Figure 2.7.



**Figure 2.6** Diamond sample DHP5.3: octahedron pretends a flat tabular form.



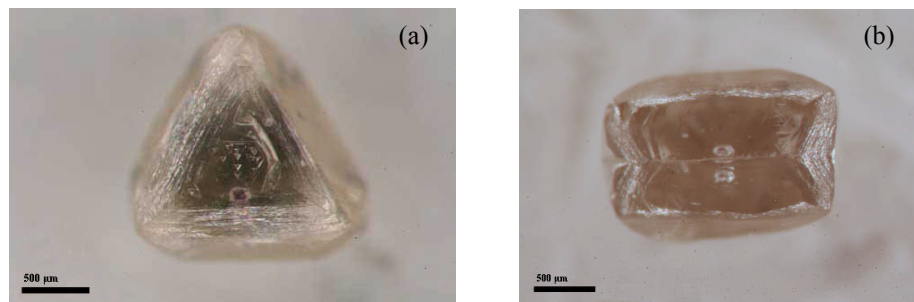
**Figure 2.7** Asymmetric deviation of octahedral habit resulting in an elongated crystal (DHP4.3).

Twinning in diamonds occurs from some variation of the growth process which produces a definite change in the crystallographic orientation of the growth

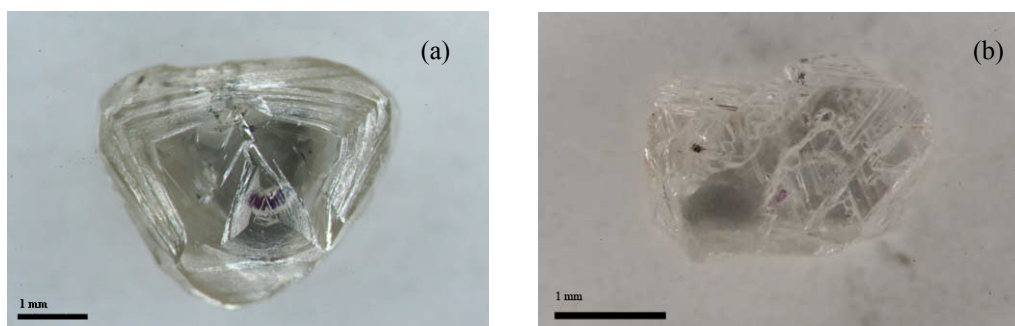
planes. The result of a change in orientation of the crystal structure during growth is a composite or double crystal with reversed parallel faces. Flat triangles shape is the most common twin form, which is called 'macle' (Bruton, 1970; Wilks and Wilks, 1991; Stachel, 2007). As shown in Figure 2.8a, the macle consists of two prominent  $\{111\}$  faces divided by a twin plane parallel to these face (Figure 2.8b) (Harris et al., 1973).

As a result of orientation change during the growth process, contact twinning is one of the simple twinning rules which is found with different orientation (Figure 2.9a). The rotation occurs through  $180^\circ$  and grows parallel to the original growth of one octahedrally growing crystal.

Sometimes twinning occurs over only part of the growing surface, thus producing complex crystals (Wilks and Wilks, 1991) as can be observed in DHV12.1 (Figure 2.9b).



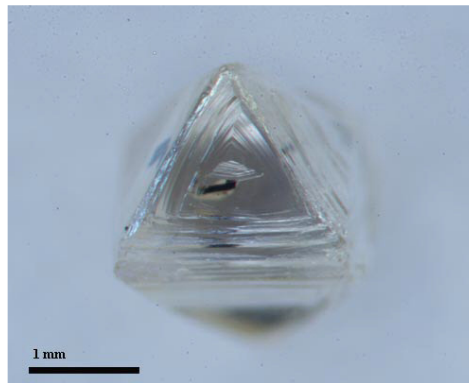
**Figure 2.8** (a) Flat triangular or macle shaped diamond (DHV12.2); (b) two prominent  $\{111\}$  faces divided by a twin plane parallel (spinel-twin-law).



**Figure 2.9** Twining in diamond (a) contact twin (D10) and (b) the complex crystal caused by twinning over only part of the growing surface (DHV12.1).

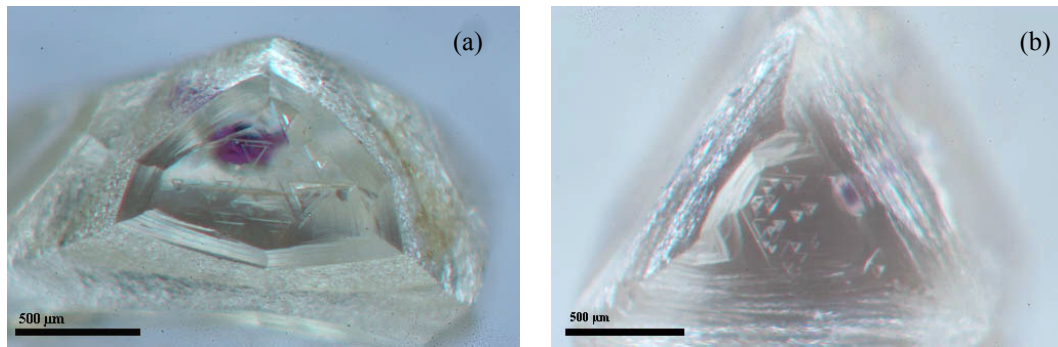
### 2.3 Surfaces Features

Surface and morphological features of the diamond samples were described from examination with an optical microscope. The growth of diamond crystals obviously occurs in layers. Crystal faces are often marked by lines which are seen to be shallow steps or terraces (Bruton, 1970). Many diamond samples present triangular plates on octahedral faces, called stacked growth layers (Stachel, 2007) as shown in Figure 2.10, which depend on their growth processes (Wilks and Wilks, 1991). Censier and Tourenq (1995) examined the surface morphology of diamond samples from the Western Region of the Central African Republic using a scanning electron microscope (SEM) and proposed that all the stepped figures on octahedral faces of diamonds result from the superposition of octahedral planes.



**Figure 2.10** Diamond crystal (DHU3.1) showing stacked growth layers on its octahedral face.

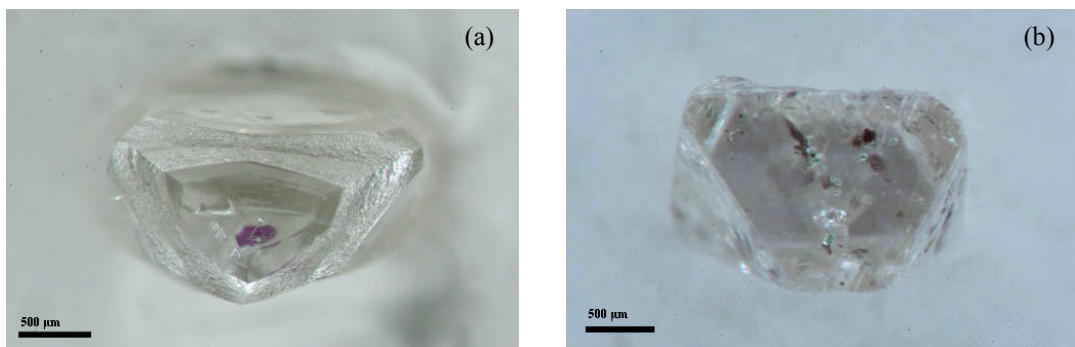
The triangular etch pits, known as ‘trigons’ are the common secondary feature which may be seen on octahedral faces of natural diamonds. There are either positive trigons parallel to the orientation of the octahedral face or negative trigons with an inverse orientation, depending upon the conditions of etching. The majority of trigons on natural diamonds are negative trigons (Patel and Ramanathan, 1962; Verma, 1967; Bruton, 1970; Harris, 1987; Wilks and Wilks, 1991; Haggerty, 1999) that are either flat-bottomed or point-bottomed with inclined sides (Stachel, 2007). In Figure 2.11 a number of negative trigons on octahedral faces of diamonds are shown.



**Figure 2.11** Groups of negative trigons on octahedral faces of diamonds (a) DHU2.1 and (b) DHV12.2.

The octahedral growth of diamond crystal may result in a layering in the form of terraces and as discontinuous ridges called ‘hillocks’ (Figure 2.12a), which is a surface feature on rounded dodecahedral faces.

Percussion marks and edge abrasion (Figure 2.12b) are related to the wear of diamonds during sedimentary transport on the Earth’s surface.



**Figure 2.12** Surface features in diamond (a) hillocks on diamond surfaces (DHU2.1) and (b) edge abrasion (DHP5.3).

### 3. CHARACTERIZATION OF DIAMOND SAMPLES RELATED TO INTERNAL PROPERTIES

#### 3.1 Optical or Colour Centres due to Nitrogen Impurities

Impurities induced by foreign atoms (other than C) in the diamond crystal structure can act as optical centres which create optical absorption effects. Nitrogen is the common impurity in diamond (Evans and Qi, 1982). About 98% of natural diamonds contain a concentration of nitrogen atoms between about 0.003 and 0.3 wt% as an impurity (Allen and Evans, 1981). Bulanova (1995) suggested that after finishing growth, diamonds remain in the mantle at a high temperature ( $\geq 900$  °C) and nitrogen aggregation takes place during this time through a process of diffusion to and into the diamond crystalline lattice. Carbon atoms in the diamond crystal structure are easily replaced by nitrogen atoms because they are relatively similar by size and electronic behavior, shown by their adjacent position in the periodic table (Schönfeld's rule at least at half), so nitrogen atoms are rather similar in size to carbon but contain more valence electrons than carbon. Four of the outer electrons from nitrogen will bond with the four nearest carbon neighbours leaving one electron free. The optical centres are now caused by either a single nitrogen atom or a small group of them.

The optical absorption in a perfect diamond displays no absorption of visible light. Impurity related atoms in the diamond structure can act as optical centres which create typical optical absorption effects (Wilks and Wilks 1991) and may thus have a resulting colour.

#### **Diamond Type**

Diamond has been classified into two main types, based on their specific optical absorption characters and differences in their electronic properties (Kaiser and Bond, 1959; Davies, 1976; Evans and Qi, 1982; Harris, 1987; Berman et al., 1975; Wilks and Wilks, 1991 and Mainwood, 1994).

*Type I:* Natural diamonds contain nitrogen atoms in their structure. There are two subdivisions according to whether nitrogen is present in various forms of

aggregates within the carbon lattice (Type Ia) or whether nitrogen is acting as a single substitutional atom (Type Ib), with nitrogen atoms randomly replacing carbon atoms.

**Type II:** The diamonds are appreciably purer, containing little or no nitrogen atoms. A very few of these show some electrical conductivity, which is due to the presence of boron impurities. Type II diamonds can be subdivided on the basis of their electrical conductivity. Type IIa is the purest diamond form, which is relatively free from any kind of impurity. Type IIb diamonds contain boron atoms, they are usually blue and behave as p-type semiconductors (Berman, 1965).

The type I diamonds show the optical centres, so-called A and B centres.

*The A centre* contains two nitrogen atoms on adjacent lattice sites in the diamond lattices (Allen and Evans, 1981; Mainwood, 1994). An absorption peak in the infrared spectroscopic region at  $1282\text{ cm}^{-1}$  is the most intensive feature of the one-phonon absorption of the A-aggregates of nitrogen occurring within a range from  $1050$  to  $1330\text{ cm}^{-1}$  (Zaitsev, 2001).

*The B centre* is an aggregate consisting of a small number (greater than three) of nitrogen atoms (Allen and Evans, 1981; Mainwood, 1994). An absorption peak in the infrared spectrum at  $1175\text{ cm}^{-1}$  is the most intensive peak of the one-phonon absorption of the B-aggregates of nitrogen within a spectral range from  $850$  to  $1330\text{ cm}^{-1}$ . The B-aggregates are naturally occurring defects in almost of all type Ia natural diamonds (Zaitsev, 2001).

The colour centres in diamond were studied by Collins (1982) and Weikusat (2005) reported the nomenclature of diamond related to its defect structure.

From the previous work, Evans et al. (1982) suggested that type Ia and type Ib diamonds were stable in the upper mantle at temperatures of between  $1000$  -  $1400\text{ }^{\circ}\text{C}$  and at about  $800\text{ }^{\circ}\text{C}$ , respectively. Diamond formation in type IaA is stable at lower temperatures ( $1050$  -  $1100\text{ }^{\circ}\text{C}$ ) than in type IaB ( $1200$  -  $1400\text{ }^{\circ}\text{C}$ ) (Hahherty, 1999).

The diamond samples from Udachnaya (Siberia/Russia) in this study show the optical absorptions comparable to diamonds from Udachnaya studied by Weikusat (2005).

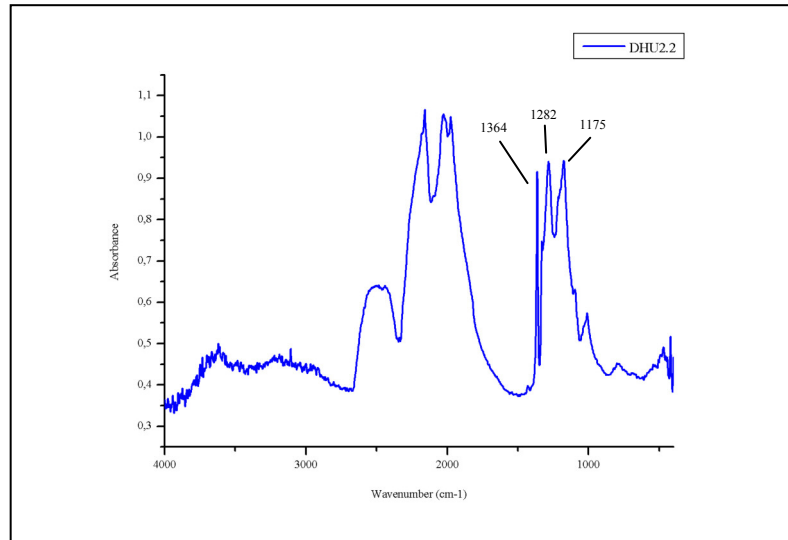
### 3.2 Fourier Transform Infrared Spectrophotometer (FTIR)

The infrared spectroscopy is used to study the lattice dynamic of materials under investigation. The absorption of material in the infrared region of the electromagnetic spectrum, which is referred to as the energy range between  $13,000\text{ cm}^{-1}$  and  $33\text{ cm}^{-1}$ , is usually caused by structural vibrations, i.e. rocking, stretching or bending, of building units of different size and shape in the crystal structures.

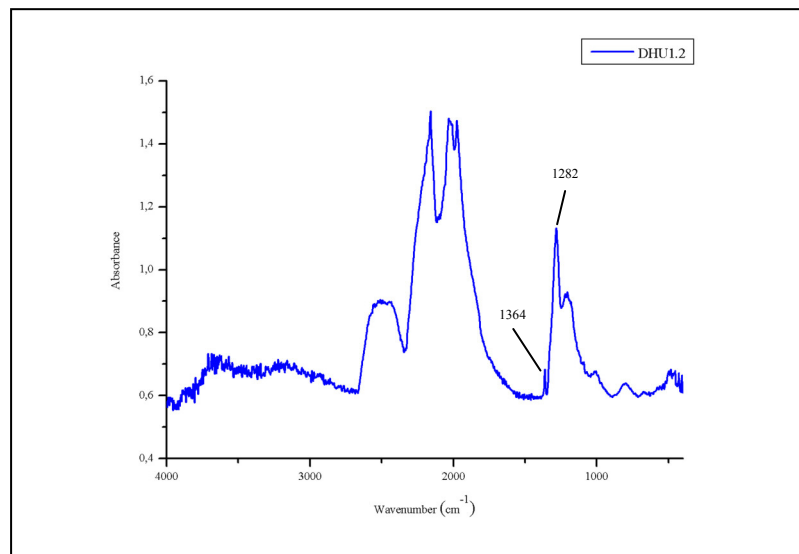
The infrared absorption spectra of diamonds were collected using a Perkin-Elmer 1725X Fourier Transform Infrared Spectrophotometer. The transmission spectra in mid IR region were recorded, ranging from  $400\text{ cm}^{-1}$  to  $4000\text{ cm}^{-1}$  with a  $4\text{ cm}^{-1}$  resolution.

The infrared absorption spectroscopy revealed that the majority of the diamond samples in this study demonstrated a concentration of nitrogen and aggregated nitrogen impurities, consistent with type IaAB. The diamond types and optical centres are given in Table 3.1. Representative samples for type IaAB and IaA are illustrated in Figure 3.1 and Figure 3.2, respectively. The absorption bands between  $5000$  and  $1500\text{ cm}^{-1}$  are lattice bands of the diamond lattice, which are found in all diamonds (Sutherland et al., 1954; Lax and Burstein, 1955; Kaiser and Bond, 1959; Wilks and Wilks, 1991). Type I diamonds contain impurities which destroy the local symmetry of the lattice and allow one-phonon processes to occur in the  $1400 - 1000\text{ cm}^{-1}$  region (Walker, 1979). The strength of the absorption in this region varies from diamond to diamond (Sutherland and Willis, 1945). The presence of nitrogen in diamonds show two main components, A centres at  $1282\text{ cm}^{-1}$  (Brozel et al., 1978 and Zaitsev, 2001) and B centres at  $1175\text{ cm}^{-1}$  (Zaitsev, 2001).

The platelets line at  $1364\text{ cm}^{-1}$ , which has never been observed without the A and/or B centre, is observed in nitrogen-containing type Ia diamonds (Walker, 1979). The precise position of this line ( $1358$  to  $1380\text{ cm}^{-1}$ ) depends on the size of the platelets, the larger the platelets the more the position moves to the maximum (Zaitsev, 2001).



**Figure 3.1** Typical infrared spectrum of an IaAB diamond including a narrow peak at  $1364\text{ cm}^{-1}$  due to the presence of nitrogen platelets.



**Figure 3.2** Typical infrared spectrum of an IaA diamond.

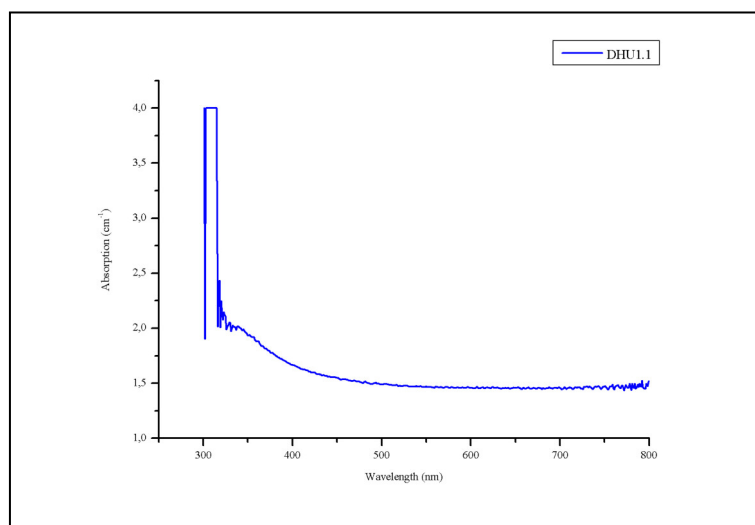


### 3.3 UV-Vis Spectrophotometer

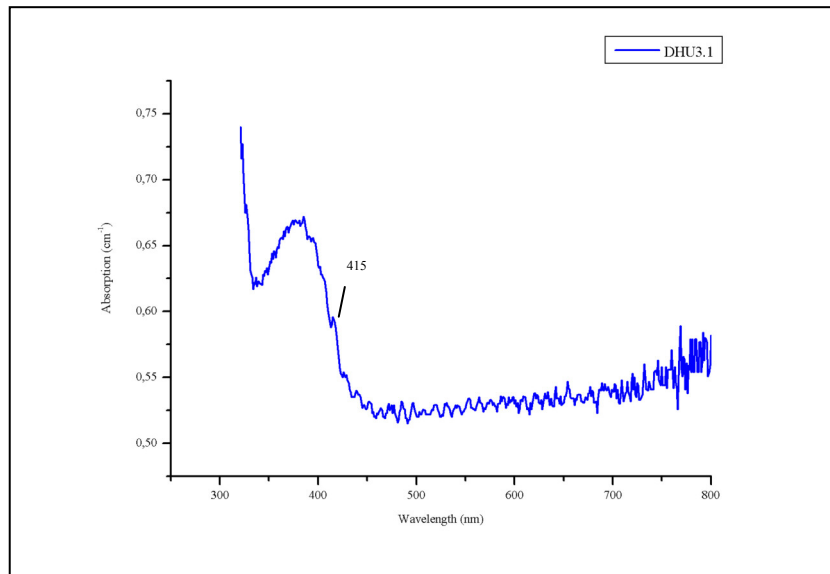
The specific absorption of radiation within the UV-Vis range corresponds to the excitation of outer electrons, which are promoted from their ground state to an excited state when an atom or molecule absorbs energy.

Absorption spectra in the ultraviolet to visible (UV-Vis) range were obtained using LEITZ MPV-SP Spectrophotometer equipped with a microscope with 16x UV-objective between a range from 250 to 800 nm. In Figure 3.3, the visible absorption spectra, where the absorption is due to impurity atoms, arise in absorption from 300 nm confirmed that most samples are belonging to type I, the A-centre group (Kaiser and Bond, 1959; Wilks and Wilks, 1991). The shift in absorption corresponds to the lattice expansion of diamond with increasing nitrogen content, and indicates considerable changes from the normal diamond lattice in the neighbourhood of the nitrogen impurity (Kaiser and Bond, 1959).

UV-Vis spectroscopy of some diamonds which contain a N3 centre, which is found in nitrogen-rich diamonds (Walker, 1979), showed absorption bands at 415 nm together with a band extending to shorter wavelengths (Wilks and Wilks, 1991) as presented in Figure 3.4.



**Figure 3.3** UV-Vis absorption spectrum of diamond in which A centres are the predominant impurities.



**Figure 3.4** UV-Vis absorption spectrum of a diamond in which N3 centre contribute to the absorption.

**Table 3.1** Diamond types, optical absorption and cathodoluminescence effects.

Sample No.	Type	IR	UV-Vis	CL-effect
DHU1.1	IaAB	AB, platelets	-	blue
DHU1.2	IaA	A, platelets	-	inert
DHU1.3	IaAB	AB, platelets	N3	inert
DHU2.1	IaAB	AB, platelets	N3	inert
DHU2.2	IaAB	AB, platelets	N3	inert
DHU3.1	IaAB	AB, platelets	N3	blue
DHU3.2	IaAB	AB, platelets	-	blue
DHP4.1	IaA	A	-	yellow – blue oscillation
DHP4.2	IaAB	AB, platelets	-	yellow – blue oscillation
DHP4.3	IaAB	AB, platelets	-	yellow – blue oscillation
DHP5.1	IaAB	AB, platelets	-	yellow – blue oscillation
DHP5.2	IaAB	AB, platelets	-	yellow – blue oscillation
DHP5.3	IaAB	AB, platelets	-	yellow – blue oscillation
DHK6.2	IaAB	AB, platelets	-	blue with yellow striated
DHK6.3	IaAB	AB, platelets	-	blue
DHK7	IaAB	AB	N3	blue
DHD8.1	IaAB	AB, platelets	-	blue
DHD8.2	IaA	A, platelets	-	blue
DHD8.3	IaAB	AB, platelets	-	blue with yellow striated
D10	IaA	A, platelets	-	yellow – blue oscillation

**Table 3.1** (continued)

Sample No.	Type	IR	UV-Vis	CL-effect
DHF10.1	IaA	A	-	yellow – blue oscillation
DHF10.2	IaAB	AB, platelets	-	yellow – blue oscillation
DHF11	IaA	A, platelets	-	blue
DHV12.1	IaB	B, platelets	N3	yellow – blue oscillation
DHV12.2	IaAB	AB, platelets	-	green
DHV12.3	IaA	A, platelets	-	yellow – blue oscillation
DHK13	IaAB	AB, platelets	N3	yellow – blue oscillation
DHK14	IaA	A	-	yellow – blue oscillation

### 3.4 Internal Growth Features

Cathodoluminescence visualizes some optical phenomena whereby an electron beam impacts on a samples surface, causing the material to emit visible light. The luminescence images contribute to elucidating the growth structure of diamonds, for example. A typical octahedron has grown outwards on {111} faces. Various changes (i.e. variations of the temperature, chemical and impurity content) of the parental ‘melt’ that occurred in its environment during growth can produce changes in the structure of diamonds (Wilks and Wilks, 1991).

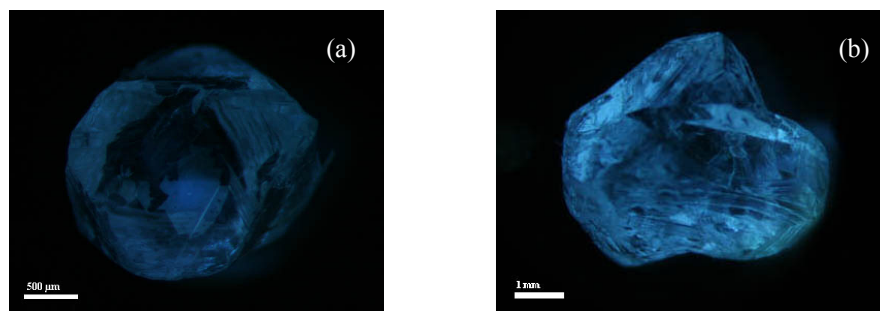
The near-surface effects of diamonds were investigated through the bombarded faces by CITL Cold Cathode Luminescence 8200, mk3 equipped with Zeiss Stemi SV 11 stereo-microscope. Electron beam energies used to excite the CL were 10-15 keV. The light emitted by the samples under electron bombardment has been detected.

Diamonds containing mineral inclusions were polished parallel to {110} or {111} faces, this has been carried out till the mineral inclusions (chrome-pyrope, chrome-diopside, chromite and olivine) were exposed. As the cathodoluminescence technique is a near-surface effect, the internal structures were to be observed.

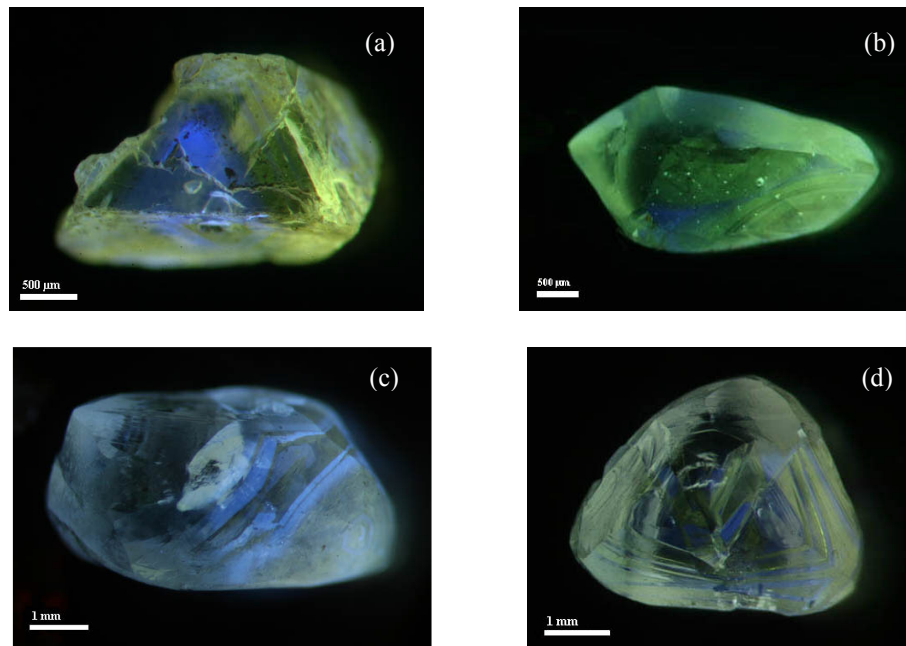
The cathodoluminescence observations of twenty-nine diamond samples have been carried out by visual microscopy on the whole stones in their natural crystal forms. Photographs of the cathodoluminescence were taken individually. The

luminescence of the diamond samples may be caused by the different factors nominated above, i.e. nitrogen content in diamond structures or deformation of the individual crystal structure.

Cathodoluminescence images of diamonds usually show a variety of growth patterns (Table 3.1). Few samples of the specimen investigated here are inert and some samples show dark blue and blue colour (Figure 3.5), since the samples have less deformation. Some samples show the blue-yellow luminescence bands in regions of crystal growth (Figure 3.6).



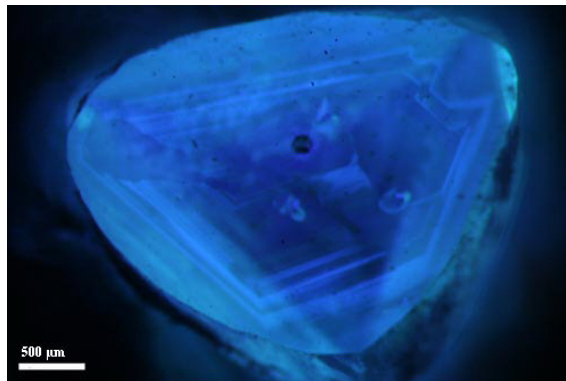
**Figure 3.5** Cathodoluminescence images of diamonds showing blue colour: (a) DHU1.1 and (b) DHK6.1.



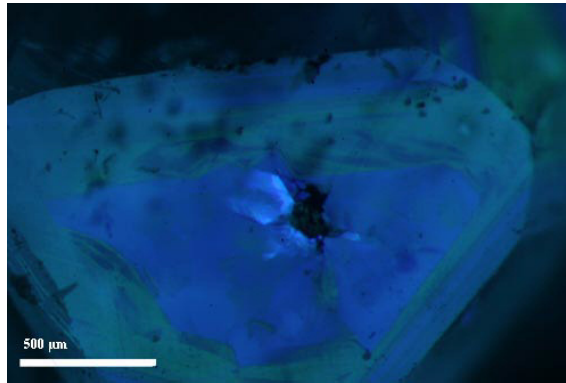
**Figure 3.6** Cathodoluminescence images of diamonds showing yellow-blue oscillation on their surfaces: (a) DHP4.2, (b) DHP4.3, (c) DHP5.1 and (d) D10.

Since cathodoluminescence is a near-surface effect, it is better to observe the internal structure through the polished face. Nine from twenty-nine diamond samples were polished parallel to  $\{110\}$  faces, which is the easy direction of abrasion (Wilks and Wilks, 1991). Only one sample (DHK7) was polished along its  $\{111\}$  face due to the position of the prominent inclusion within the crystal host. The mineral inclusions captured in their hosts are thus exposed to accessible surfaces. The internal structures of diamonds were observed by imaging of cathodoluminescence effects. Some of them show a close relationship between inclusions and the internal morphology of the host diamonds.

The colour of luminescence effects of the central zones in most of the diamond samples usually is blue with growth zoning in some samples. In Figure 3.7, sample DHK13 shows the internal growth zone, showing slightly evidence of resorption at any intermediate stage of crystal formation. One sample (DHK14) shows yellow luminescence zones with slightly rounded corners (Figure 3.8).

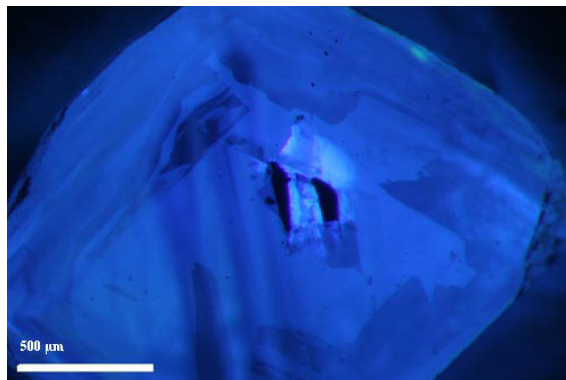


**Figure 3.7** Cathodoluminescence image of DHK13, polished along  $\{110\}$  faces, showing blue colour luminescence parallel to internal zones.



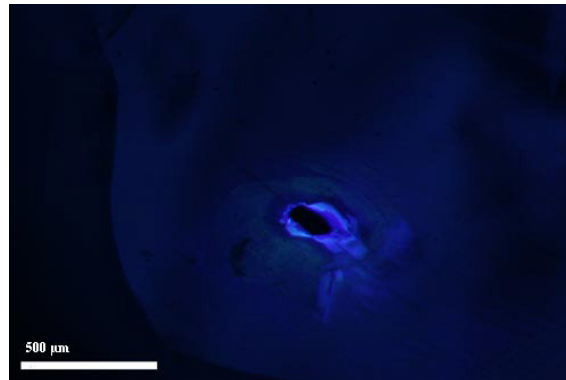
**Figure 3.8** Cathodoluminescence image of DHK14, polished along  $\{110\}$  faces, showing the yellow luminescence internal structure with rounded corner.

DHU3.1 shows the relationship between chromite inclusions and diamond internal structures (Figure 3.9). The image of the local area near the inclusions show that the diamond growth zones are interrupted by the crystal inclusions contact, it corresponds to the evidence for the synchronous growth of diamonds and their syngenetic inclusions (Bulanova, 1995).



**Figure 3.9** Internal structure of diamond (DHU3.1) and its inclusions. Cathodoluminescence images of polished faces on  $\{110\}$  diamond face.

The diamond surrounding a coexisting couple of chrome-pyrope + enstatite in sample DHF10.2 shows a much brighter cathodoluminescence than the outer area (Figure 3.10), since the luminescence effects are responding to the defect concentration within the diamond structure.



**Figure 3.10** Cathodoluminescence image of DHF10.2, polished along the {110} face, showing the brighter luminescence around the chrome-pyrope + enstatite inclusion.

## **4. MINERAL INCLUSIONS IN DIAMOND SAMPLES**

### **4.1 Raman Spectroscopy**

Raman spectroscopy is a non-destructive technique measuring lattice vibrations or rotations of structural units induced by light, which is routinely used to identify mineral inclusions in diamonds. In this study, Raman spectra were recorded on a Jobin Yvon confocal micro-LASER-Raman-spectrometer (LabRam HR800), equipped with an Olympus BX41 microscope. A 50x objective was used to focus the laser beam. The mineral inclusions were analysed with the Argon ion 514.53 nm and the Nd-YAG 532.21 nm laser lines. The spectra were collected by a CCD detector. The mineral inclusion measurements were operated in confocal mode (confocal hole was 400  $\mu\text{m}$ ) and a grating with 1800 grooves per mm and a slit width of 100  $\mu\text{m}$ . The method can be applied to inclusions in their actual position within the host crystal being uncut or unpolished diamonds.

### **4.2 Mineral Inclusions Identification**

Mineral inclusions in natural diamonds are samples coming with their hosts from the Earth's mantle at depths exceeding 120 to 150 km; there is a high probability of their crystallization within the upper mantle, then being retained in diamonds, which are the strongest possible container for transport to the earth surface. They probably represent the physical and chemical conditions during diamond growth (Meyer, 1968; Sobolev et al., 2000, 2008 and Nasdala et al., 2003). Inclusions in diamonds are divided into three groups, i.e. protogenetic, syngenetic and epigenetic. This classification is based on their formation, which may be accompanied or followed by crystallization of their diamond hosts. Protogenetic inclusions are the mineral inclusions that have formed before the encapsulation by the host diamond. The external shape of protogenetic inclusions is governed depending on their own crystal system, but may be altered by the host crystallization. Syngenetic inclusions are presumed to have formed simultaneously within the crystallization process of their hosts. Epigenetic inclusions are secondary minerals which result from the penetration of fluids or melts

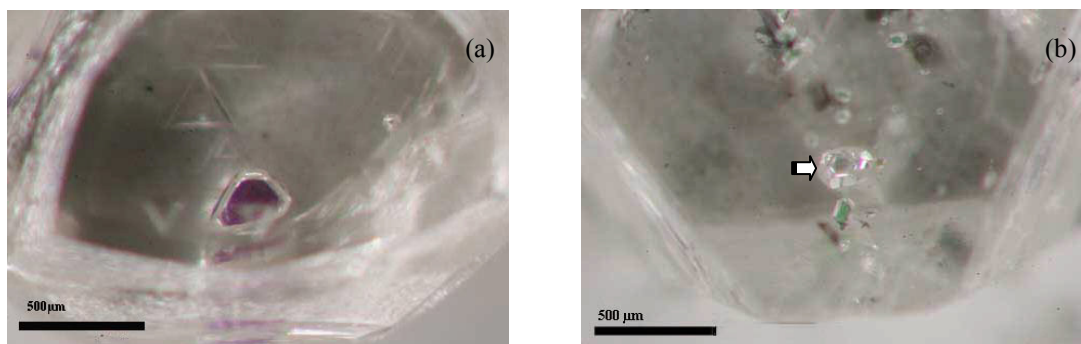


into diamonds along cracks, which are typically associated with crustal processes (Meyer, 1987; Wilks and Wilks, 1991; Taylor et al., 2003; Stachel and Harris, 2008) or it may be crystallization of graphite, due to phase related stabilization processes.

The inclusions in diamonds can be grouped according to their major element chemistry into two suites. Olivine, enstatite, pyrope garnet, diopside and chromite belong to the *ultramafic* suite or *peridotitic* suite, which can be divided into a *lherzolitic* (clinopyroxene bearing) and a *harzburgitic* paragenesis (clinopyroxene absent), whereas pyrope-almandine garnet, omphacite, coesite and kyanite are assigned to the *eclogitic* suite (Meyer and Tsai, 1976; Richardson et al., 1984; Griffin et al., 1992; Shirey et al., 2003; Stachel, 2003; King et al., 2005 and Sobolev et al., 2008).

Various euhedral and subhedral crystal inclusions trapped in 29 diamonds from 7 mines in Siberia (Russia) and South Africa were observed by optical stereo-microscope and were photographed using the natural faces of diamonds as windows for optical access. Most diamond samples in this study contain more than one crystal inclusion. The mineral inclusions approximately range from 50 to 200  $\mu\text{m}$  and were characterized using confocal micro-LASER-Raman-spectroscopy as chrome-diopside, chrome-pyrope, chromite, olivine and graphite, respectively (Table 4.1). Some black material occurred as partial coats on the surfaces of some single-crystal inclusions in diamonds and platelets. The black platelets were identified as graphite inclusions. The black mineral coating the surface of inclusions was not possible to be identified because of thin and tiny size.

Most inclusions in this study have unaltered appearance, no visible fractures leading to diamond hosts and have polyhedral morphology, which had been controlled by the host diamond. Therefore they are interpreted as syngenetic mineral inclusions (Prinz et al., 1975 and Davies et al., 2004). The mineral inclusions usually exhibit some well-developed faces, but have habits dominated by octahedral faces (Prinz et al., 1975). Many syngenetic inclusions display a cubo-octahedral morphology (Figure 4.1) that is imposed by their cubic diamond hosts, whereas some others may be tabular and flattened parallel to the octahedral plane of diamonds (Meyer, 1985; Meyer, 1987; Stachel and Harris, 2008).



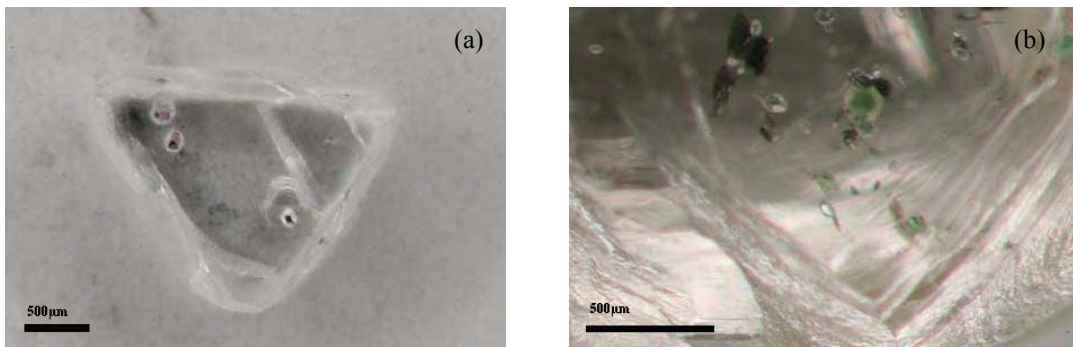
**Figure 4.1** The octahedral form of mineral inclusions in diamonds: (a) chrome-pyrope inclusion in diamond DHU2.1 and (b) olivine inclusion in diamond DHP5.3.

**Table 4.1** Mineral inclusions in diamonds from Russia and South Africa.

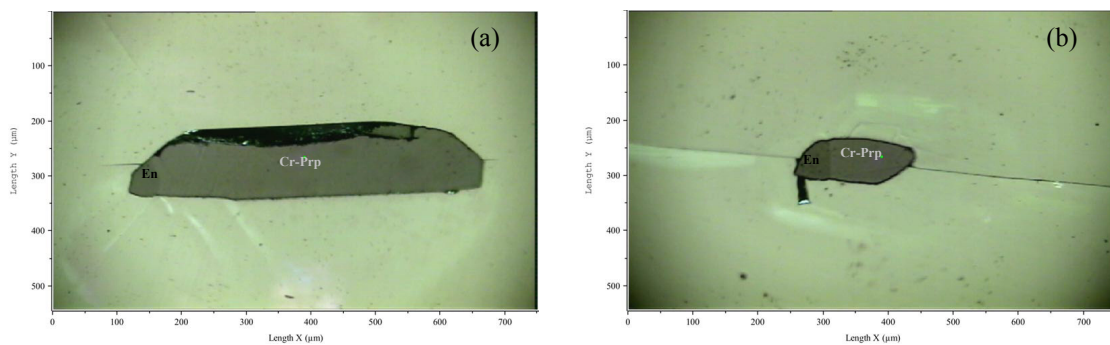
Samples	Inclusions					
	Chrome-diopside	Chrome-pyrope	Chromite	Olivine	Graphite	Enstatite *
DHU1.1	X					
DHU1.2	X					
DHU1.3	X			X	X	
DHU2.1		X		X		
DHU2.2		X				
DHU3.1			X	X		
DHU3.2			X			
DHP4.1		X			X	
DHP4.2		X				
DHP4.3		X				
DHP5.1	X					
DHP5.2	X					
DHP5.3	X			X		
DHK6.1		X				
DHK6.2		X				X
DHK6.3		X				
DHK7	X					
DHD8.1		X				
DHD8.2		X		X		
DHD8.3		X				
D10		X				
DHF10.1		X				
DHF10.2		X				X
DHF11	X					
DHV12.1		X		X		
DHV12.2		X				
DHV12.3		X				
DHK13	X	X		X		
DHK14	X	X				

\* Enstatite inclusions were observed and identified from exposed inclusions after polishing.

Some diamond samples contain two or more mineral inclusions co-existing in a single diamond. Most of the co-existing inclusions are separate from each other (non-touching) as shown in Figure 4.2, and intergrowths (touching) of two minerals were also found in a single host diamond (Figure 4.3).



**Figure 4.2** Co-existing inclusions within individual diamonds: (a) graphite (black) and chrome-pyrope (purplish red) inclusions in diamond DHP4.1 and (b) chrome-diopside (green) and olivine (colourless) inclusions trapped in DHK14.

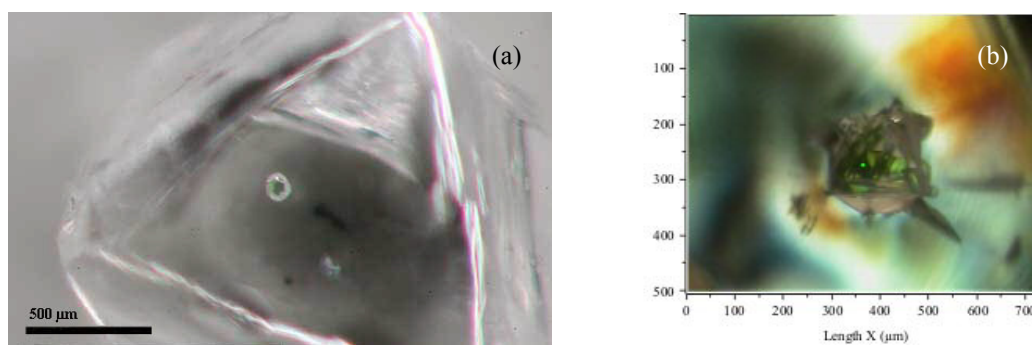


**Figure 4.3** Intergrowths of two mineral inclusions (chrome-pyrope + enstatite) trapped in single host (a) DHK6.2 and (b) DHF 10.2.

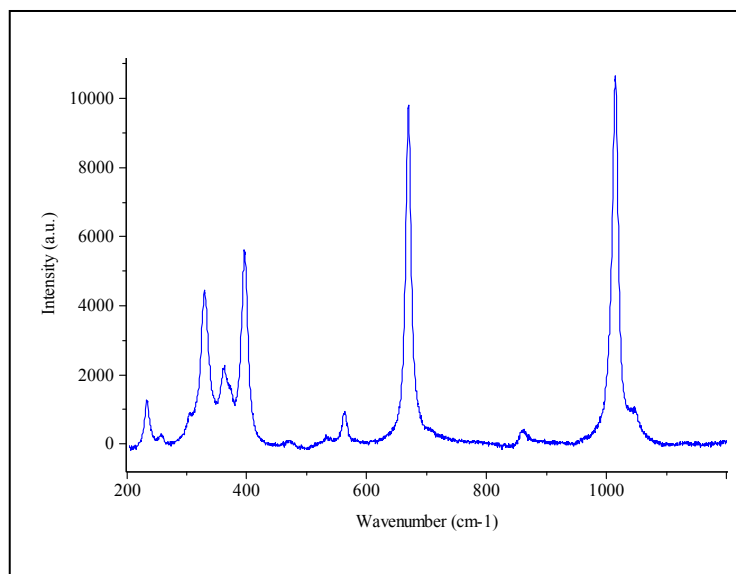
### *Chrome-diopside*

Diopside is a member of the pyroxene group of the chain silicates, which crystallises in the monoclinic system. Space group  $C2/c$ ;  $a = 9.73 \text{ \AA}$ ,  $b = 8.91 \text{ \AA}$ ,  $c = 5.25 \text{ \AA}$ ,  $z = 4$ ;  $\beta = 105.5^\circ$  (Klein and Hurlbut, 1993); unit of cell volume:  $438.58 \text{ \AA}^3$  (Smyth and Bish, 1988) are the starting parameters for further investigation. Diopside is a calcium magnesium silicate ( $\text{CaMg}[\text{SiO}_3]_2$ ), but some magnesium is always replaced by iron which may increase in quantity until the crystals become dark green. The chromium contained in diopside causes a bright green (Webster, 1994). The  $\text{Cr}^{3+}$  ion should usually be accompanied by some  $\text{Na}^+$ -content, which means that there may be some ureyite component replacing the diopside crystal chemistry.

Green crystal inclusions are visually interpreted – as being observed by stereo-microscope - as chrome-diopside (Figure 4.4a). Monoclinic inclusions with stepping of octahedral faces (Figure 4.4b) are indicative of imposed morphology during syngenetic growth (Stachel and Harris, 2008). The typical Raman spectrum of chrome-diopside is shown in Figure 4.5.



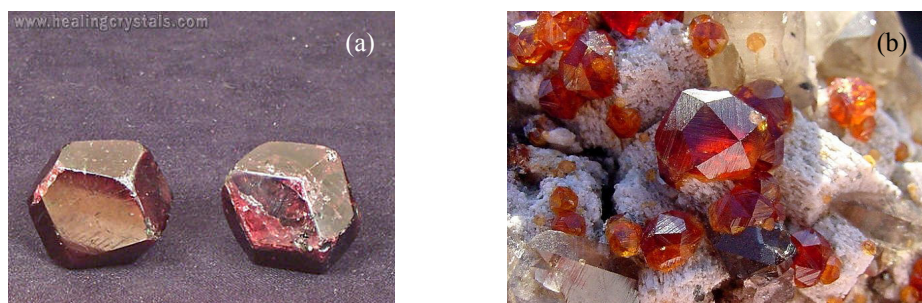
**Figure 4.4** Chrome-diopside inclusions in diamonds: (a) DHU1.2 observed under stereo-microscope and (b) chrome-diopside crystal inclusion in DHF11 with stepping of octahedral faces.



**Figure 4.5** In situ Raman spectrum of a chrome-diopside inclusion in diamond DUH1.1.

### *Chrome-pyrope garnet*

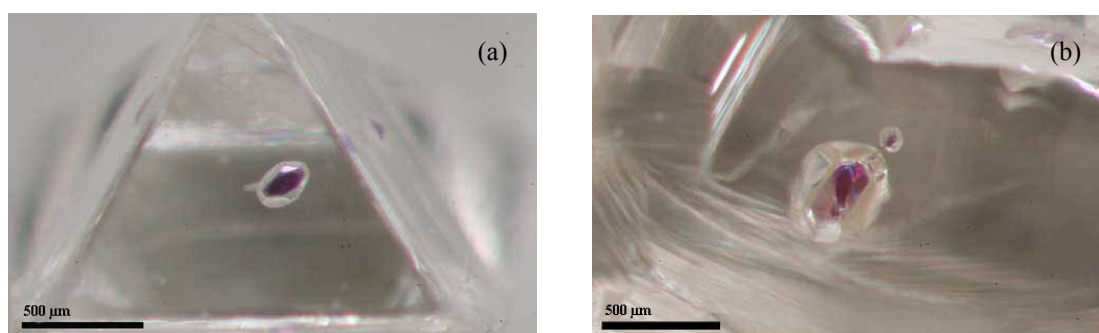
Chrome-pyrope garnets crystallise in the cubic system, space group  $Ia\bar{3}d$ ;  $a = 11.46 \text{ \AA}$ ; unit of cell volume:  $1504.70 \text{ \AA}^3$  (Klein and Hurlbut, 1993; Smyth and Bish, 1988), as starting structural parameters. Common crystal morphologies are a twelve-faced rhombic-dodecahedron and the twenty-four-faced trapezohedron (Figure 4.6), often in combinations of these two forms.



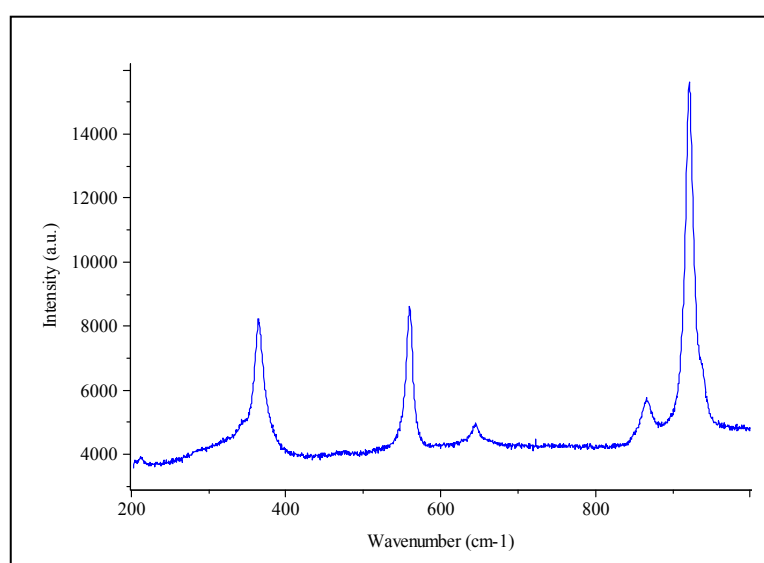
**Figure 4.6** The common crystal morphologies of garnet: (a) a twelve-faced rhombic-dodecahedron ([www.healingcrystal.com](http://www.healingcrystal.com)) and (b) twenty-four-faced trapezohedron ([skywalker.cochise.edu](http://skywalker.cochise.edu)).

Pyrope garnet, if pure, would be colourless and would have the formula  $\text{Mg}_3\text{Al}_2[\text{SiO}_4]_3$ , but natural pyropes are usually deep-red in colour due to the presence of  $\text{Fe}^{2+}$  (Klein and Hurlbut, 1993 and Webster, 1994).

The purplish-red inclusions are visually identified by stereo-microscope as pyrope garnets (Figure 4.7) as found in a peridotitic paragenesis, whereas the eclogitic paragenesis garnets are orange-red (Richardson et al., 1984; Meyer, 1987; Kunz et al., 2002 and Stachel and Harris, 2008). The purplish-red inclusions were also recognized by Raman spectroscopy. A typical Raman spectrum characteristic of pyrope garnet is usually observed as depicted in Figure 4.8.



**Figure 4.7** Chrome-pyrope inclusions embedded in diamonds: (a) DHU2.2 and (b) DHF10.1.

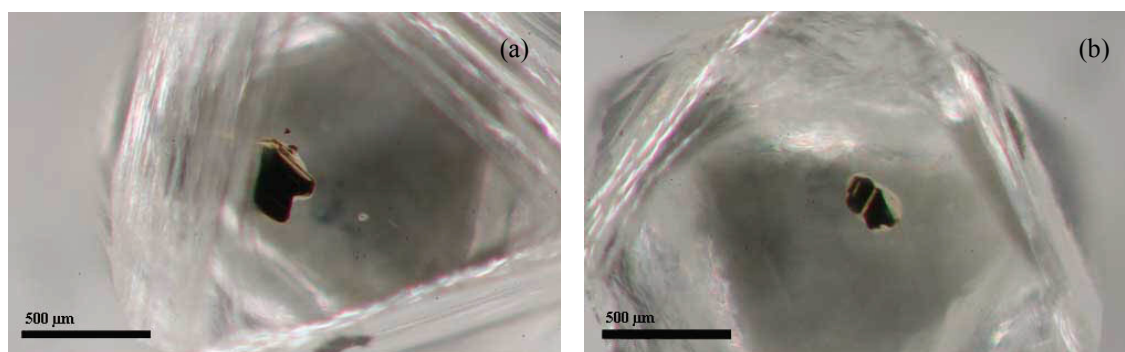


**Figure 4.8** In situ Raman spectrum of a chrome-pyrope inclusion in diamond DHF10.2.

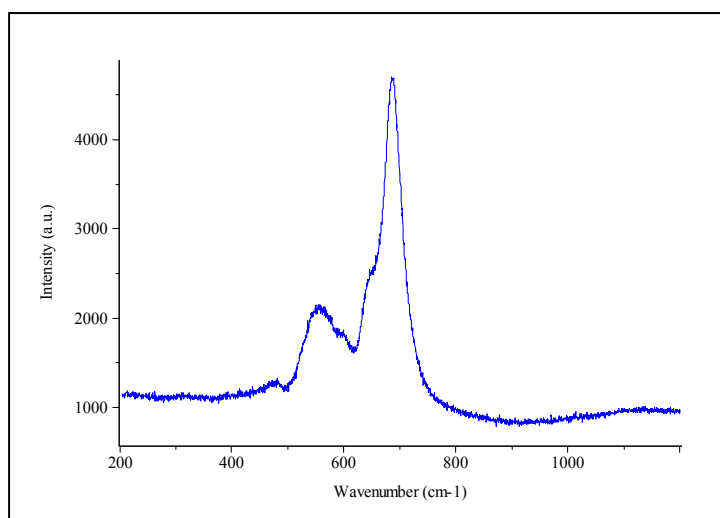
### ***Chromite***

Chromite is a spinel with iron and chromium oxide ( $\text{FeCr}_2\text{O}_4$ ), which crystallises in the isometric system and is generally opaque. Normally, it crystallizes in typical octahedrally dominated morphologies, but the crystals as inclusions are small and rare. They are commonly massive, granular and compact. Space group  $Fd3m$ ;  $a = 8.10 \text{ \AA}$ ,  $z = 8$  (Klein and Hurlbut, 1993); unit of cell volume:  $588.31 \text{ \AA}^3$  (Smyth and Bish, 1988) are the starting parameters.

Black crystal inclusions in diamonds DHU3.1 and DHU 3.2 are identified as chromite (Figure 4.9). The Raman spectrum of a typical chromite inclusion is portrayed in Figure 4.10.



**Figure 4.9** Chromite inclusions in diamonds: (a) DHU3.1 and (b) DHU3.2.



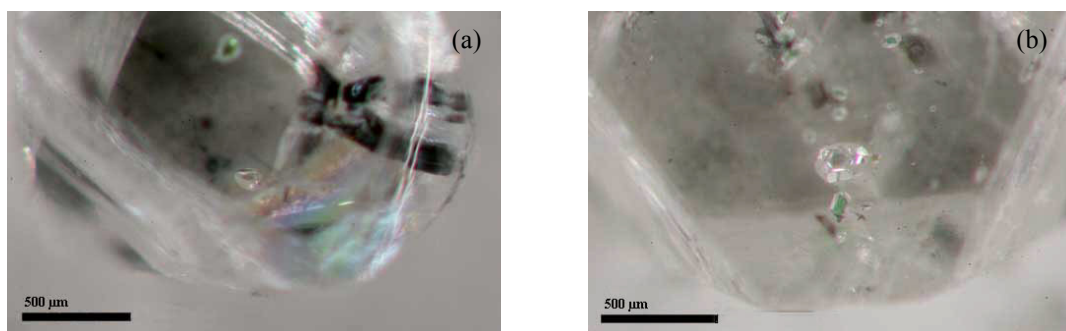
**Figure 4.10** In situ Raman spectrum of a chromite inclusion in diamond DHU3.1.



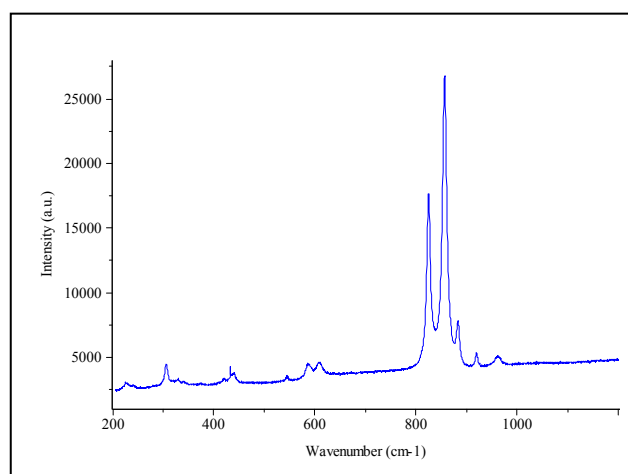
### *Olivine*

Olivine ( $\text{Mg,Fe}$ ) $_2\text{SiO}_4$ , belongs to an orthorhombic orthosilicate group. Olivines vary in composition from forsterite ( $\text{Mg}_2\text{SiO}_4$ ) to fayalite ( $\text{Fe}_2\text{SiO}_4$ ). The more common olivines are richer in Mg than in  $\text{Fe}^{2+}$ . Space group  $Pbnm$ ;  $z = 4$ .  $\text{Mg}_2\text{SiO}_4$ :  $a = 4.75 \text{ \AA}$ ,  $b = 10.20 \text{ \AA}$ ,  $c = 5.98 \text{ \AA}$ , unit of cell volume:  $289.58 \text{ \AA}^3$ .  $\text{Fe}_2\text{SiO}_4$ :  $a = 4.82 \text{ \AA}$ ,  $b = 10.48 \text{ \AA}$ ,  $c = 6.09 \text{ \AA}$ , unit of cell volume:  $307.42 \text{ \AA}^3$  (Deer et al., 1966; Smyth and Bish, 1988; Klein and Hurlbut, 1993) are used as principally characterizing structural parameters. The crystals usually exhibit a combination of prisms, pinacoids and a dipyramid.

Colourless crystal inclusions are observed and identified as olivine (Figure 4.11). The typical Raman spectrum obtained from an olivine inclusion is shown in Figure 4.12.



**Figure 4.11** Olivine inclusions in diamonds: (a) DHU1.3 and (b) DHP5.3.



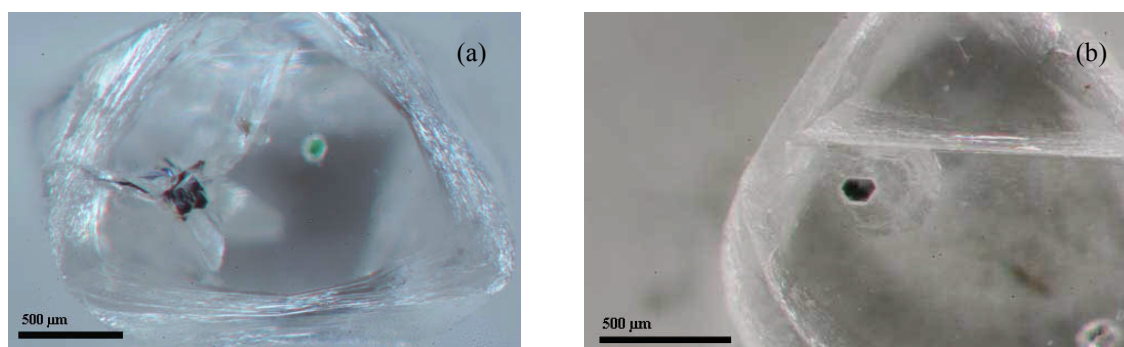
**Figure 4.12** In situ Raman spectrum of an olivine inclusion in diamond DHK13.



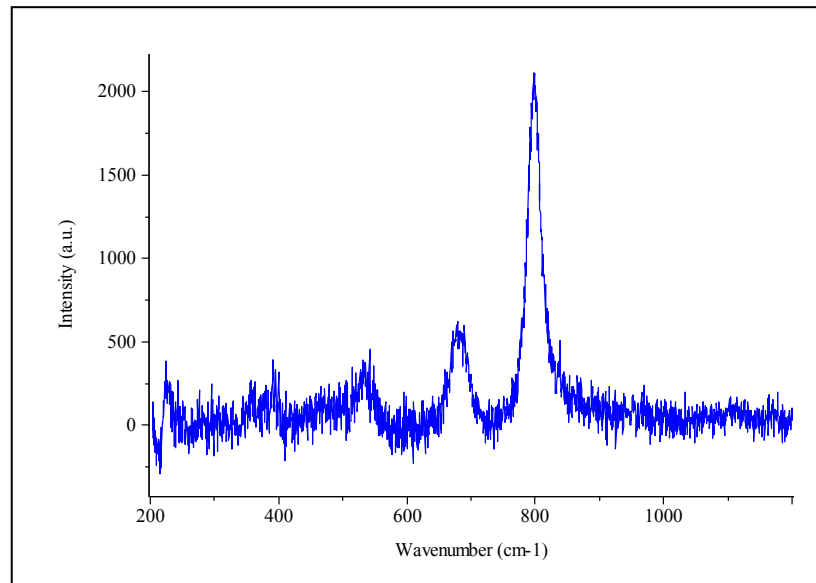
### ***Graphite***

Graphite (C) is one polymorph of crystalline carbon which develops as a stable form at ordinary pressure and temperature (Webster, 1994), the phase diagram of carbon is shown in Figure 1.3, Chapter 1. The carbon atoms in the crystal structure of graphite lie in honeycomb sheets, with extremely strong covalent bonds between the atoms in each sheet but the interlayer bonds are relatively weak (Zhao et al., 1989). Graphite crystallises in the hexagonal crystal system in tabular crystals of hexagonal outline with prominent basal plane. Space group  $P6_3/mmc$ ;  $a = 2.46 \text{ \AA}$ ,  $c = 6.74 \text{ \AA}$ ,  $z = 4$  (Klein and Hurlbut, 1993); unit of cell volume:  $35.42 \text{ \AA}^3$  are the principal values of graphite crystallography.

Graphite inclusions were initially recognized by their colour and hexagonal habit which are accompanied by fractures reaching into the diamond host (Figure 4.13a). As shown in Figure 4.13b, the graphite inclusion may be an idiomorphic crystal, with its (001) face oriented parallel to a (111) diamond plane. This graphite slab is surrounded by hexagonal-shaped fractures in the same (111) diamond plane. A typical Raman spectrum of a graphite inclusion is depicted in Figure 4.14.



**Figure 4.13** Graphite inclusions in diamonds: (a) DHU1.3 and (b) DHP4.1.

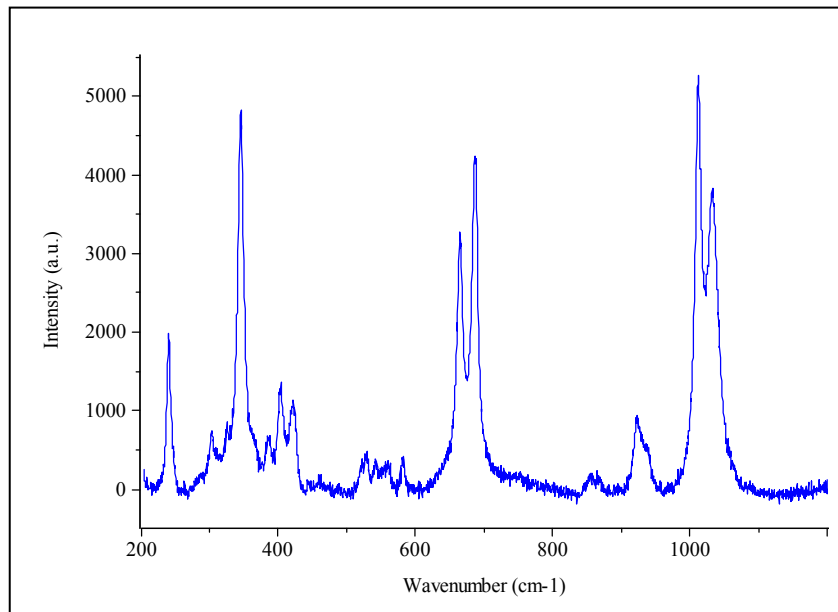


**Figure 4.14** In situ Raman spectrum of a graphite inclusion in diamond DHP4.1.

### *Enstatite*

Enstatite belongs to the pyroxene family, a member of the chain silicate group, which crystallises usually in orthorhombic system (though polymorphic phases are well known). The chemical composition is  $\text{MgSiO}_3$ . Space group *Pbca*;  $a = 18.22 \text{ \AA}$ ,  $b = 8.81 \text{ \AA}$ ,  $c = 5.17 \text{ \AA}$  (Klein and Hurlbut, 1993); volume of unit cell:  $829.88 \text{ \AA}^3$  may serve a starting parameters of crystal structure basics.

In this study, enstatite inclusions were characterized after polishing. Raman spectroscopy confirmed the presence of enstatite as intergrowth (touching) inclusion with chrome-pyrope in diamonds DHK6.2 and DHF10.2 as show above in Figure 4.3. A typical Raman spectrum of an enstatite is shown in Figure 4.15.



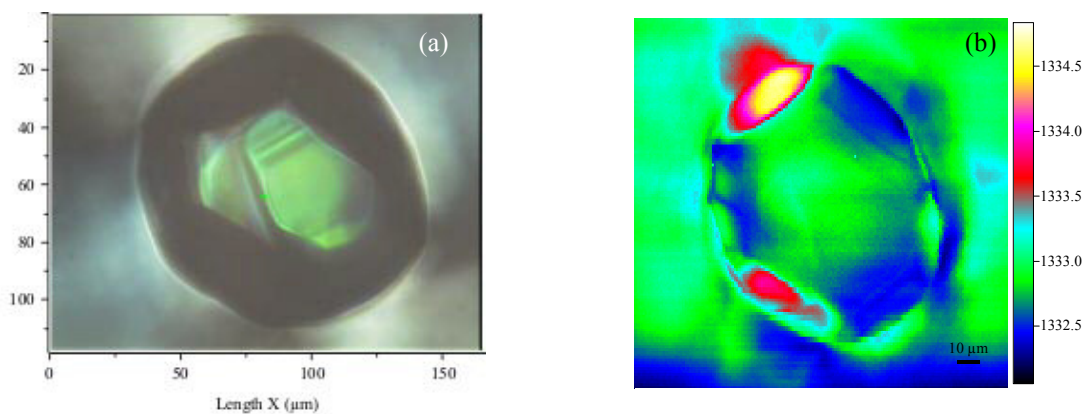
**Figure 4.15** Raman spectrum of an enstatite inclusion in diamond DHF10.2.

### **4.3 Pressure Differences between Diamond Host Crystals and Their Guest Inclusions**

Diamonds, due to their very high bulk modulus and thermal expansion coefficients, can preserve compressed mineral inclusions at an effective pressure up to several GPa without plastic deformation. The preserved pressure depends on the difference in compressibility and expandability of the host diamond relative to the inclusion (Sobolev et al., 2000). Stresses in the surrounding diamond and internal pressure within coexisting mineral inclusions can be measured and eventually used to estimate pressures of the diamond source condition.

Twenty-seven crystal inclusions from seventeen diamond samples were selected for in situ microanalysis of pressure relations. There are almost no fractures reaching from the outer surface of the inclusion into the outer surface of the diamond (Figure 4.16a). The non-destructive Raman in situ point-by-point mappings were done in confocal mode. A 2-dimensional Raman spectral map was made of the diamond-volume or more correctly area adjacent to an inclusion. The residual pressure can be estimated by the shift of the first-order Raman spectrum band of diamond (Barron et al.,

2008; Izraeli et al., 1999 and Nasdala et al., 2003, 2005). A colour-code image generated from a data set of Raman spectra in the actual diamond-inclusion pair is shown in Figure 4.16b.



**Figure 4.16** (a) Chrome-diopside inclusion in diamond DHU1.2, (b) Raman map of diamond DHU1.2 (view through  $\{111\}$ ) around the chrome-diopside inclusion. The colour-code represents the shift of the first-order Raman band of diamond. The relative pressure between diamond and chrome-diopside inclusion is 1.13 GPa.

In special cases, Raman peaks for a certain mineral will shift due to an increased confining pressure (Baron et al., 2008). Two-dimensional Raman spectral mapping was carried out using a frequency doubled Nd:YAG laser (532.21 nm) with a software-controlled x-y-stage. The sample was moved step-by-step relative to the fixed microscope objective. The step width was chosen depending on the size of the mapped area. The 50x microscope objective was used to focus the excitation laser to the micrometer-sized beam. The octahedral faces of the diamonds were flat and even enough to allow full optical examination. The Raman signal was excited and measured perpendicular to the diamond-inclusion interface. The diamonds were observed through their octahedral  $\{111\}$  faces, view direction  $[111]$  on to the diamond. A Raman spectrum was acquired at each sampling point, resulting in many thousands of collected single spectra, making the recording of mapping files a lengthy process. Individual maps consisted of thousands of spectra, depending on size and resolution. The spectra were then individually curve fitted, using symmetrical mixed Gaussian-Lorentzian line shape adaptations. A colour-code image was generated from a complete data set of

Raman spectra. The measurements were carried out to obtain the information on the residual pressure under which the inclusions were trapped, which can be estimated by the shift of the first-order Raman spectrum band of diamond ( $\sim 1332 \text{ cm}^{-1}$ ).

The quantitative barometric information can be provided from vibrational spectra, since the energy of a phonon in a material is affected by the average bond distances within the material and therefore, the strain is represented by a shift in the Raman bands of the material pairs under investigation (Nugent et al., 1998). The calibration of the pressure-induced band shift has been reported in previous studies of the first-order Raman spectra of diamond (Boppart et al., 1985 and Hanfland et al., 1985).

The remnant pressures are calculated, according to factor from Grimditch et al., (1978), the pressure shift factor for the main Raman peak of diamond is different for different crystallographic directions. The respective calibration of uniaxial stress is  $2.2 \text{ cm}^{-1}/\text{GPa}$  along  $\{111\}$  direction and  $0.7 \text{ cm}^{-1}/\text{GPa}$  in the  $\{001\}$  direction.

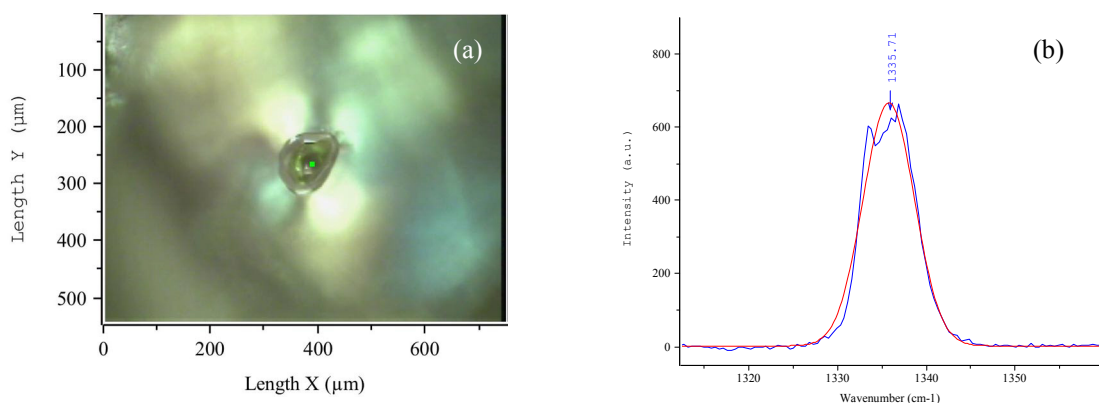
The remnant pressures are derived from the shift of first-order Raman diamond spectra shown in Table 4.2.

**Table 4.2** Relative pressure differences between host diamond crystals and their guest inclusions.

Samples	Pressure (GPa)				
	Chrome- diopside	Chrome- pyrope	Chromite	Olivine	Graphite
DHU1.1	1.01				
DHU1.2	1.13				
DHU1.3	1.77			0.77	
DHU2.1		0.91		0.59	
DHU2.2		0.77			
DHU3.1			1.00, 0.23	0.32	
DHU3.2			0.68		
DHP4.1		0.45, 0.43			0.48
DHP4.3		0.65			
DHP5.1	0.97				
DHP5.3				1.27	
DHK7	2.01, 0.97, 0.49				
DHF10.1		0.90			
DHF11	1.41				
DHV12.3		0.68			
DHK13	0.59	0.86		1.14	
DHK14	1.02				

In some samples, individual diamonds contain multiple inclusions of the same species, i.e. DHK7 contains twelve chrome-diopside inclusions, of which three were measured. The mineral inclusions trapped in the host show the different remnant pressures depending on their sizes. Three chrome-diopside inclusions captured in individual diamond have dimensions of approximately  $200 \times 460 \mu\text{m}$ ,  $200 \times 250 \mu\text{m}$  and  $20 \times 70 \mu\text{m}$ , which have remnant pressures of 2.01, 0.97 and 0.49 GPa, respectively. Whereas, the two chrome-pyrope inclusions captured in diamond DHP4.1 have similar dimensions of approximately  $180 \times 200 \mu\text{m}$  and  $170 \times 190 \mu\text{m}$ , which have similar remnant pressures of 0.45 and 0.43 GPa, respectively.

The mineral inclusions are under compression. They stress the diamond around them, deform it and remove its cubic symmetry (Izraeli et al., 1999). The remnant pressure of the inclusion is the cause of the strain in the diamond lattice that results in anomalous birefringence (Howell et al., 2008). As a result, stress-induced birefringence can be observed in the diamond adjacent to the inclusion (Figure 4.17a). In particular, a splitting of the non symmetric Raman peak into a doublet was also observed. The splitting was considered to be the result of the presence of anisotropic stresses within crystal host and guest (Stuart et al., 1993; Vlasov et al., 1997). The line is broadened and shifted to higher wave-numbers (Grimsditch et al., 1978) as is displayed in Figure 4.17b.



**Figure 4.17** (a) Strain birefringence around a chrome-diopside inclusion in the adjacent diamond DHU1.3. (b) The first-order Raman peak of diamond DHU1.3 on {111} direction which splits into a spectral doublet.

## 5. ORIENTATION OF CRYSTAL INCLUSIONS IN DIAMONDS

The orientation relationship between diamond samples and their crystal inclusions was studied by an in situ method based on a single crystal X-ray diffraction technique which reveals a combined crystallographic orientation study and a crystallographic mineral characterization of the inclusions. The measurements were carried out using the Xcalibur four-circle X-ray diffractometer with sapphire 3 CCD detector (Oxford Diffraction) with  $\text{MoK}_\alpha$  radiation during a two week stay at the Institute of Physics, University of Silesia, Katowice, Poland.

The single crystal diamond samples were mounted on a sample holder and the inclusions were centered visually using a video camera on a Kappa geometry diffractometer. The centring procedure of the crystals was difficult in some samples because of the lack of parallel faces on the diamond hosts. The optical refractive index of the diamond host crystal had to be introduced being a significant possibility of error in the crystal centring by microscopic techniques. Data were collected between  $0^\circ \leq \varphi < 360^\circ$  for  $\omega = 0^\circ$ ,  $\kappa = 0^\circ$  for two  $2\theta$  settings, at  $35^\circ$  and  $-35^\circ$ , respectively. The diffraction experiments revealed the values of the lattice parameters for the inclusion crystals in addition to the very strong reflections of the host diamond crystals. Based on the lattice parameters, these reflections could be attributed to different mineral inclusions, which must confirm the optical observation on the mineral inclusions in the special diamonds. From orientation matrices, principle angles between the lattices of the host diamonds and the lattices of their inclusions could be determined.

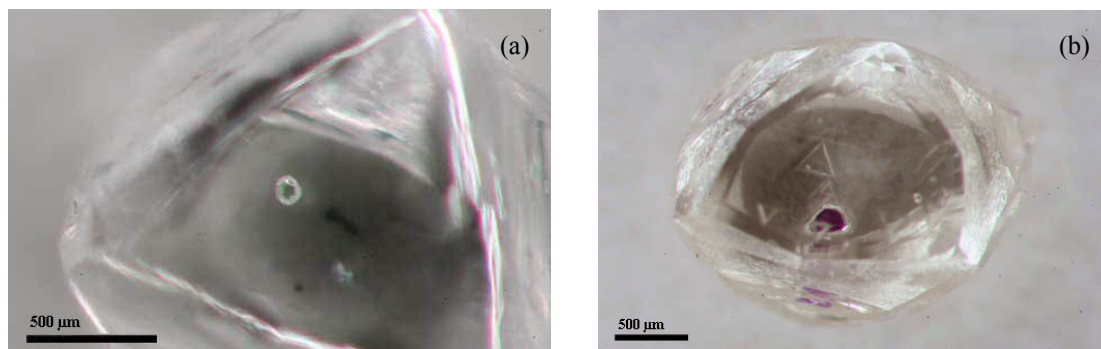
The crystallographic orientation of crystal inclusions in single crystal diamonds represent the observational evidence that principal surfaces of the common syngenetic inclusions are often closely related to the  $\{111\}$  and/or  $\{100\}$  planes of the diamond crystals (Harris et al., 1979). Sobolev et al. (1970, 1972) cited in Harris et al. (1979) reported for the inclusions with planar surfaces that the inclusions of chromite, diopside, orange and purple garnets and olivine in diamonds from Yakutia, in particular from the Mir kimberlite diatreme, possess octahedral morphologies either in the form of single octahedra or as parallel octahedral intergrowths, and in all cases, the inclusion facets are strictly parallel to the diamond octahedral faces.

According to previous works, the morphology of syngenetic crystal inclusions has been imposed by the diamond lattice and morphology (Harris, 1993). The physical relationship between diamonds and their inclusions is sometimes reflected by the crystal form of the silicate inclusions, which take over the morphology of the host diamonds rather than that of their own species (Kirkley et al., 1991). The presence of mineral inclusions, i.e., olivine and enstatite, having cubo-octahedral morphology, is a common feature, despite their origin out of the orthorhombic system (Meyer, 1987 and Taylor et al., 2003). Eppler (1961) considered the parallelism of dodecahedral faces of pyrope garnets to the octahedral plane of the diamond host.

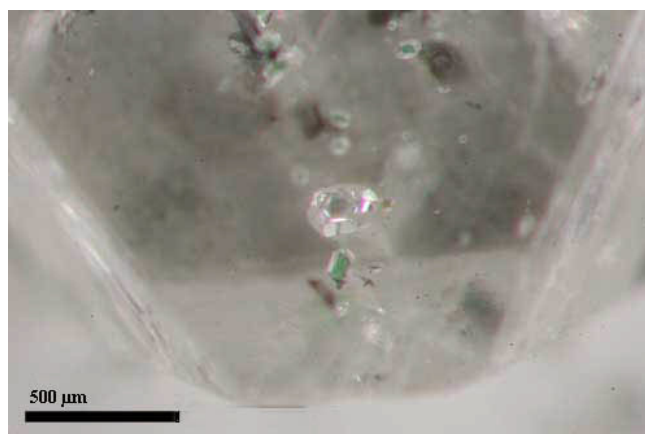
The chrome-diopside inclusion in diamond sample DHU1.2 and chrome-pyrope inclusion crystallized in diamond sample DHU2.1 from Udachanaya (Siberia/Russia) in Figure 5.1a, b respectively (observed under optical microscope), show that the diamonds obviously have controlled mineral morphologies resulting in corresponding faces between inclusion and their host. Furthermore, in sample DHP5.3 (Figure 5.2) it is shown that the olivine inclusion has an octahedral morphology. The olivine inclusion faces correspond to the enclosing octahedral diamond. The occurrence of euhedral, unaltered olivine inclusions, often with orientation and morphological influence by the host diamond suggest these inclusions were closely syngenetic with their hosts (Mitchell and Giardini, 1977).

Chrome-diopside is a typical monoclinic clinopyroxene and olivine is an orthorhombic mineral, but both species may exhibit pseudo-cubo-octahedral morphology within diamond host crystals. Moreover, a syngenetic garnet has typically octahedral morphology, whereas a protogenetic garnet inclusion should have a dodecahedral form. These relationships indicate that there are periods when a diamond and its inclusion grow simultaneously (Harris, 1993); whereas the inclusions that existed prior to their encapsulation in the diamonds typically should have either irregular morphologies or euhedral morphologies that are entirely consistent with the crystal structure and morphological symmetry and habit of the mineral. It has been suggested that the simultaneous growth of both, mineral inclusions and diamond hosts, results from the inclusions nucleated on the octahedral or cubic plane of the growing diamond crystal (Harris et al., 1979 and Meyer, 1987).





**Figure 5.1** Octahedral diamonds from Udachnaya (Siberia/Russia), showing the octahedrally shaped inclusions which are imposed by the diamonds: (a) chrome-diopside inclusion in diamond DHU1.2 and (b) chrome-pyrope inclusion in diamond sample DHU2.1.



**Figure 5.2** Octahedral shape inclusions in octahedral diamond DHP5.3 from Premier Mine, showing the octahedron face of olivine inclusion, which are imposed by the diamond host.

The occurrence of euhedral chrome-pyrope inclusions and peridotitic minerals i.e., chrome-diopside and olivine, suggests that the diamonds formed over a more extended range of pressure and temperature (Mitchell and Giardini, 1977).

## 5.1 The Structural Relationships of Inclusions in Diamonds

The crystallographic cell parameters of mineral inclusions in diamonds from Udachnaya (Siberia/Russia) and various mines in South Africa are shown in Table 5.1 to Table 5.4.

**Table 5.1** Crystallographic cell parameters of chrome-pyropes in diamonds.

Sample No.	a (Å)	v (Å <sup>3</sup> )
DHU2.1	11.567(1)	1548(1)
DHU2.2	11.634(6)	1575(4)
DHP4.2_1	11.644(3)	1579(1)
DHP4.2_2	11.466(3)	1508(1)
DHP4.3	11.556(1)	1543(1)
DHP5.1_2	11.553(1)	1542(1)
DHK6.1_1	11.583(1)	1554(1)
DHK6.1_2	11.444(2)	1499(1)
DHK6.2_1	11.520(3)	1530(1)
DHK6.2_2	11.576(6)	1532(1)
DHK6.3_1	11.494(1)	1519(1)
DHK6.3_2	11.576(2)	1551(1)
DHD8.1_1	11.667(5)	1588(2)
DHD8.1_2	11.521(6)	1529(1)
DHD8.2	11.529(1)	1532(1)
DHD8.3	11.407(2)	1484(4)
D10	11.535(2)	1535(1)
DHF10.1_1	11.528(2)	1532(1)
DHF10.1_2	11.525(2)	1531(1)
DHF10.2_1	11.325(4)	1453(1)
DHF10.2_2	11.725(5)	1612(1)
DHV12.1_3	11.409(8)	1485(3)
DHV12.2	11.559(2)	1545(1)
DHV12.3_1	11.499(2)	1520(1)
DHV12.3_2	11.518(1)	1528(1)
DHV12.3_3	11.527(7)	1530(2)
DHV12.3_4	11.585(2)	1555(1)
DHV12.3_5	11.575(1)	1551(1)
DHV12.3_6	11.558(4)	1544(3)
DHK13_1	11.391(1)	1478(4)
DHK13_4	11.691(1)	1598(5)

**Table 5.2** Crystallographic cell parameters of chromite inclusions in diamonds.

Sample No.	a (Å)	v (Å <sup>3</sup> )
DHU3.1_1	8.333(1)	579(1)
DHU3.1_2	8.321(2)	576(1)
DHP3.2	8.332(1)	578(1)

**Table 5.3** Crystallographic cell parameters of chrome-diopside inclusions in diamonds.

Sample No	a (Å)	b (Å)	c (Å)	$\beta$ (°)	v (Å <sup>3</sup> )
DHU1.1_1	9.706(3)	8.920(2)	5.243(3)	105.9(1)	437(1)
DHU1.1_2	9.677(5)	9.024(1)	5.172(3)	105.6(1)	435(1)
DHU1.2_1	9.670(1)	8.879(4)	5.229(3)	106.1(1)	432(1)
DHU1.2_2	9.660(2)	8.879(7)	5.256(4)	106.2(1)	433(1)
DHP5.1_1	9.681(1)	8.890(1)	5.236(2)	106.2(3)	433(1)
DHP5.2_1	9.720(1)	8.917(9)	5.253(6)	106.2(2)	437(1)
DHP5.2_2	9.630(1)	8.890(1)	5.250(1)	105.3(2)	435(1)
DHP5.2_3	9.670(2)	8.930(2)	5.210(1)	106.0(2)	433(1)
DHP5.2_4	9.530(3)	8.850(2)	5.280(2)	106.5(4)	428(2)
DHP5.3_1	9.638(6)	8.838(3)	5.243(3)	106.8(1)	428(1)
DHP5.3_2	9.650(8)	8.843(6)	5.245(5)	106.7(1)	429(1)
DHP5.3_3	9.610(8)	8.839(5)	5.268(5)	106.4(1)	429(1)
DHP5.3_5	9.610(8)	8.839(5)	5.268(5)	106.4(1)	429(1)
DHK7_1	9.570(2)	8.828(9)	5.180(1)	103.8(2)	425(1)
DHK7_2	9.670(1)	8.914(8)	5.235(5)	107.4(1)	431(1)
DHK7_3	9.660(2)	8.750(1)	5.230(2)	107.6(3)	421(2)
DHK7_4	9.480(3)	8.800(2)	5.250(3)	104.2(4)	425(2)
DHK7_5	9.240(6)	8.670(2)	5.300(2)	105.9(6)	408(3)
DHK7_6	9.660(3)	8.800(10)	5.250(2)	107.7(4)	425(2)
DHF11	9.930(2)	8.940(1)	5.260(1)	107.0(3)	447(1)
DHK13_1	9.560(4)	9.000(3)	5.280(4)	105.1(7)	439(2)
DHK13_2	9.300(3)	9.150(3)	5.390(6)	101.0(2)	450(2)
DHK14_1	9.642(3)	8.827(4)	5.245(2)	106.4(4)	428(1)
DHK14_2	9.659(9)	8.842(9)	5.236(6)	106.6(1)	429(1)
DHK14_3	9.550(2)	8.805(8)	5.282(9)	105.4(2)	428(1)
DHK14_4	9.810(2)	8.830(4)	5.300(1)	106.9(2)	439(1)
DHK14_5	9.480(2)	8.850(3)	5.184(7)	105.6(2)	419(1)
DHK14_6	9.530(3)	8.720(2)	5.164(9)	105.8(2)	413(1)
DHK14_7	9.547(9)	8.846(7)	5.217(8)	104.7(1)	426(1)
DHK14_8	9.840(5)	8.730(8)	5.249(8)	105.3(3)	435(2)
DHK14_9	9.510(2)	8.780(2)	5.222(9)	107.0(3)	417(2)

**Table 5.4** Crystallographic cell parameters of olivine inclusions in diamonds.

Sample No.	a (Å)	b (Å)	c (Å)	v (Å <sup>3</sup> )
DHU3.1_3	4.811(3)	10.175(9)	5.907(3)	289(1)
DHP5.3_4	4.742(3)	10.429(9)	5.990(5)	296(1)
DHP5.3_6	4.724(3)	10.266(9)	5.852(8)	284(1)
DHD8.1_3	4.787(2)	10.252(9)	5.888(8)	289(1)
DHV12.1_1	4.769(1)	10.224(2)	5.995(2)	292(1)
DHV12.1_2	4.770(2)	10.247(3)	5.987(2)	293(1)
DHV12.1_4	4.777(3)	10.216(8)	6.004(4)	293(1)

Due to their chemical compositions, natural garnets are commonly divided into two groups with ideal formulae  $(\text{Mg,Fe}^{2+},\text{Mn,Ca})_3(\text{Al,Fe}^{3+},\text{Cr})_2(\text{Si,Al})_3\text{O}_{12}$  (Deer et al., 1992). The cell parameters and unit of cell volumes as shown above in Table

5.1 are typical for the garnets with general composition  $(\text{Fe,Mg,Ca})_3\text{Al}_2(\text{SiO}_4)_3$ . The mol% end-member pyrope are 78.5 – 85.0 (see Appendix 3).

The chromite minerals belong to the spinel group, subdivided into chromite series according to the  $\text{Cr}^{3+}$  (Deer et al., 1992). The crystallographic cell parameters and volumes in Table 5.2 are typical for chromite, comparable to the unit cell database of chromite compiled by Smyth and Bish (1988).

The pyroxene group include both orthopyroxenes (chemical series of  $(\text{Mg,Fe})\text{SiO}_3$  and clinopyroxenes which have a wide range of chemical composition, as members of the four-component system  $\text{CaMgSi}_2\text{O}_6 - \text{CaFeSi}_2\text{O}_6 - \text{Mg}_2\text{Si}_2\text{O}_6 - \text{Fe}_2\text{Si}_2\text{O}_6$ . The cell parameters and unit of cell volumes as show above in Table 5.3 are comparable to data of the unit cell database of diopside compiled by Smyth and Bish (1988). The atomic percentages (see Appendix 5) are comparable to diopside compiled by Deer et al. (1992).

The olivine minerals have a general formula  $\text{M}_2\text{SiO}_4$ , which have compositions in range  $\text{Mg}_2\text{SiO}_4$  (forsterite:  $\text{Fo}_{100-90}$ ) to  $\text{Fe}_2\text{SiO}_4$  (fayalite:  $\text{Fo}_{10-0}$ ). The cell parameters and volumes of cells as show above in Table 5.4 are typical for olivine high in forsterite content compiled by Smyth and Bish (1988), corresponding to the chemical compositions, which show high atomic percentages of Mg between 91.4 and 94.2 (see Appendix 6) compiled by Deer et al. (1992).

The data sets of diamond hosts and their crystal inclusions have been combined by matrix calculation, and thus the mutual orientation of the crystallographic directions of both substances could be determined. Thus, the crystallographic orientation of diamond hosts and mineral inclusions encapsulated inside may now be characterized by comparisons of appropriate vector calculations according to the three dimensional unit cell orientations.

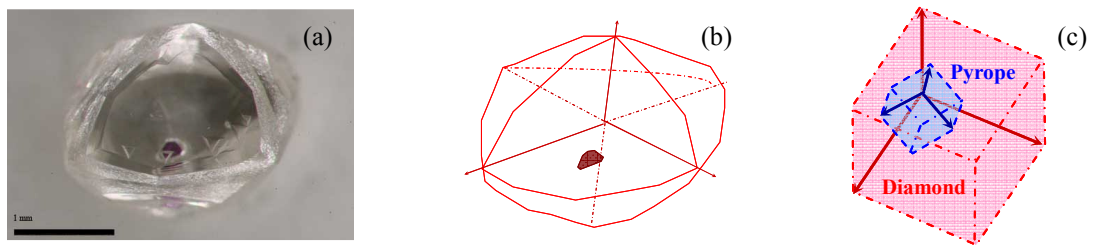
Typical angles between diamond vectors and inclusion vectors can be calculated by

$$\alpha^\circ = \arccos \left( \frac{\vec{d} \cdot \vec{i}}{|\vec{d}| \cdot |\vec{i}|} \right) \cdot 180/\pi$$

where  $\vec{d}$  and  $\vec{i}$  are vectors of diamond and inclusion, respectively.

Angle calculations between [111] direction of diamonds and inclusions is shown in Appendix 1.

In Figure 5.3, an orientation matrix of the inclusion crystal was found and a unit cell parameter for a typical garnet crystal was calculated. The lattice parameters of the garnet calculated from the diffraction pattern are  $a = 11.567(1) \text{ \AA}$ ,  $\alpha = 90.0(1)$  and  $V = 1548(1) \text{ \AA}^3$ . The crystallographic orientation of the diamond host crystal lattice and the chrome-pyrope inclusion shows a principal deviation of the pyrope lattice to the diamond lattice of approximately  $25^\circ$  between the a axis,  $12^\circ$  between the b axis and  $23^\circ$  between the c axis, respectively. The correlation angle between [111] directions of diamond and [111] direction of chrome-pyrope inclusion in DHU2.1 is approximately  $25.28^\circ$ .



**Figure 5.3** (a) Diamond sample DHU2.1 with chrome-pyrope inclusion (view along [111] perpendicular through the octahedral face), (b) the directions of diamond crystallographic axes, (c) the directions of the two sets of axes show the orientation of diamond lattice and chrome-pyrope inclusion.

The unit cell dimension between diamond hosts and their inclusions were indexed. To determine and quantify the degree of orientation or miss-orientation of mineral inclusions in diamonds it has been decided to correlate the [111] direction of diamonds with the [111], [010] and [100] directions of mineral inclusions belonging to the cubic, monoclinic and orthorhombic crystal systems, respectively. The degree of relative orientation of mineral inclusions in the corresponding diamond lattices are shown in Table 5.5 and Figure 5.4.

The angle correlations and principal lattice direction deviations between diamonds and chrome-pyrope, chromite, chrome-diopside and olivine inclusions from various mines in this study are shown in Figure 5.5 to Figure 5.8, respectively.

The plots in Figure 5.5 show the angle correlation between diamonds and their inclusions from various mines in this study. The different symbols and colour exhibit each mineral inclusion captured in diamonds.

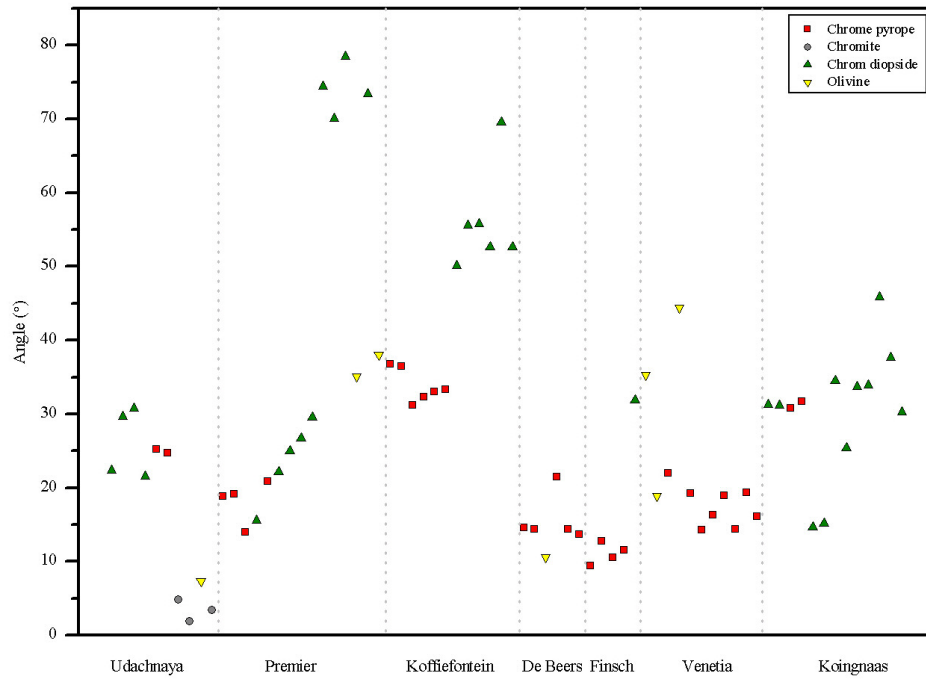
In Figure 5.5 to Figure 5.8 show the angle correlation and standard deviation between diamonds from various mines and chrome-pyrope, chromite, chrome-diopside and olivine inclusions, respectively. The different colour of symbol exhibit that inclusions captured in different diamond samples.

**Table 5.5** The angle and deviation between the [111] direction of diamonds and their inclusions.

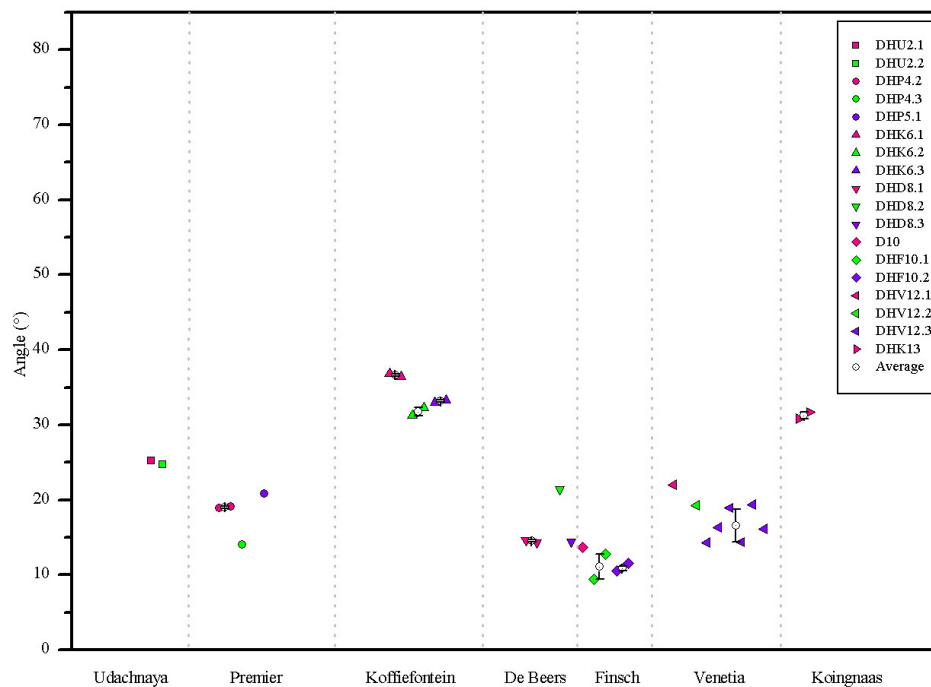
Samples	Chrome-Pyrope [111]		Chromite [111]		Chrome-Diopside [010]		Olivine [100]	
	Angle (°)	Deviation	Angle (°)	Deviation	Angle (°)	Deviation	Angle (°)	Deviation
DHU1.1_1 DHU1.1_2					22.35 29.69	3.67		
DHU1.2_1 DHU1.2_2					30.78 21.54	4.62		
DHU2.1	25.28							
DHU2.2	24.68							
DHU3.1_1 DHU3.1_2 DHU3.1_3			4.86 1.88	1.49			7.38	
DHU3.2			3.38					
DHP4.2_1 DHP4.2_2	18.90 19.12	0.11						
DHP4.3	14.01							
DHP5.1_1 DHP5.1_2					15.59			
DHP5.2_1 DHP5.2_2 DHP5.2_3 DHP5.2_4					22.12 25.00 26.74 29.49	3.09		
DHP5.3_1 DHP5.3_2 DHP5.3_3 DHP5.3_4 DHP5.3_5 DHP5.3_6					74.44 70.06 78.48 73.35	3.47	35.12 38.06	1.47

Table 5.5 (continued)

Samples	Chrome-Pyrope [111]		Chromite [111]		Chrome-Diopside [010]		Olivine [100]	
	Angle (°)	Deviation	Angle (°)	Deviation	Angle (°)	Deviation	Angle (°)	Deviation
DHK6.1_1 DHK6.1_2	36.81 36.44	0.18						
DHK6.2_1 DHK6.2_2	31.23 32.30	0.54						
DHK6.3_1 DHK6.3_2	32.99 33.33	0.17						
DHK7_1 DHK7_2 DHK7_3 DHK7_4 DHK7_5 DHK7_6					50.12 55.58 55.77 52.66 69.53 52.65	6.93		
DHD8.1_1 DHD8.1_2 DHD8.1_3	14.65 14.38	0.14					10.57	
DHD8.2	21.46							
DHD8.3	14.41							
D10	13.65							
DHF10.1_1 DHF10.1_2	9.43 12.74	1.66						
DHF10.2_1 DHF10.2_2	10.59 11.61	0.28						
DHF11					31.86			
DHV12.1_1 DHV12.1_2 DHV12.1_3 DHV12.1_4							35.36 18.94 44.41	12.91
DHV12.2	19.28							
DHV12.3_1 DHV12.3_2 DHV12.3_3 DHV12.3_4 DHV12.3_5 DHV12.3_6	14.34 16.36 18.91 14.36 19.38 16.16	2.16						
DHK13_1 DHK13_2 DHK13_3 DHK13_4					31.29 31.11	0.09		
	30.82 31.69	0.43						
DHK14_1 DHK14_2 DHK14_3 DHK14_4 DHK14_5 DHK14_6 DHK14_7 DHK14_8 DHK14_9					14.61 15.13 34.49 25.35 33.65 33.94 45.80 37.64 30.28	10.23		



**Figure 5.4** Plot of angle correlations between [111] directions of diamond and [111] of chrome-pyrope, chromite [111], chrome-diopside [010] and olivine [100] inclusions from various mines in this study.

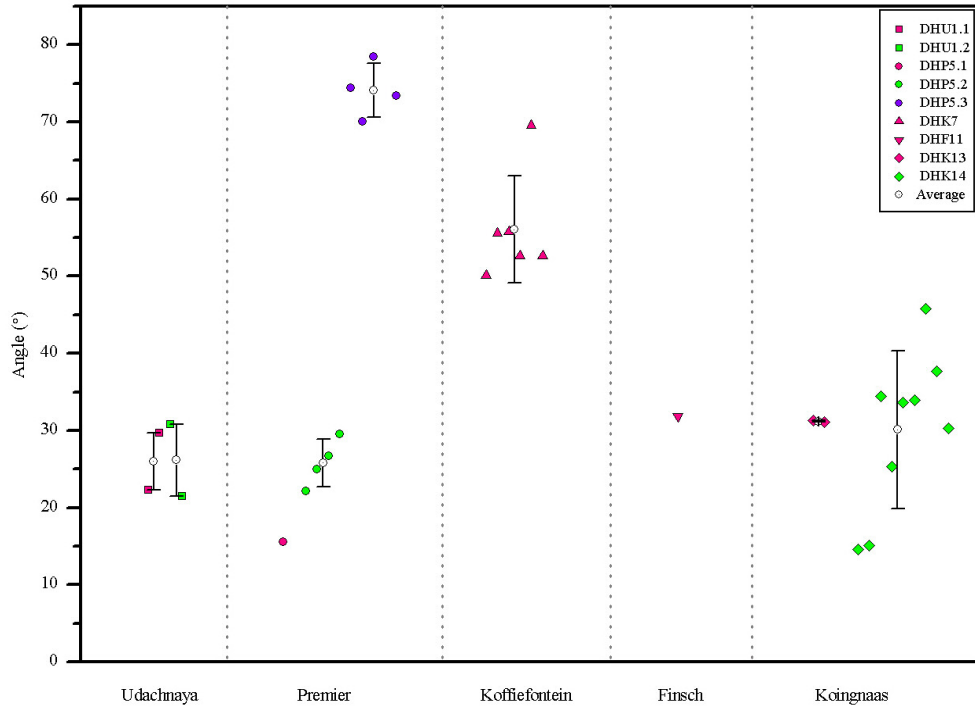


**Figure 5.5** Plot of angle correlation between [111] directions of diamond and chrome-pyrope inclusions [111] from various mines.

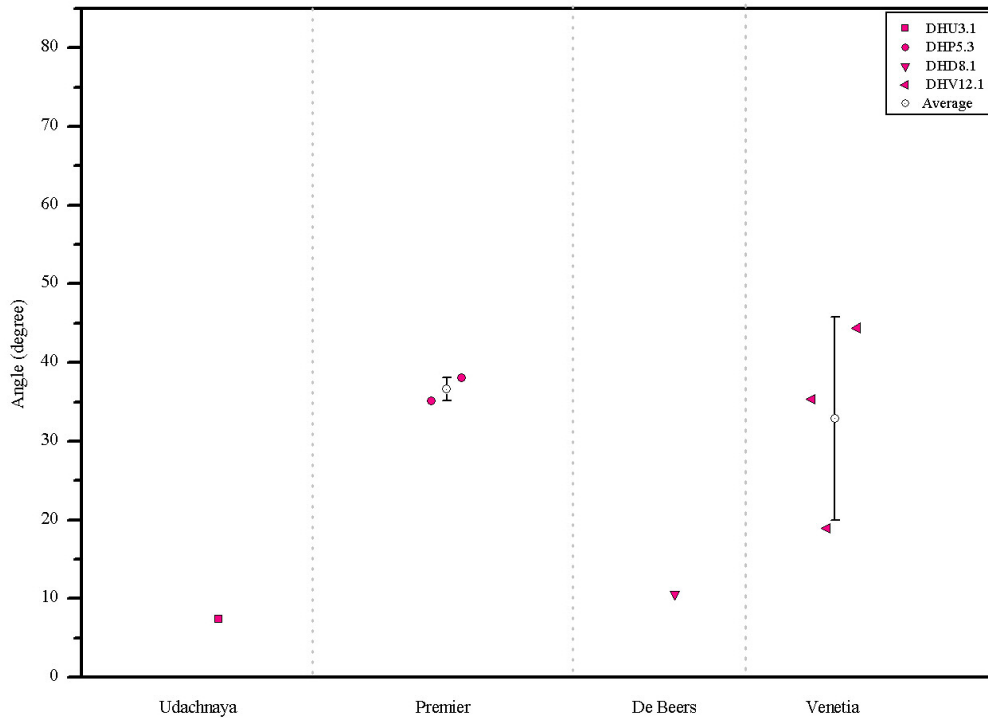




**Figure 5.6** Plot of angle correlation between [111] directions of diamond and chromite inclusions [111] from Udachnaya (Siberia/Russia).



**Figure 5.7** Plot of angle correlation between [111] directions of diamond and chrome-diopside inclusions [010] from various mines.



**Figure 5.8** Plot of angle correlation between [111] directions of diamond and olivine inclusions [100] from various mines.

The chrome-pyrope or chromite inclusions, being captured in the same diamond hosts, showed the angle correlation between diamond [111] and chrome-pyrope [111] or chromite [111] with small misalignments up to  $2.2^\circ$  and  $3.4^\circ$  between the chrome-pyrope (Figure 5.5) and chromite inclusions (Figure 5.6), respectively.

Additionally, the chrome-pyrope and chromite inclusions, which crystallized as inclusions in each diamond localities, showed also relatively similar angle correlations with only small degrees in difference.

The chrome-diopside and olivine inclusions showed the degrees of misorientation between diamond [111] and chrome-diopside [010], olivine [100] up to  $10.2^\circ$  and  $12.9^\circ$  for chrome-diopside (Figure 5.7) and olivine (Figure 5.8), respectively.

## 5.2 The Twin Law Approach to Mineral Inclusions in Diamonds

Twinning is a crystallographically controlled intergrowth, which may be interpreted as a deviation from perfection. Two or more crystals may form a symmetrical intergrowth under certain conditions of growth. The lattice directions of one crystal in a twin develop a definite crystallographic relation to the lattice directions of the other crystal (Klein and Hurlbut, 1993).

Based on certain twin laws (symmetrically formulated rules of congruently transformable patterns), the twinning matrices were deduced from the diamonds and their inclusions component orientation matrices. According to the twinning matrices, the rotation angles and rotation vectors of diamond hosts and their inclusions were indicated (see Appendix 2). The degree of rotation angles and deviation of diamonds and their inclusions in this study are shown in Table 5.6 and Figure 5.9.

**Table 5.6** The rotation angle for twinning of lattices and the deviation angles between diamonds and their inclusions.

Samples	Chrome-Pyrope		Chromite		Chrome-Diopside		Olivine	
	Angle (°)	Deviation	Angle (°)	Deviation	Angle (°)	Deviation	Angle (°)	Deviation
DHU1.1_1					54.72			
DHU1.1_2					72.40	8.83		
DHU1.2_1					43.50			
DHU1.2_2					40.32	1.59		
DHU2.1	25.71							
DHU2.2	40.73							
DHU3.1_1			10.73					
DHU3.1_2			11.46	0.36				
DHU3.1_3							56.96	
DHU3.2			8.35					
DHP4.2_1	62.90							
DHP4.2_2	62.57	1.69						
DHP4.3	38.93							
DHP5.1_1					50.47			
DHP5.1_2	51.04							

Table 5.6 (continued)

Samples	Chrome-Pyrope		Chromite		Chrome-Diopside		Olivine	
	Angle (°)	Deviation	Angle (°)	Deviation	Angle (°)	Deviation	Angle (°)	Deviation
DHP5.2_1 DHP5.2_2 DHP5.2_3 DHP5.2_4					36.50 55.56 44.88 44.23	7.83		
DHP5.3_1 DHP5.3_2 DHP5.3_3 DHP5.3_4 DHP5.3_5 DHP5.3_6					51.31 55.59 46.76 52.51	3.66	23.30 36.02	6.36
DHK6.1_1 DHK6.1_2	53.37 53.36	0.00						
DHK6.2_1 DHK6.2_2	31.85 29.26	1.30						
DHK6.3_1 DHK6.3_2	39.17 39.06	0.05						
DHK7_1 DHK7_2 DHK7_3 DHK7_4 DHK7_5 DHK7_6					60.69 51.78 58.56 60.20 58.33 57.37	3.20		
DHD8.1_1 DHD8.1_2 DHD8.1_3	38.24 38.13	0.05					48.91	
DHD8.2	36.17							
DHD8.3	45.84							
D10	45.95							
DHF10.1_1 DHF10.1_2	53.37 58.64	2.64						
DHF10.2_1 DHF10.2_2	39.43 39.73	0.15						
DHF11					40.23			
DHV12.1_1 DHV12.1_2 DHV12.1_3 DHV12.1_4	60.25						40.98 47.48 43.03	3.32
DHV12.2	38.99							
DHV12.3_1 DHV12.3_2 DHV12.3_3 DHV12.3_4 DHV12.3_5 DHV12.3_6	67.31 68.95 36.55 66.84 59.83 40.60	14.43						
DHK13_1 DHK13_2 DHK13_3 DHK13_4	41.92 43.63	0.85			61.47 30.73	15.36		

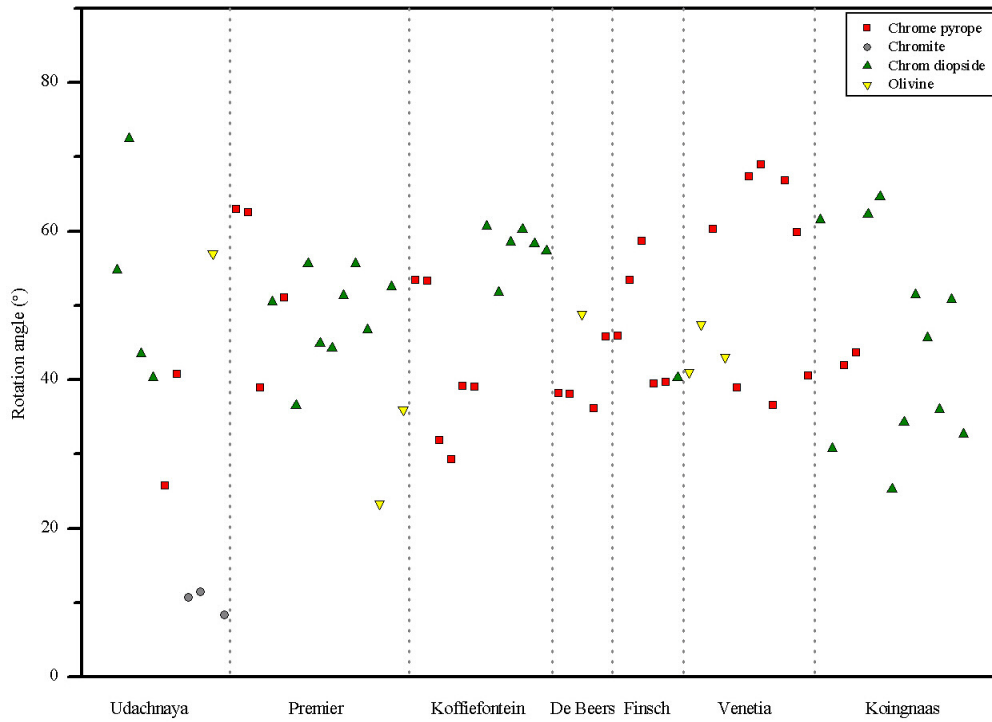
**Table 5.6** (continued)

Samples	Chrome-Pyrope		Chromite		Chrome-Diopside		Olivine	
	Angle (°)	Deviation	Angle (°)	Deviation	Angle (°)	Deviation	Angle (°)	Deviation
DHK14_1					62.24	13.66		
DHK14_2					64.61			
DHK14_3					25.32			
DHK14_4					34.31			
DHK14_5					51.43			
DHK14_6					45.62			
DHK14_7					35.96			
DHK14_8					50.80			
DHK14_9					32.65			

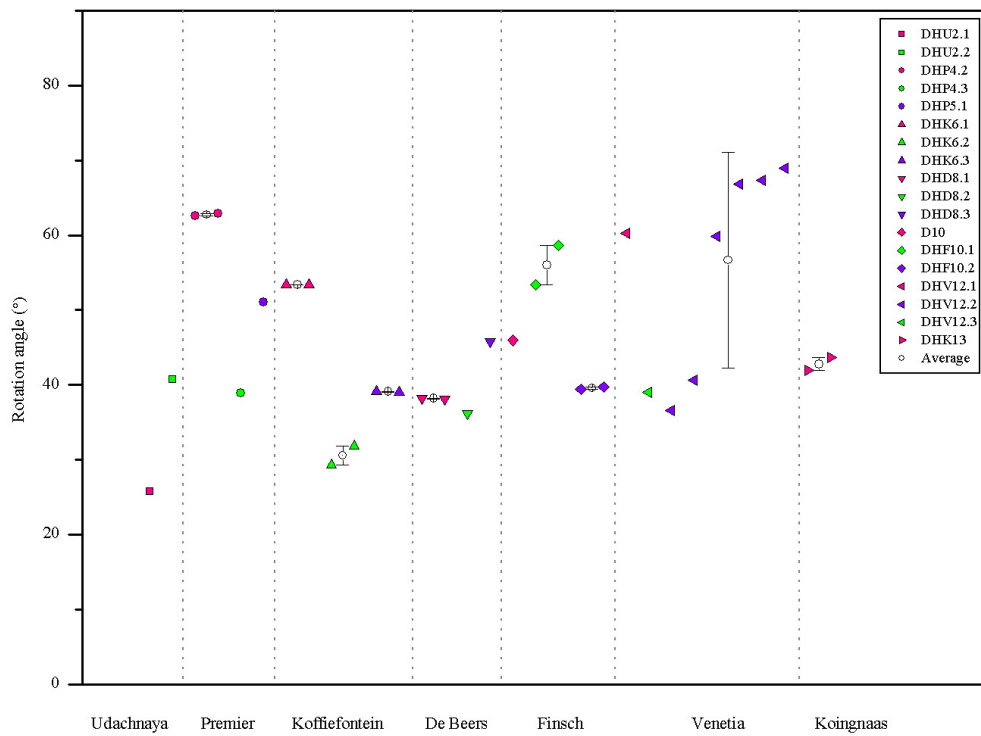
The twinning rotation angles and the corresponding deviation angles of diamonds and chrome-pyrope, chromite, chrome-diopside and olivine inclusions from various mines in this study are shown in Figure 5.10 to Figure 5.13, respectively.

Figure 5.9 show the rotation angle for diamonds and their inclusions from various mines in this study. The different symbols and colour exhibit each mineral inclusion captured in diamonds.

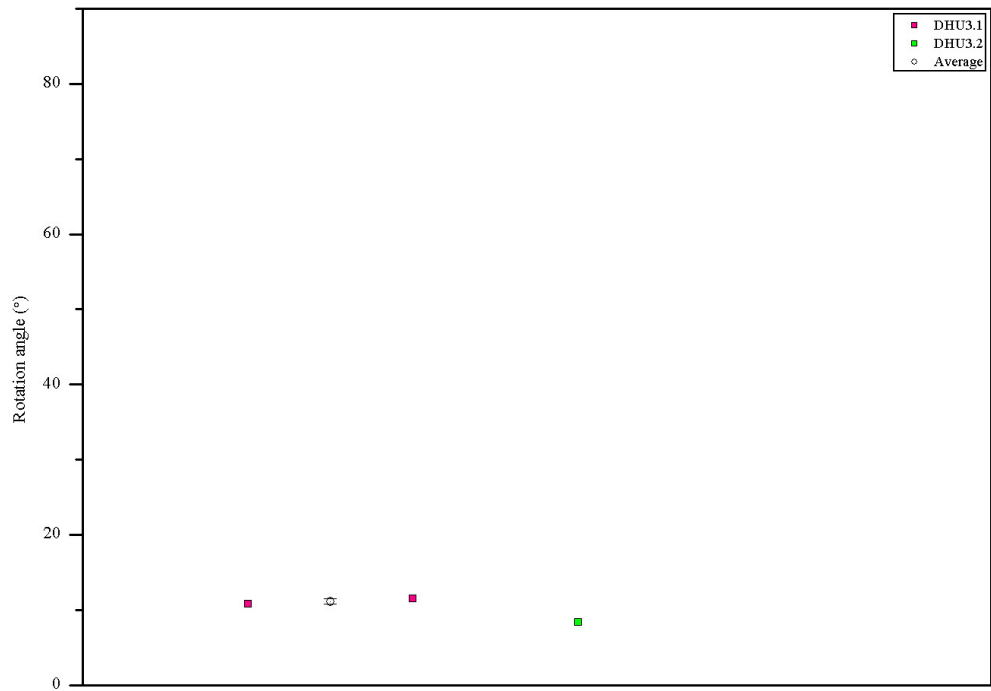
Figure 5.5 to Figure 5.8 show the rotation angle and standard deviation between diamonds from various mines and chrome-pyrope, chromite, chrome-diopside and olivine inclusions, respectively. The different colours of symbols exhibit inclusions captured in different diamond samples.



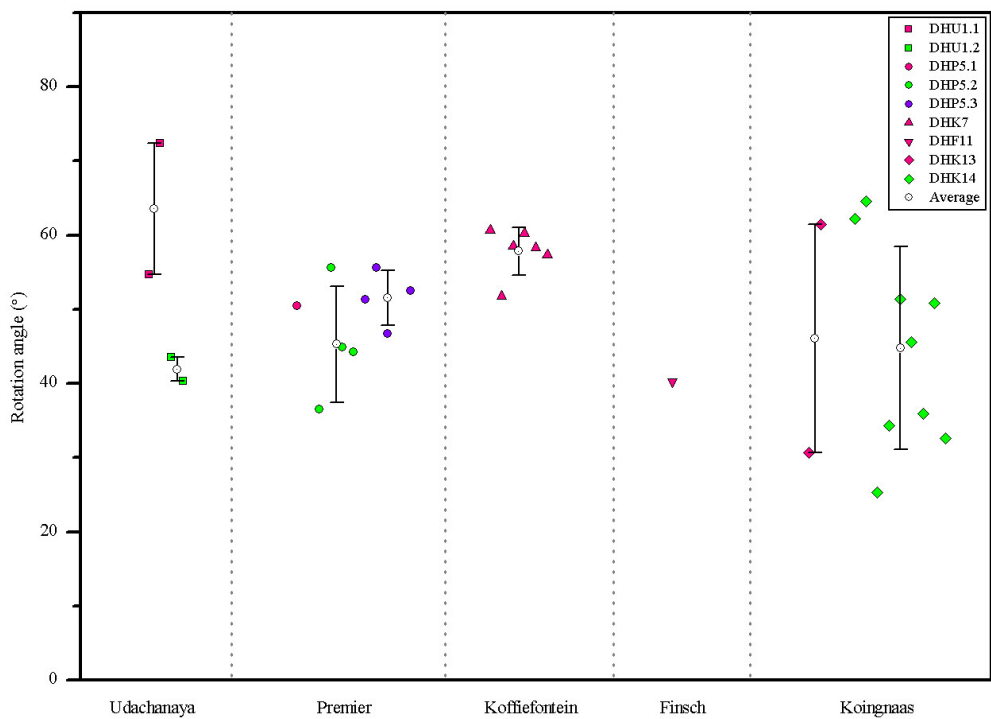
**Figure 5.9** Plot of rotation angles for inclusions and diamonds from Udachnaya (Siberia/Russia) and various mines in South Africa.



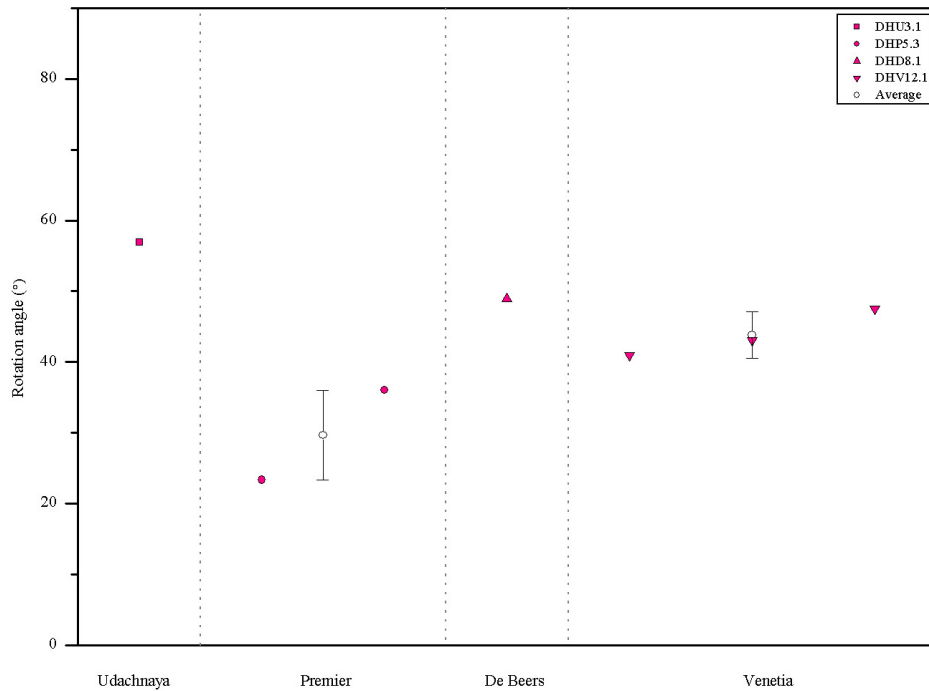
**Figure 5.10** Plot of twinning rotation angles for chrome-pyrope inclusions in diamonds from various mines.



**Figure 5.11** Plot of twinning rotation angles for chromite inclusions in diamonds from Udachanaya (Siberia/Russia).



**Figure 5.12** Plot of twinning rotation angles for chrome-diopside inclusions in diamonds from various mines.



**Figure 5.13** Plot of twinning rotation angles for olivine inclusions in diamonds from various mines.

Most of the diamonds which contain more than one crystal of chrome-pyropite inclusions showed the twinning rotation angles with small misalignments (Figure 5.10), excluding the six crystals of chrome-pyropite inclusions in diamond DHV12.3 which showed the deviation from the average value of twinning rotation angle up to  $14.43^\circ$ .

The chromite inclusions captured in diamonds showed the deviation from the average value of rotation angles with small misalignments up to  $0.36^\circ$  (Figure 5.11).

The chrome-diopside and olivine inclusions in diamonds showed the deviation from the average value of degree of twinning rotation up to  $15.36^\circ$  and  $6.36^\circ$  for chrome-diopside (Figure 5.12) and olivine (Figure 5.13), respectively.

As mentioned above, the degree of angle correlation between [111] directions of diamond and [111] direction of chrome-pyropite and chromite inclusions in the same diamond samples also show the small misalignments as the twinning rotation angles of diamonds and chrome-pyropite or chromite inclusions; the chrome-diopside and olivine inclusions show a larger spread in deviation.



## 6. MINERAL CHEMISTRY OF INCLUSIONS IN DIAMONDS

The geo- and crystal chemistry of the mineral inclusions in diamonds is an important source of information on the composition of the Earth's mantle at depths exceeding 120 – 150 km. The diamond formation in peridotitic (or ultramafic) and/or eclogitic environments may be preserved and demonstrated by mineral inclusions in diamonds (Sobolev et al., 2008).

Mineral inclusions in natural diamonds are usually monomineralic, however, bimineralic and polymineralic inclusions consisting of the different phases, i.e. chrome-pyrope + enstatite inclusions in diamond in this study, peridotitic garnet + orthopyroxene + chromite inclusion in diamond from De Beers Pool (Phillips et al., 2004) do occur. These multiphase mineral inclusions are particularly important not only in discriminating peridotitic or eclogitic origin, but also because analyses of the chemical composition of two or more coexisting minerals allow estimating the pressure and temperature environments in which the inclusions and the host diamond had formed (Boyd et al., 1980 and Kirkley et al., 1991).

In this study, 12 diamond samples were selected for study of the mineral inclusion content. Diamonds were polished parallel to {110} face in the easy directions of abrasion (Wilks and Wilks, 1991) and only one diamond sample (DHK7) was polished in the hard direction of abrasion {111} face (Wilks and Wilks, 1991), due to the position of inclusion. Mineral inclusions i.e. chrome-pyrope, chrome-pyrope + enstatite, chrome-diopside, chromite and olivine have been exposed thus to have a direct contact with the inclusion for material analyses. After surface polishing, 9 crystal inclusions are exposed from 9 diamond samples (Table 6.1). Two diamonds were broken and one crystal inclusion was lost during polishing. It has to be mentioned here, that diamond polishing is not at all a straight forward operation in this research project: Diamond cutting and polishing has to be performed with a profound knowledge on the orientation of the individual guest crystal, it has to be performed on special diamond polishing tools and it is very time consuming; we are especially grateful to MEDIDIA company, Idar-Oberstein, which supplied the institute with a very properly working diamond polishing device.

**Table 6.1** Mineral inclusions exposed from diamond samples.

<b>Inclusion species</b>	<b>No. of diamonds</b>
Chrome-diopside	3
Chromite	1
Olivine	2
Chrome-pyrope	1
Chrome-pyrope + enstatite	2

Considering the silicate and oxide mineral inclusions, the diamonds and their inclusions in this study are classified as the peridotitic paragenesis (P-type), containing chrome-pyrope, diopside, enstatite, chromite or olivine (Meyer, 1968; Meyer and Boyd, 1972, Meyer and Tsai 1976; Harris et al., 1979 and Harte et al., 1980).

The major and trace element contents of the mineral inclusions in the diamonds investigated were analyzed using both, Electron Probe Micro-Analysis (EPMA), and Laser Ablation Inductively Coupled Plasma Mass Spectrometry (LA-ICP-MS) methods.

### **6.1 Electron Probe Micro-Analysis (EPMA)**

Electron Probe Micro-Analysis (EPMA) is a non-destructive technique using a high-energy focused beam of electrons to generate X-rays, characteristic for the elements within a sample. Measurements can be carried out qualitatively and quantitatively with the proper standard materials. It can provide quantitative analyses of elements ranging from beryllium (in some cases) to uranium at levels as low as 100 ppm (Abduriyim et al., 2006).

Major element compositions of the mineral inclusions were analysed by electron microprobe, which is generally made on the polished surfaces of the exposed inclusions and preserve the crystals for further study. The diamond samples were embedded in an epoxy resin and were coated with carbon. The exposed inclusions were determined using JEOL JXA 8900 equipped with the EDXRF system, using 15 kV gun potential and 12 nA beam current. The concentration of eleven elements (i.e. Na, Si, K, Ti, Fe, Al, Mg, Ca, Cr, Mn and Ni) were determined on silicate with a Ni and Cr

program. The chemical composition of each sample was then corrected by ZAF correction program. At least four analytical points were investigated separately in each inclusion to check their homogeneity.

## **6.2 Laser Ablation Inductively Coupled Plasma Mass Spectrometry (LA-ICP-MS)**

Laser Ablation Inductively Coupled Plasma Mass Spectrometry (LA-ICP-MS) is a rapid quantitative method of analysis for trace elements with high accuracy and low detection limits. In principle this technique causes relatively little damage to the samples, because it usually only leaves ablation pits of around 25 – 55  $\mu\text{m}$  across.

Minor and trace elements of silicate and oxide mineral inclusions, i.e., chrome-pyrope, chrome-diopside, chromite, olivine and enstatite were determined by LA-ICP-MS. Analyses were achieved with a New Wave Research UP-213 Nd:YAG laser with a 10 Hz frequency and an ablation energy of 3 J/cm<sup>2</sup>. The ablated material was carried through to an Agilent 7500s ICP-MS with Helium. The variation of the beam diameter of around 25 to 55  $\mu\text{m}$  was used depending on the sizes of the inclusions. Background was measured for 30 s followed by 150 s of mineral ablation product measurement. Data reduction was carried out using the Glitter 4.4.2 software (Macquarie University, Sydney).

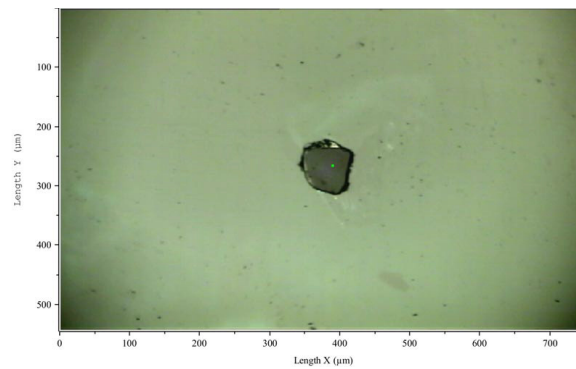
The silicate glass reference material NIST SRM 612 was used as external standard for analysis, which was measured for 60 s with a 100  $\mu\text{m}$  beam diameter. The concentrations of elements were calculated via an internal standard element. <sup>43</sup>Ca with CaO concentrations determined by electron microprobe, was used as internal standard for chrome-pyrope and chrome-diopside analyses. <sup>29</sup>Si was used as internal standard for olivine and enstatite and <sup>27</sup>Al was used as internal standard for chromite analyses. At least two analytical points were measured in each inclusion to check their homogeneity. The detection limits were 0.1- 17 ppm for different elements.

The major and trace element compositions of nine mineral inclusions (i.e., chrome-pyrope, enstatite, chromite, chrome-diopside and olivine) in diamonds

from various mines presented in this study are given as oxide-wt% and ppm for the major and trace elements, respectively, as presented in Table 6.2 to Table 6.7.

### *Chrome-pyrope ( $Mg_3Al_2[SiO_4]_3$ )*

Three chrome-pyrope inclusions are exposed within three different diamond samples DHK6.2, DHF10.2 and DHV12.3 from Koffiefontein, Finsch and Venetia mines, respectively. One diamond (DHV12.3) contains only a chrome-pyrope inclusion (Figure 6.1), whereas two samples (DHK6.2 and DHF10.2) enclose intergrowths (touching inclusions) of chrome-pyrope + enstatite inclusions (Figure 6.5).



**Figure 6.1** Chrome-pyrope inclusion in diamond DHV12.3.

The chrome-pyrope inclusion in DHV12.3 contains 3.6-3.8 wt.%  $Cr_2O_3$ , 3.6-3.7 wt.% CaO, 5.8-6.0 wt.% FeO and 22.6-22.8 wt.% MgO (Table 6.2). The composition is also comparable to a peridotitic garnet from the “Venetia database” compiled by Stachel et al. (2004).

**Table 6.2** Chemical analyses of chrome-pyrope inclusions in diamond DHV12.3.

	1	2	3	4	5
<b>SiO<sub>2</sub></b>	42.24	42.87	42.41	42.56	42.69
<b>TiO<sub>2</sub></b>	0.26	0.20	0.23	0.21	0.25
<b>Al<sub>2</sub>O<sub>3</sub></b>	20.77	21.03	21.13	20.80	20.71
<b>Cr<sub>2</sub>O<sub>3</sub></b>	3.83	3.76	3.77	3.74	3.66
<b>FeO</b>	5.89	5.93	5.92	5.82	6.07
<b>MgO</b>	22.61	23.03	22.82	22.68	22.86
<b>CaO</b>	3.72	3.65	3.65	3.63	3.74
<b>MnO</b>	0.24	0.31	0.26	0.26	0.26
<b>NiO</b>	b.d.	b.d.	0.04	0.02	b.d.
<b>Na<sub>2</sub>O</b>	0.04	0.01	0.05	0.05	0.07
<b>K<sub>2</sub>O</b>	0.02	0.01	0.01	0.02	0.01
<b>Total</b>	99.62	100.80	100.29	99.79	100.32
<i>Trace elements (ppm)</i>					
<b>Sc</b>			98.0		98.3
<b>Ti</b>			1799		1781
<b>V</b>			223		222
<b>Cr</b>			25950		25784
<b>Mn</b>			2016		1993
<b>Co</b>			43.9		42.4
<b>Ni</b>			79.8		79.8
<b>Sr</b>			0.374		0.428
<b>Y</b>			6.48		6.31
<b>Zr</b>			35.2		37.2
<b>Nb</b>			<0.120		<0.137
<b>La</b>			<0.111		<0.120
<b>Ce</b>			0.165		0.187
<b>Nd</b>			1.06		1.04
<b>Sm</b>			0.97		0.99
<b>Eu</b>			0.294		0.38
<b>Gd</b>			1.21		<0.66
<b>Tb</b>			0.181		0.104
<b>Dy</b>			1.22		1.40
<b>Er</b>			0.70		0.70
<b>Yb</b>			1.06		1.14
<b>Lu</b>			0.152		0.152
<b>Hf</b>			1.22		1.05
<b>Ta</b>			<0.098		<0.097
<b>Th</b>			<0.098		<0.096
<b>U</b>			<0.085		<0.087

\* b.d. = value below the detection limit.

Coexisting mineral pairs of chrome-pyrope + enstatite inclusions occur in two diamond samples, DHK6.2 and DHF10.2. The chrome-pyrope inclusions have 6.6-7.5 wt.% Cr<sub>2</sub>O<sub>3</sub>, 1.3-2.3 wt.% CaO, 5.3-5.8 wt.% FeO and 23.7-24.8 wt.% MgO (Table 6.3). These compositions fall within the representative analyses of chrome-pyrope inclusion in typically peridotitic suites, as compiled by Meyer (1987).

**Table 6.3** Chemical analyses of chrome-pyrope inclusions from the Cr-Prp + En pairs in diamonds DHK6.2 and DHF10.2.

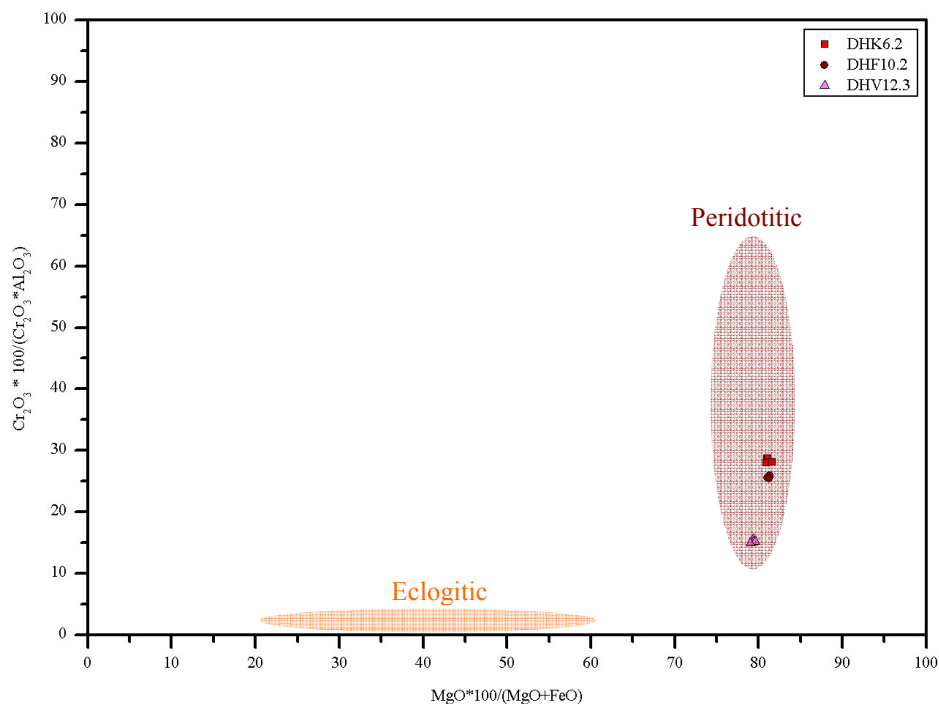
	DHK6.2				DHF10.2			
	1	2	3	4	1	2	3	4
SiO <sub>2</sub>	42.33	42.30	42.30	42.17	42.53	42.46	42.80	42.81
TiO <sub>2</sub>	0.09	0.09	0.12	0.07	0.02	0.02	0	0
Al <sub>2</sub> O <sub>3</sub>	18.58	18.60	18.74	18.70	19.37	19.28	19.30	19.38
Cr <sub>2</sub> O <sub>3</sub>	7.49	7.51	7.31	7.32	6.68	6.75	6.63	6.63
FeO	5.58	5.59	5.59	5.37	5.60	5.61	5.80	5.68
MgO	23.78	24.04	23.78	23.85	24.38	24.36	24.84	24.62
CaO	2.28	2.20	2.34	2.33	1.40	1.44	1.36	1.40
MnO	0.21	0.26	0.21	0.24	0.30	0.34	0.26	0.27
NiO	0.01	b.d.	0.01	0.03	0.04	0.02	b.d.	b.d.
Na <sub>2</sub> O	0.04	0.04	0.03	0.02	0.02	b.d.	b.d.	b.d.
K <sub>2</sub> O	0.02	0.02	0.02	0.02	b.d.	b.d.	0.01	0.02
<b>Total</b>	100.41	100.65	100.45	100.12	100.34	100.28	101.00	100.81
<i>Trace elements (ppm)</i>								
	DHK6.2 (1)		DHK6.2 (2)		DHF10.2 (1)		DHF10.2 (2)	
Sc	119		118		121		112	
Ti	646		635		50.0		47.6	
V	457		449		316.29		284.08	
Cr	49412		48499		51141		46834	
Mn	1681		1653		2246		2063	
Co	45.6		43.6		55.07		47.54	
Ni	83.1		81.8		80.43		66.98	
Ga	n.a.		n.a.		3.67		2.87	
Rb	n.a.		n.a.		<1.41		<0.202	
Sr	2.54		6.93		3.08		2.42	
Y	1.73		1.60		<0.85		0.407	
Zr	72.0		71.1		10.55		9.66	
Nb	0.347		0.22		<0.93		0.143	
Cs	n.a.		n.a.		<0.97		<0.127	
Ba	n.a.		n.a.		<6.78		<1.10	
La	0.203		0.199		<0.92		<0.111	
Ce	3.20		3.16		<0.80		0.92	
Nd	8.28		8.50		5.05		4.43	
Sm	2.80		2.96		<4.59		1.44	
Eu	1.121		1.07		<1.09		0.27	
Gd	3.82		4.24		<4.41		<0.68	
Tb	0.36		0.345		<0.62		<0.091	
Dy	1.21		1.06		<2.55		<0.43	
Ho	n.a.		n.a.		<0.61		<0.103	
Er	<0.162		<0.169		2.13		<0.30	
Yb	<0.210		<0.216		<3.02		<0.49	
Lu	<0.049		<0.051		<0.77		<0.097	
Hf	1.74		1.83		1.75		<0.31	
Ta	<0.048		<0.050		<0.70		<0.099	
Pb	n.a.		n.a.		2.15		<0.32	
Th	<0.047		<0.051		<0.55		<0.113	
U	<0.046		0.088		<0.66		<0.093	

\* n.a. not analyzed.

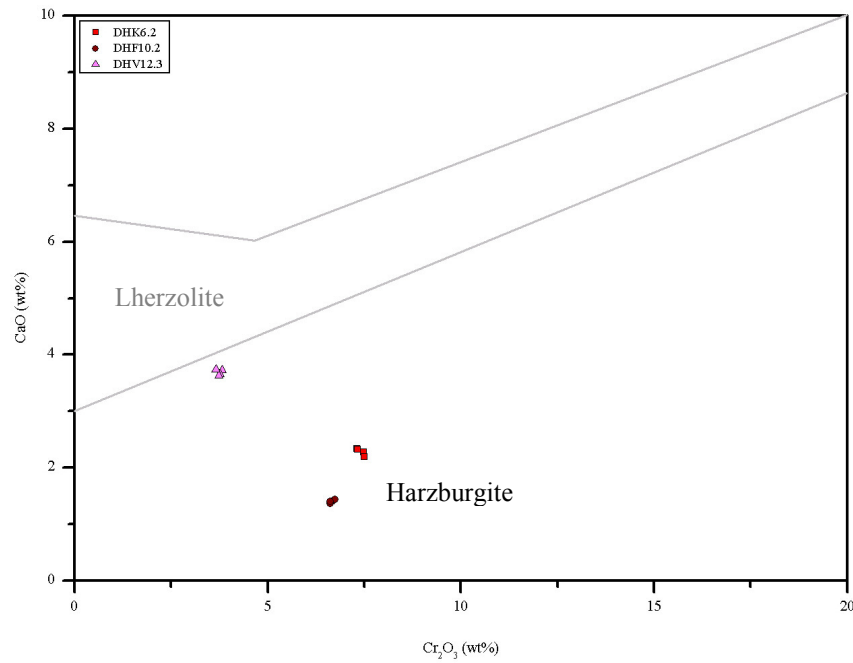
b.d. = value below the detection limit.

The chrome-pyrope compositions in DHK6.2 and DHF10.2 are comparable to garnet inclusions from Koffiefontein mine (Rickard et al., 1989) and the Finsch mine (Shee et al., 1982), respectively. The chromium content of the chrome-pyrope inclusion in DHF10.2 from the Finsch mine corresponds to the data given by Gurney and Switzer (1973), which indicated that the garnet inclusions in diamonds from the Finsch mine may contain 5.8 to 15.9 %  $\text{Cr}_2\text{O}_3$ .

Chrome-pyrope inclusions in this study can usually be assigned to the peridotite suite on the basis of the chemical composition (Figure 6.2), since peridotitic garnets tend to be Cr rich, whereas those from eclogites are mostly Cr poor (Boyd et al., 1980). They exhibit typical chrome-pyrope chemistries and are dominated by a harzburgitic paragenesis as demonstrated by their calcium and chromium contents (Figure 6.3).



**Figure 6.2** Chrome-pyrope inclusions in diamonds DHK6.2, DHF10.2, and DHV12.3, plotted in terms of four major oxides. The chrome-pyrope inclusions lie in the peridotitic fields. The outlines of the peridotitic and eclogitic fields are taken from Meyer (1987).

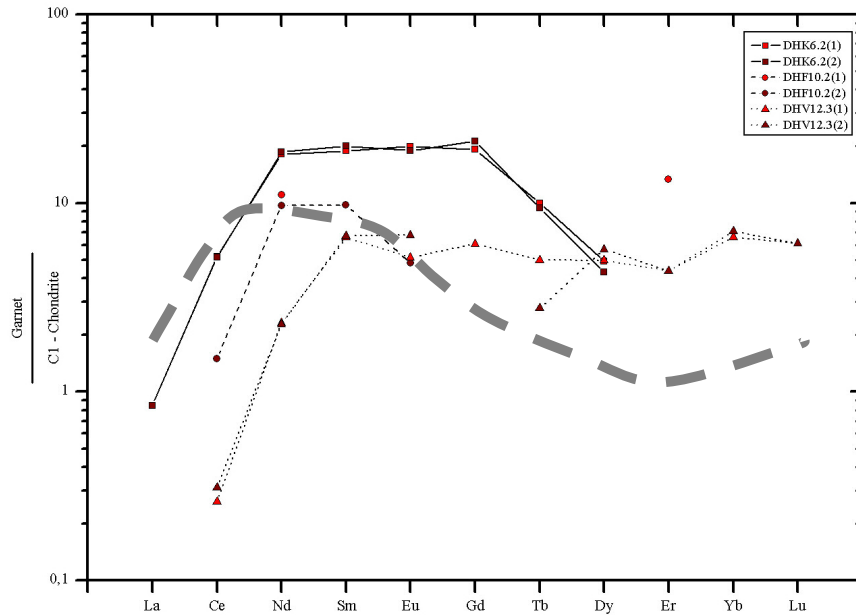


**Figure 6.3** Plot of  $\text{Cr}_2\text{O}_3$  versus  $\text{CaO}$  (wt%) for garnets from diamond samples DHK6.2, DHF10.2 and DHV12.3. The chrome-pyrope inclusions lie in the harzburgite fields. The compositional field for lherzolite field is taken from Sobolev et al. (1973).

The rare-earth elements (REE) concentrations in chrome-pyrope garnets are normalized to chondrite to visualizing the behavior of REE, since garnet inclusions in diamonds were known as the most useful mineral from which to obtain REE information. Three chrome-pyrope inclusions examined belong to the peridotitic diamond inclusion suite, assigned to the harzburgitic paragenesis as mentioned above. The REE for the three chrome-pyrope inclusions in diamonds from Finsch, Koffiefontein and Venetia mines are illustrated in Figure 6.4. Some REE data are not shown on the diagram as laser ablation measurements revealed that the concentrations were below detection limits.

The chondrite normalized REE ( $\text{REE}_N$ ) patterns for chrome-pyrope inclusion in DHK6.2 from Koffiefontein mine, the LREE increase from La to Nd, the REE patterns are flat from Nd to Gd then decrease with a minimum at Dy, but Er to Lu were not detected.





**Figure 6.4** REE concentration diagram for the three chrome-pyrope inclusions in diamonds from three different mines. The grey dot line is average compositions of harzburgitic garnet inclusions from worldwide sources (Stachel et al., 2004). All elements are normalized to the C1-chondrite composition given by McDonough and Sun (1995).

The REE<sub>N</sub> patterns for chrome-pyrope inclusion in DHF10.2 from Finsch mine show the short patterns from two different analysis spots, the first spot show only two elements (Nd and Er). The second spot begins at Ce, peaking at Nd to Sm then decrease at Eu. The HREE, Gd to Lu were not detected.

The REE<sub>N</sub> patterns for the chrome-pyrope inclusion in DHV12.3 from Venetia mine, the LREE increase from Ce to Sm and the MREE and HREE are variable in composition from Sm to Lu.

Hoal et al. (1994) suggested that the segments of the sinusoidal REE patterns can be interpreted as interrupted stages in the equilibration of garnets. Sinusoidal REE patterns represent a state of disequilibrium during the re-equilibration process of garnet. In normal garnets, the MREE (Sm – Ho) and HREE (Eu – Lu) are in equilibrium with the LREE. The flat HREE patterns of the normal garnets represent the fully equilibrated metasomatic garnet compositions, therefore garnet with sinusoidal REE patterns were evolving. Most sinusoidal garnet REE patterns peak at Sm, probably because of the order of magnitude differences in distribution coefficients for the LREE

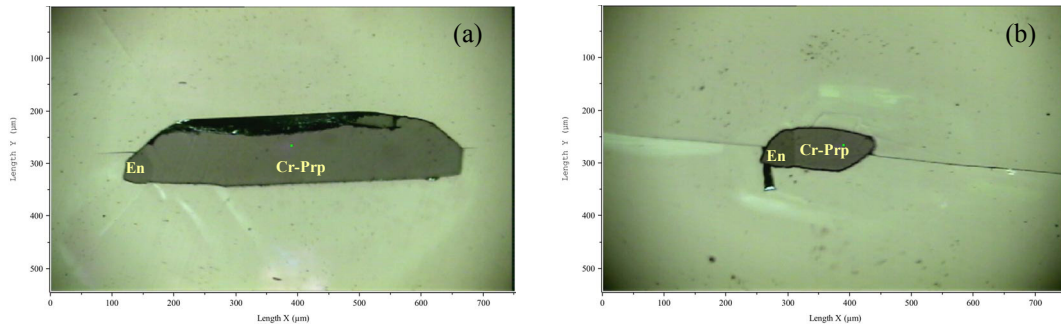
and HREE in garnet. The chrome-pyrope inclusions have sinusoidal REE patterns which peak at Nd suggesting that Sm had not yet re-equilibrated to the same extent as Nd at the time the chemical system closed.

The chondrite normalized REE patterns for three chrome-pyrope inclusions, characterized by sinusoidal REE<sub>N</sub> pattern are similar to harzburgitic garnet inclusions in diamonds from worldwide sources, whereas the normal patterns positive slope within the LREE, flat and enriched MREE –HREE are typical for lherzolitic garnets (Stachel et al., 2004). The sinusoidal REE<sub>N</sub> patterns are also characteristic for harzburgitic garnets from peridotite and kimberlite concentrates (Shimizu and Richardson, 1987; Hoal et al., 1994; Stachel et al., 1998). The sinusoidal REE<sub>N</sub> pattern of chrome-pyrope inclusions may be reflected an evolutionary sequence of increasing metasomatic re-enrichment (Stachel and Harris, 2008).

### *Enstatite (Mg<sub>2</sub>[SiO<sub>3</sub>]<sub>2</sub>)*

Enstatite inclusions in diamonds are relatively uncommon (Meyer and Boyd, 1972), normally are colourless or for large inclusions may show a yellowish green hue (Stachel and Harris, 2008). In this study only two touching inclusion assemblages of enstatite + chrome-pyrope are exposed from 2 diamond samples, DHK6.2, DHF10.2 (Figure 6.5).

The chemical compositions of enstatite inclusions are presented in Table 6.4. The enstatite compositions in DHK6.2 and DHF10.2 are comparable to orthopyroxene inclusions from the Koffiefontein mine (Rickard et al., 1989) and the Finsch mine (Harris and Gurney, 1979, and Shee et al., 1982), respectively, and similar to those reported from other diamond hosts from African localities (Meyer and Boyd, 1972).



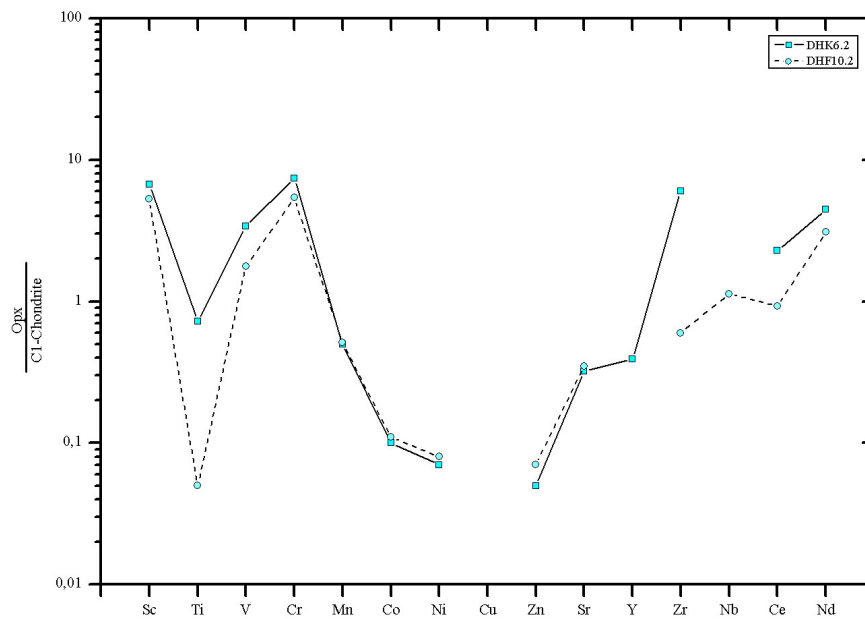
**Figure 6.5** Touching inclusions of chrome-pyrope and enstatite in diamonds (a) DHK6.2 and (b) DHF10.2.

**Table 6.4** Chemical analyses of enstatite inclusions from Cr-Prp + En pairs in diamonds DHK6.2 and DHF10.2.

	<b>DHK6.2</b>	<b>DHF10.2</b>
<b>SiO<sub>2</sub></b>	57.82	57.97
<b>TiO<sub>2</sub></b>	0.09	b.d.
<b>Al<sub>2</sub>O<sub>3</sub></b>	0.60	0.60
<b>Cr<sub>2</sub>O<sub>3</sub></b>	0.45	0.43
<b>FeO</b>	3.66	3.48
<b>MgO</b>	36.89	37.11
<b>CaO</b>	0.22	0.13
<b>MnO</b>	0.10	0.15
<b>NiO</b>	0.14	0.10
<b>Na<sub>2</sub>O</b>	0.06	0.07
<b>K<sub>2</sub>O</b>	0.01	0.04
<b>Total</b>	100.04	100.08
<i>Trace elements (ppm)</i>		
<b>Ca</b>	5625	2905
<b>Sc</b>	39.9	31.3
<b>Ti</b>	316	21.8
<b>V</b>	190	98.9
<b>Cr</b>	19525	14274
<b>Mn</b>	958	981
<b>Co</b>	52.8	55.6
<b>Ni</b>	736	883
<b>Cu</b>	<2.90	<1.09
<b>Zn</b>	14.6	23.1
<b>Sr</b>	2.29	2.57
<b>Y</b>	0.62	<0.146
<b>Zr</b>	22.9	2.31
<b>Nb</b>	<0.42	0.271
<b>Ce</b>	1.40	0.573
<b>Nd</b>	2.04	1.41
<b>Sm</b>	<2.00	<0.70
<b>Dy</b>	<1.05	<0.41
<b>Yb</b>	<1.13	<0.46
<b>Hf</b>	<0.81	<0.35
<b>Ta</b>	<0.276	<0.112

\* b.d. = value below the detection limit.

Two enstatite inclusions in this study belong to the peridotitic diamond inclusion suite, assigned directly to the harzburgitic paragenesis, since they occur as coexisting mineral pairs with chrome-pyrope in DHK6.2 and DHF10.2. The enstatite inclusion in diamond DHK6.2 has a Mg# of 94.20 and DHF10.2 has a Mg# of 94.56, which fall in the Mg# range of peridotitic orthopyroxene inclusions suggested by Stachel and Harris (2008). Furthermore, enstatite inclusions never occur together with clinopyroxene or lherzolitic garnet and contain low Ca contents (Stachel and Harris, 1997b). The chondrite normalized element patterns for enstatite inclusions in diamonds DHK6.2 and DHF10.2 are shown in Figure 6.6. The patterns of enstatite inclusions in diamonds from two different mines (Koffiefontein and Finsch mine) displaying some variation in the shape of pattern. The REE<sub>N</sub> patterns begin at Ce, peaking at Nd and trend to decreasing values for the HREE (HREE are below detection limit).

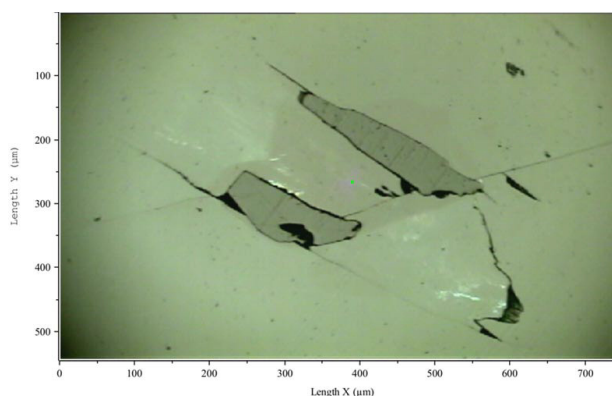


**Figure 6.6** Chondrite normalized trace elements concentration diagram for the two enstatite inclusions in diamonds from two different mines. All elements are normalized to the C1-chondrite composition given by McDonough and Sun (1995).

**Chromite ( $FeCr_2O_4$ )**

Two chromite inclusions in the diamond DHU3.1 from Udachnaya were polished (Figure 6.7) to surface exposure.

The chromite inclusions contain 63.9-64.5 wt.%  $Cr_2O_3$ , 0.1 wt.%  $TiO_2$ , 14.4-14.7 wt.%  $FeO$ , 13.8-14.3 wt.%  $MgO$ , 0.2-0.3 wt.%  $MnO$  and 0.2-0.3 wt.%  $NiO$  (Table 6.5). The compositions are comparable to chromite inclusions from the chromite inclusions in diamonds from Udachnaya compiled by Sobolev et al. (2004) and to data of the worldwide database compiled by Meyer and Boyd (1972).



**Figure 6.7** Two parts of chromite inclusions exposed on the surface of diamond DHU3.1.

**Table 6.5** Chemical analyses of chromite from diamond sample DHU3.1.

	1a	2a	3a	4a	5a	1b	2b	3b	4b	5b
<b>SiO<sub>2</sub></b>	0.14	0.17	0.19	0.14	0.11	0.12	0.14	0.19	0.14	0.16
<b>TiO<sub>2</sub></b>	0.12	0.19	0.15	0.16	0.20	0.16	0.20	0.13	0.17	0.11
<b>Al<sub>2</sub>O<sub>3</sub></b>	7.11	7.18	7.19	7.24	7.17	7.08	7.06	7.15	7.03	7.13
<b>Cr<sub>2</sub>O<sub>3</sub></b>	63.99	64.35	64.50	64.43	64.57	64.25	64.51	64.50	64.40	64.56
<b>FeO</b>	14.71	14.53	14.48	14.49	14.36	14.47	14.77	14.61	14.61	14.72
<b>MgO</b>	13.82	14.24	13.99	13.81	14.22	13.87	14.11	14.15	14.30	14.39
<b>CaO</b>	0.01	0.01	b.d.	b.d.	b.d.	0.01	b.d.	0.01	0.02	0.01
<b>MnO</b>	0.38	0.31	0.28	0.28	0.30	0.24	0.31	0.30	0.27	0.32
<b>NiO</b>	0.15	0.06	0.12	0.11	0.17	0.07	0.03	0.06	0.09	0.10
<b>Na<sub>2</sub>O</b>	0.02	0.04	b.d.	0.01	b.d.	b.d.	b.d.	b.d.	b.d.	0.04
<b>K<sub>2</sub>O</b>	0.00	0.01	b.d.	0.01	0.01	b.d.	b.d.	b.d.	b.d.	b.d.
<b>Total</b>	100.45	101.09	100.90	100.68	101.11	100.27	101.13	101.10	101.03	101.54

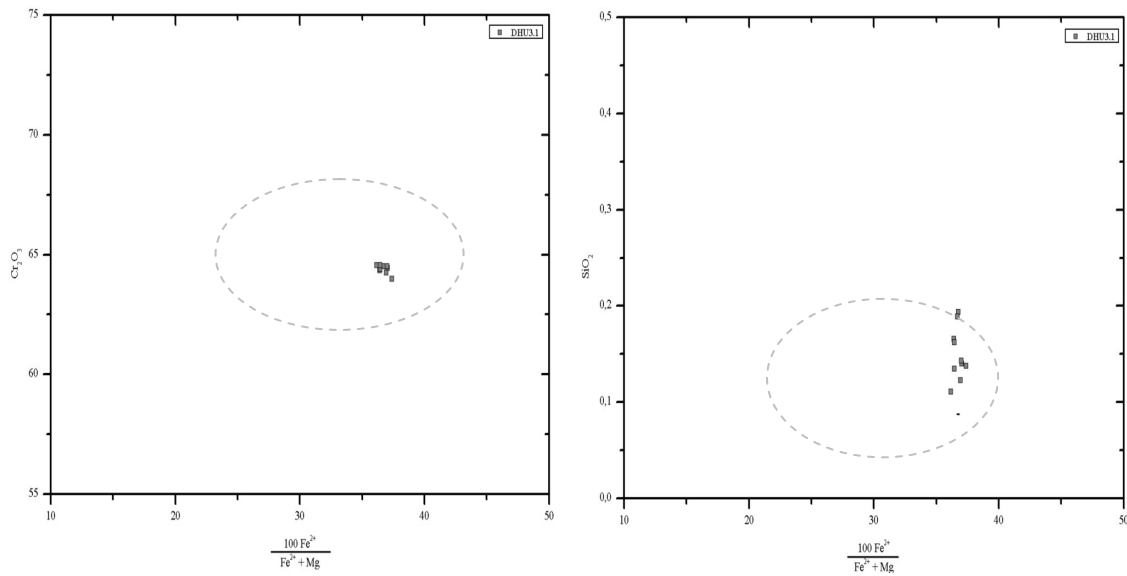
**Table 6.5** (continued)

<i>Trace elements (ppm)</i>				
	<b>DHU3.1 (1)</b>	<b>DHU3.1 (2)</b>	<b>DHU3.1 (3)</b>	<b>DHU3.1 (4)</b>
<b>Li</b>	<0.40	<0.67	<0.62	<0.64
<b>Ca</b>	5300	1365	<98.38	<98.98
<b>Sc</b>	5.16	5.33	5.35	5.55
<b>V</b>	1716	1774	1808	1864
<b>Cr</b>	414378	414741	413061	400266
<b>Mn</b>	1392	1402	1556	1490
<b>Co</b>	226	237	235	248
<b>Ni</b>	747	682	732	717
<b>Cu</b>	3.96	5.43	3.91	4.59
<b>Zn</b>	662	599	616	609
<b>Ga</b>	13.3	12.1	12.7	12.4
<b>Ge</b>	1.17	<1.85	<1.63	<1.70
<b>Zr</b>	1.89	1.21	0.71	0.83
<b>Nb</b>	1.08	2.57	1.17	1.97
<b>Mo</b>	<0.50	<0.86	0.82	<0.76
<b>Sn</b>	0.43	1.18	<0.50	0.51
<b>Sb</b>	0.44	0.69	<0.38	<0.43
<b>Hf</b>	<0.188	<0.33	<0.27	<0.29
<b>Ta</b>	0.16	0.46	0.14	0.11
<b>W</b>	<0.235	<0.43	<0.36	<0.36
<b>Pb</b>	0.84	0.55	<0.253	<0.238
<b>Th</b>	<0.061	<0.112	0.11	<0.096
<b>U</b>	0.50	0.84	0.42	<0.084

\* b.d. = value below the detection limit.

The chromite inclusion in DHU3.1 has a Cr# of 85.6 – 86.0 and a Mg# of 62.6 – 63.6 (Appendix 4). Due to the Cr# of spinel, Stachel and Harris (2008) predicted that within the diamond stability field only spinels with a Cr# of at least about 80 will be stable in cratonic peridotite.

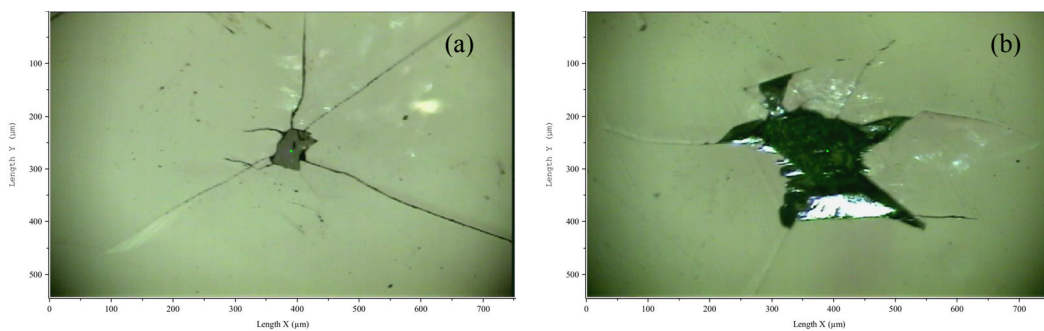
The FFM ratio  $[\text{Fe}^{2+}/(\text{Fe}^{2+} + \text{Mg})]$  vs.  $\text{Cr}_2\text{O}_3$  and  $\text{SiO}_2$  plots for chromite inclusions are shown in Figure 6.8 (a) and (b), respectively. The chromite inclusions fall in the peridotitic world-wide field given representatively by Stachel and Harris (1997a).



**Figure 6.8** (a) FFM ratio vs.  $\text{Cr}_2\text{O}_3$  and (b) FFM ratio vs.  $\text{SiO}_2$  plots for chromite inclusions in diamond DHU3.1 from Udachnaya (Siberia/Russia). The chromite inclusions lie in the world-wide peridotitic chromite fields. The outline of the world-wide peridotitic chromite inclusion field is modified from Stachel and Harris (1997a).

### *Chrome-diopside ( $\text{CaMg}[\text{SiO}_3]_2$ )*

Typical peridotitic clinopyroxenes are emerald green chrome-diopside inclusion crystals (Stachel et al., 2008). Three chrome-diopside inclusions encapsulated in the three diamonds DHU1.1, DHK7, and DHK14, were selected for chemical analysis (Figure 6.9, Table 6.6). The compositions are comparable to diopside inclusions (peridotitic suite) from the worldwide database compiled by Meyer (1987).



**Figure 6.9** Chrome-diopside inclusions (a) DHK7 and (b) DHK14.

**Table 6.6** Chemical analyses of chrome-diopside from diamond sample DHU1.1, DHK7 and DHK14.

	DHU1.1								
	1	2	3	4	5				
SiO <sub>2</sub>	55.29	51.17	54.19	58.62	54.33				
TiO <sub>2</sub>	0.03	b.d.	0.01	b.d.	0.04				
Al <sub>2</sub> O <sub>3</sub>	0.63	0.61	0.61	0.57	0.58				
Cr <sub>2</sub> O <sub>3</sub>	1.08	1.26	1.16	0.96	1.07				
FeO	2.16	6.38	3.99	2.27	3.96				
MgO	18.46	16.48	17.92	21.58	17.93				
CaO	21.91	20.50	21.41	19.60	21.32				
MnO	0.11	0.18	0.13	0.11	0.09				
NiO	0.05	0.05	0.03	0.06	0.04				
Na <sub>2</sub> O	0.73	0.61	0.60	0.48	0.63				
K <sub>2</sub> O	0.11	0.13	0.12	0.13	0.12				
<b>Total</b>	100.56	97.37	100.17	104.38	100.11				
	DHK7					DHK14			
	1	2	3	4	5	1	2	3	4
SiO <sub>2</sub>	55.31	55.29	55.04	55.04	55.75	55.53	50.09	51.03	56.15
TiO <sub>2</sub>	0.39	0.40	0.32	0.39	0.33	b.d.	0.05	b.d.	b.d.
Al <sub>2</sub> O <sub>3</sub>	5.12	5.11	5.24	5.20	4.74	1.02	1.10	0.96	1.11
Cr <sub>2</sub> O <sub>3</sub>	1.46	1.56	1.50	1.44	1.46	2.00	1.97	2.03	1.98
FeO	4.79	4.79	4.92	4.72	4.87	1.70	2.74	1.70	1.84
MgO	15.33	15.52	15.25	15.28	15.58	18.32	15.59	16.51	19.13
CaO	12.82	12.82	13.01	12.92	12.73	20.54	20.08	20.41	20.21
MnO	0.08	0.12	0.12	0.15	0.10	0.08	0.11	0.10	0.08
NiO	0.09	0.06	0.14	0.09	0.10	0.05	0.09	0.04	0.00
Na <sub>2</sub> O	3.49	3.46	3.58	3.45	3.07	0.64	0.81	0.68	0.57
K <sub>2</sub> O	0.18	0.18	0.17	0.18	0.20	1.07	1.11	1.14	0.99
<b>Total</b>	99.06	99.31	99.29	98.86	98.93	100.95	93.74	94.60	102.06
<i>Trace elements (ppm)</i>									
	DHU1.1	DHK7			DHK14 (1)		DHK14 (2)		
Sc	7.44	12.9			10.3		11.1		
Ti	112	2430			21.5		25.8		
V	87.0	240			245		242		
Cr	7116	10051			13185		13150		
Mn	672	744			514		510		
Co	24.4	37.5			21.4		21.0		
Ni	492	779			428		428		
Sr	235	293			1076		1070		
Y	<0.28	1.58			0.188		0.152		
Zr	<0.49	9.65			0.544		0.597		
Nb	<0.28	<0.121			<0.121		<0.104		
La	8.52	2.73			16.34		16.30		
Ce	15.4	7.50			30.69		30.77		
Nd	4.76	5.01			10.56		10.53		
Sm	<1.44	0.89			1.49		<0.59		
Eu	<0.41	0.423			0.194		0.215		
Gd	<1.31	<0.55			<0.51		<0.50		
Tb	<0.176	<0.079			<0.075		<0.072		
Dy	<0.89	0.64			<0.31		<0.33		
Er	<0.60	<0.256			<0.229		<0.246		
Yb	<0.95	<0.42			<0.36		<0.36		

\* b.d. = value below the detection limit.



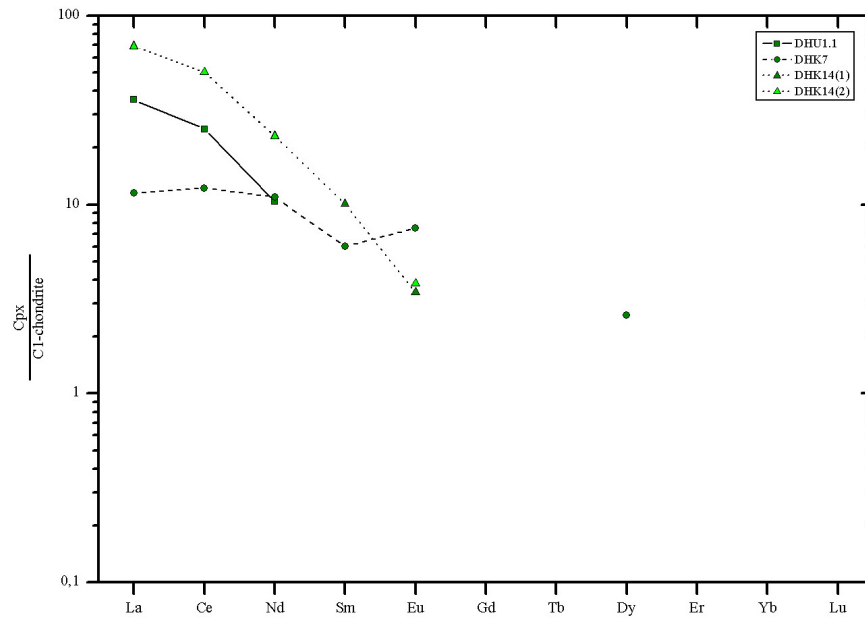
**Table 6.6** (continued)

<i>Trace elements (ppm)</i>				
	<b>DHU1.1</b>	<b>DHK7</b>	<b>DHK14 (1)</b>	<b>DHK14 (2)</b>
<b>Lu</b>	<0.213	<0.089	<0.079	<0.082
<b>Hf</b>	<0.56	0.48	<0.240	<0.248
<b>Ta</b>	<0.228	<0.077	<0.084	<0.092
<b>Th</b>	<0.217	<0.092	0.153	0.094
<b>U</b>	<0.171	<0.080	0.075	<0.074

The composition of chrome-diopside inclusion in DHK7 are comparable to peridotitic clinopyroxenes in diamonds from Koffiefontein as compiled by Rickard et al. (1986).

The composition of chrome-diopside inclusions in DHU1.1 in Table 6.6 is similar to diopsides (peridotitic suite) in diamonds from Siberia, as reported by Sobolev et al. (1971, 1976) in Meyer (1987).

On the basis of the chemical composition, chrome-diopside in this study can usually be assigned to the peridotite paragenesis, whereas clinopyroxene from the peridotitic assemblages tend to be Cr rich (Boyd et al., 1980). DHU1.1 contain 0.9 – 1.2 wt% Cr<sub>2</sub>O<sub>3</sub> with a Mg# of 81.7 – 93.5, DHK7 has 1.4 – 1.5 wt% Cr<sub>2</sub>O<sub>3</sub> with a Mg# of 84.8 – 84.9 and DHK14 contain 1.9 – 2.0 wt% Cr<sub>2</sub>O<sub>3</sub> with a Mg# of 90.7 – 94.8. Stachel and Harris (2008) suggested that typical peridotitic clinopyroxenes are emerald-green chrome-diopside inclusions, and 80% of chrome-diopside inclusions contain Cr<sub>2</sub>O<sub>3</sub> between 0.6 and 2.4 wt% with high Mg# (means between 92.5 and 93.5).



**Figure 6.10** REE concentrations in chrome-diopside inclusions in diamonds from three different mines normalized to the composition of C1-chondrites (McDonough and Sun, 1995).

Chrome-diopside inclusions have negative slopes in  $LREE_N - MREE_N$  (Figure 6.10), which generally decrease with increasing Ni (Stachel and Harris, 1997b). The patterns of  $REE_N$  show the slope down and a trend to decreasing values for the HREE, similar to  $REE_N$  pattern of clinopyroxene inclusions in diamonds from Akwatia, Ghana (Stachel and Harris, 1997b) and Kankan region of Guinea (Stachel et al., 2000) in West Africa. The HREE (Eu to Lu) in chrome-diopside inclusions are very low for samples used in this study. Almost all of HREE are below detection limits.

### ***Olivine* ((Mg, Fe)<sub>2</sub>[SiO<sub>4</sub>])**

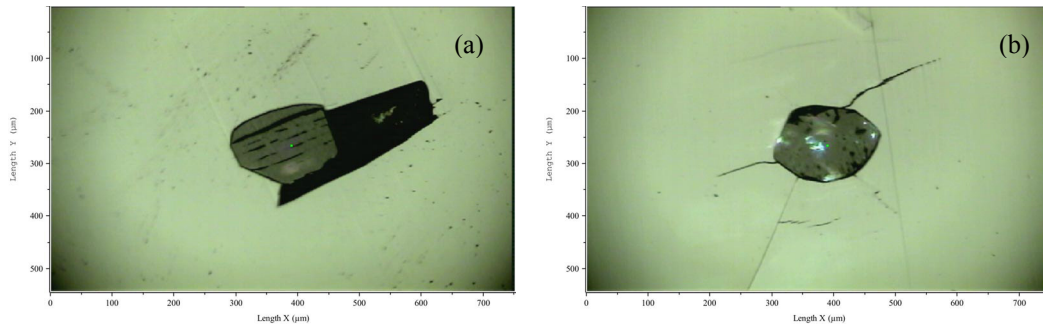
Olivine is the most typical inclusion in P-type diamonds of any size and quality (Sobolev et al., 2008). Colourless olivine inclusions are generally high in forsterite content, consistent with an origin from peridotitic sources (Stachel et al., 2008). The olivine inclusions occur as single inclusions in diamond samples DHD8.2 and DHK13 (Table 6.7 and Figure 6.11) and show only a small range in the concentrations of their major and minor elements.

**Table 6.7** Chemical analyses of olivine inclusions from DHD8.2 and DHK13.

	DHD8.2					DHK13				
	1	2	3	4	5	1	2	3	4	5
<b>SiO<sub>2</sub></b>	41.64	41.50	40.84	41.35	41.61	41.11	40.62	40.80	40.55	40.04
<b>TiO<sub>2</sub></b>	b.d.	b.d.	b.d.	0.04	b.d.	0.02	0.02	0.03	b.d.	b.d.
<b>Al<sub>2</sub>O<sub>3</sub></b>	0.01	0.02	b.d.	b.d.	0.01	0.02	0.02	0.01	0.04	0.05
<b>Cr<sub>2</sub>O<sub>3</sub></b>	0.02	0.06	0.08	0.05	0.06	0.06	0.13	0.05	0.05	0.08
<b>FeO</b>	5.43	5.33	5.46	5.35	5.35	7.66	7.70	7.65	7.68	7.59
<b>MgO</b>	52.96	53.28	52.47	52.89	53.54	51.36	50.69	50.97	50.86	49.62
<b>CaO</b>	0.03	0.02	0.05	0.02	0.03	0.05	0.02	0.04	0.05	0.08
<b>MnO</b>	0.04	0.09	0.06	0.03	0.03	0.12	0.10	0.08	0.11	0.07
<b>NiO</b>	0.39	0.31	0.35	0.36	0.34	0.41	0.34	0.41	0.40	0.36
<b>Na<sub>2</sub>O</b>	0.02	0.01	0.01	0.03	0.02	0.04	0.04	b.d.	0.01	0.04
<b>K<sub>2</sub>O</b>	0.02	0.02	0.01	0.03	0.01	0.00	0.02	b.d.	b.d.	0.01
<b>Total</b>	100.56	100.64	99.33	100.15	101.00	100.85	99.70	100.04	99.75	97.94
<i>Trace elements (ppm)</i>										
	<b>DHD8.2 (1)</b>	<b>DHD8.2 (2)</b>	<b>DHK13 (1)</b>	<b>DHK13 (2)</b>	<b>DHK13 (3)</b>					
<b>Li</b>	0.63	0.68	1.40	1.39	1.64					
<b>Al</b>	49.2	49.3	52.6	54.3	54.9					
<b>P</b>	75.1	63.2	58.0	61.2	60.4					
<b>Ca43</b>	<204.93	<129.67	162	352	340					
<b>Ca44</b>	<82.46	55.86	207	258	314					
<b>Sc</b>	1.91	2.53	2.44	2.71	2.37					
<b>Ti</b>	3.56	4.83	5.02	4.96	5.65					
<b>V</b>	5.21	5.53	6.66	6.87	6.78					
<b>Cr</b>	288	288	346	350	351					
<b>Mn</b>	531	536	775	777	800					
<b>Co</b>	118	115	134	132	133					
<b>Ni</b>	2944	2852	3041	2961	2975					
<b>Cu</b>	1.59	1.64	3.66	3.85	4.32					
<b>Zn</b>	39.9	38.8	56.0	56.8	60.4					
<b>Ga</b>	<0.194	n.a.	n.a.	n.a.	n.a.					
<b>Sr</b>	<0.117	1.824	<0.054	<0.049	<0.060					
<b>Y</b>	<0.098	<0.057	<0.047	<0.047	<0.054					
<b>Zr</b>	<0.187	<0.116	0.089	<0.084	<0.083					
<b>Nb</b>	<0.110	<0.065	<0.053	<0.046	<0.060					
<b>Hf</b>	<0.249	<0.131	<0.111	<0.106	<0.121					
<b>Ta</b>	<0.081	<0.055	<0.040	<0.034	<0.040					
<b>Th</b>	<0.090	n.a.	n.a.	n.a.	n.a.					
<b>U</b>	<0.074	n.a.	n.a.	n.a.	n.a.					

\* n.a. not analyzed.

b.d. = value below the detection limit.



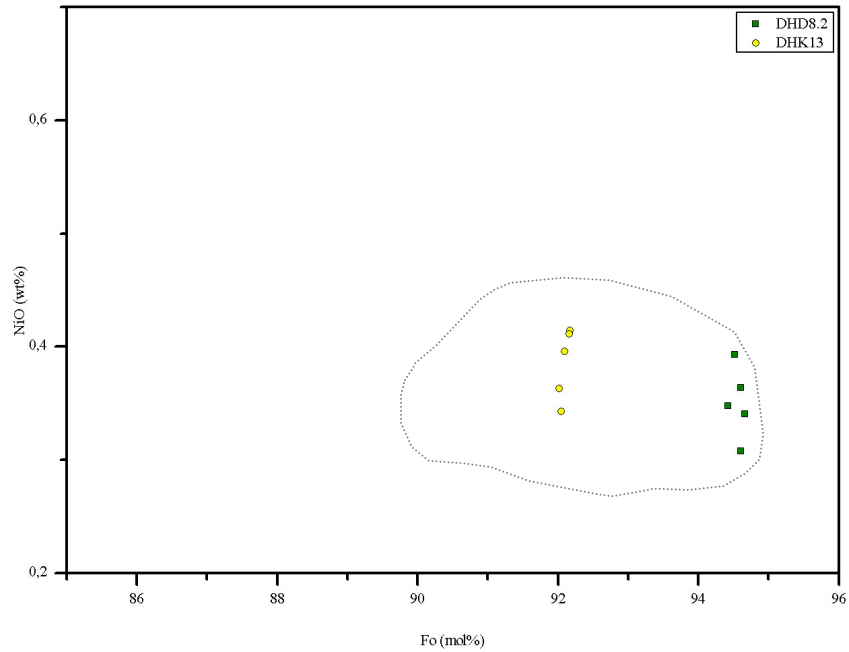
**Figure 6.11** Olivine inclusions (a) DHD8.2 and (b) DHK13.

The olivine inclusions in DHD8.2 and DHK13 have forsterite contents (Fo) 94.6 (94.42-94.66 mol%) and 92.1 (92.02-92.17 mol%), respectively. The compositions and forsterite contents (Fo) are comparable to olivine inclusions from South-West Africa (Meyer and Boyd, 1972), South Africa (Hervig et al., 1980) and to the data given by the worldwide database compiled by Meyer (1987), which are normal for olivine inclusions in diamond. Whereas olivine inclusions from diamonds range from 91 to 95 mol% Fo (Hervig et al., 1980). Meyer and Tsai (1976) reported that the olivine range from 92 to 96 mol% Fo belong to the peridotitic suite. Furthermore, the Fo contents of olivine inclusions in DHD8.2 and DHK13 fall in a range of harzburgitic olivines (Fo contents between 90.2 and 95.4) as reported by Stachel and Harris (2008).

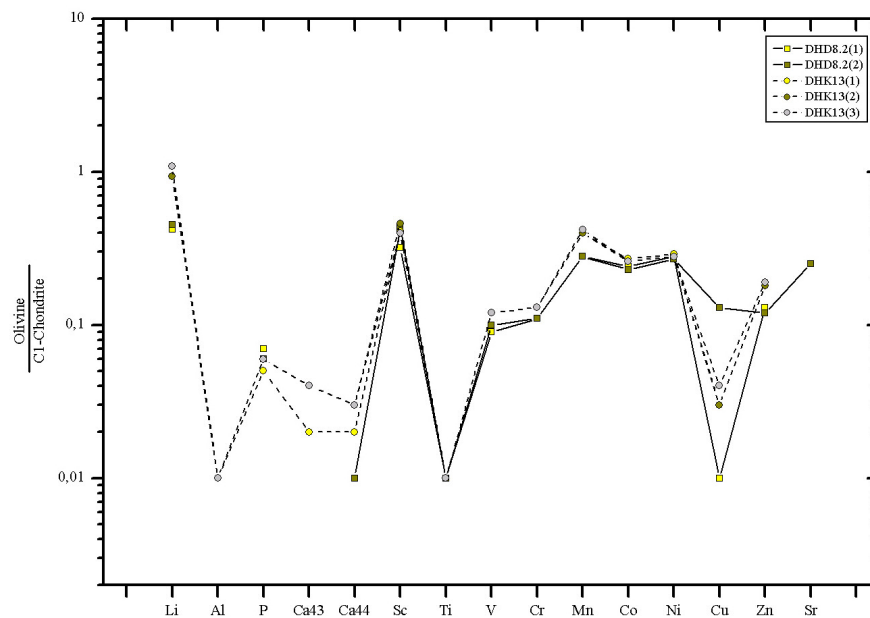
The olivine inclusion in diamond DHD8.2 has a composition and forsterite content (Fo) comparable to olivine inclusions in diamonds from De Beers Pool, South Africa compiled by Banas et al. (2008).

The information coming from NiO (wt%) and Fo (mol%) show that the majority of compositions of olivine inclusions fall in the range of the field for olivine inclusions in diamonds worldwide (Figure 6.12). The outline of the olivine inclusions field is taken from Sobolev et al. (2004).

Stachel and Harris (2008) suggested that 90% of olivine inclusions have  $\text{Cr}_2\text{O}_3 < 0.1$  wt%, which completely overlap olivines from peridotite xenoliths.



**Figure 6.12** NiO vs. Fo (forsterite contents) in olivine inclusions in diamonds from De Beers Pool and Koingnaas (alluvial) in South Africa. Plot of olivine inclusions fall in the field for olivines from diamonds world-wide as published by Sobolev et al. (2004).



**Figure 6.13** Chondrite normalized trace elements concentration diagram for the two olivine inclusions in diamonds from two different mines. All elements are normalized to the C1-chondrite composition published by McDonough and Sun (1995).

The chondrite normalized elements pattern for olivine inclusions in diamonds DHD8.2 and DHK13 are shown in Figure 6.13. The patterns of olivine inclusions in diamonds from two different mines (De Beers Pool and Koingnaas alluvial deposit) show a considerable variation in the content of trace elements with little variation in the shape of the pattern. Stachel and Harris (1997b) suggested that the harzburgitic and lherzolitic parageneses for olivine inclusions can be distinguished by a plot of Sr versus Ti, while the olivine in harzburgitic paragenesis contain higher Sr than in lherzolitic paragenesis and Ti being higher in lherzolitic paragenesis. In this study the Sr content in olivine inclusion in DHK13 are below the detection limit. This is meaningful that they contain really very low Sr and thus are interpreted to belong to the lherzolitic paragenesis.

### 6.3 Geothermobarometry

Mineral inclusions in diamonds reflect the geochemical environment of diamond hosts, which indicate that most of the diamonds were formed in peridotitic and eclogitic rocks (Meyer, 1987). Co-existing inclusion occurrences in individual diamonds are a special key to determine equilibrium mantle assemblages as well as the physical conditions prevailing in the mantle during diamond growth (Prinz et al., 1975; Meyer et al., 1976; Sobolev et al., 1997; Stachel et al., 2000 and Phillips et al., 2004). According to Harley (1984), the partitioning of Fe and Mg between two coexisting mineral phases has been recognized as potentially useful geothermometers. The temperatures and pressures determined are those that existed when the mineral systems were last in equilibrium, which may not agree precisely with the temperature and pressure of the host diamond formation (Kirkley et al., 1991). The last equilibrium temperatures between mineral assemblage diamond – chrome-pyrope – enstatite were calculated for a fixed pressure of 5.0 GPa, within the diamond stability field (Boyd et al., 1980 cited in Boyd et al., 1985 and Haggerty, 1999). Thermobarometry of peridotitic-type silicate inclusions in random diamonds gives a temperature range of 900° - 1300°C (Hervig et al., 1980).

On the other hand, Harley and Green (1982) presented the pressure evaluation, which has been estimated from alumina contents of orthopyroxenes coexisting with pyrope garnets.

Touching inclusion assemblages (chrome-pyrope + enstatite) were found in two diamonds: DHK6.2 and DHF10.2. Average estimated temperatures and pressures are shown in Table 6.8. The temperature and pressure calculations are based on the equations given by Harley (1984) and Harley and Green (1982), respectively.

$$T \text{ (}^\circ\text{C)} = \left( \frac{3,740 + 1,400 X_{gr}^{ga} + 22.86P \text{ (kb)}}{R \ln K_D + 1.96} \right) - 273$$

where  $X_{gr}^{ga} = (\text{Ca}/\text{Ca} + \text{Mg} + \text{Fe})^{ga}$

$$K_D = (\text{Fe}/\text{Mg})^{ga}/(\text{Fe}/\text{Mg})^{opx}$$

and  $R = \text{universal gas constant, } 1.9872$

$$\begin{aligned} P \text{ (kbar)} = & 1/\Delta V_r [(R \ln K - 2.93)T + 5,650 \\ & + 5,157(1-X_{Al}^{M1})(1-2X_{Al}^{M1})X_{Fe}^{opx} \\ & - 6,300[X_{Ca}^{ga}X_{Fe}^{ga} + (X_{Ca}^{ga})^2] \end{aligned}$$

where  $T$  is in Kelvin;  $K = [X_{Al}^{M1}(1-X_{Al}^{M1})/(1-X_{Ca}^{ga})^3]$

$$\Delta V_r = -[183.3 + 178.98(X_{Al}^{M1}(1-X_{Al}^{M1}))] \text{ cal kbar}^{-1}$$

**Table 6.8** Estimated equilibration temperatures and pressures for coexisting peridotitic mineral inclusions in individual diamonds.

Sample No.	Temperature* (°C)	Pressure (GPa)
DHK6.2	1087 (±15)	5.2 (±0.1)
DHF10.2	1041 (±5)	5.0 (±0.1)

\* Pressure of 5.0 GPa assumed when calculating temperature.

Average temperatures and pressure are estimated at 1087 ( $\pm 15$ ) °C, 5.2 ( $\pm 0.1$ ) GPa for diamond DHK6.2 similar to the temperature and pressure ranges predicted for diamonds from Koffiefontein by Rickard et al. (1989).

The temperature and pressure from chrome-pyrope + enstatite inclusions in DHF10.2 is calculated at 1041 ( $\pm 5$ ) °C, 5.0 ( $\pm 0.1$ ) GPa for diamond DHF10.2 from the Finsch Mine, which is close to the temperature and pressure estimated by Hervig et al. (1980) and similar to the temperature range reported by Shee et al. (1982) and Griffin et al. (1992).

According to their cubo-octahedral morphology of inclusions, the estimated temperatures and pressures in this study fall in the diamond stability field at depth below 150 km under the continental region (the pressure and temperature phase diagram of carbon is shown in Figure 1.3). The inclusions are presumed to have formed simultaneously within the crystallization process of their diamond hosts.



## 7. CONCLUSIONS

The mineral inclusions trapped in twenty-nine diamonds were observed in this study for characterization of their material properties (i.e. colour and crystallographic morphology and orientation as well as crystal chemistry). The purplish red mineral inclusions are identified as chrome-pyrope, the dark green inclusions are chrome-diopside, colourless crystal inclusions are olivine (forsterite) and black inclusions are identified as chromite and/or graphite. Most diamond samples in this study contain more than one species of crystal inclusions. The coexisting inclusions are both, either non-touching or touching inclusions. The enstatite inclusions coexisting with chrome-pyrope inclusions as touching inclusions were recovered from their different luster by the different reflection of light on the surfaces of polished diamonds.

The mineral inclusions show a variety of morphological shapes i.e. cubo-octahedral morphology, tabular and flattened parallel to octahedral plane of diamond hosts, which is obviously irrespective of their crystal systems and they have no visible fractures reaching into the diamonds. This implies that the crystal forms of inclusions were controlled by the diamond hosts. Furthermore, the principal surfaces of the syngenetic inclusions are often closely related to the [111] and/or [100] planes of the diamond guests (Harris and Gurney, 1979). The chrome-pyrope inclusions have the cubo-octahedral form, sometimes with the common crystal morphologies as a twelve-faced rhombic-dodecahedron and the twenty-four-faced trapezohedron. Some chrome-diopside and olivine inclusions show a cubo-octahedral morphology, as their crystal faces are corresponding to the enclosing octahedral diamond. The inclusions are interpreted as syngenetic mineral inclusions.

The relative residual pressures in diamonds derived from the shift of first-order Raman diamond spectra are approximately from 0.4 to 0.9 GPa. around chrome-pyrope inclusions, from 0.6 to 2.0 GPa. around chrome-diopside inclusions, from 0.3 to 1.2 GPa. around olivine inclusions, from 0.2 to 1.0 GPa. around chromite inclusions and 0.5 GPa. around graphite inclusion, respectively.

Thirty-one chrome-pyrope inclusions, three chromite inclusions, thirty-one chrome-diopside and seven olivine inclusions were discovered from twenty-seven

diamonds with respect to their cell parameters, which were obtained by the Xcalibur four-circle X-ray diffractometer. The crystallographic cell parameters and volumes are typical for chrome-pyrope, chrome-diopside, chromite and olivine in relation to their chemical composition.

The structural relationship of diamonds and their inclusions were studied by calculating the angle correlation between the [111] direction of diamonds and specifically selected directions of their distinct mineral inclusions. The chrome-pyrope or chromite inclusions, which are representing more than one trapped crystal in the individual diamond hosts, showed the angle correlation with small degrees of different orientation. The angle correlations between diamond [111] and chrome-pyrope [111] or chromite [111] showed the small misalignments up to  $2.2^\circ$  and  $3.4^\circ$  between the chrome-pyrope and chromite inclusions, respectively. The chrome-diopside and olivine inclusions showed the degree of miss-orientation between diamond [111] and chrome-diopside [010], olivine [100] up to  $10.2^\circ$  and  $12.9^\circ$  for chrome-diopside and olivine, respectively. Unfortunately, the structural relationship of diamond hosts and graphite inclusions in this study has not been investigated, no graphite single crystal information in relation to diamond hosts has been available; only one diamond sample (DHU1.3) from Udachnaya (Siberia/Russia) has a graphite inclusion which is very small and thin and did not deliver reliable single crystal data.

The cubic system inclusions (chrome-pyrope and chromite) exhibit the relatively similar orientation to diamond hosts, when the inclusions have grown together in individual diamonds. The crystal inclusions show the typical small misalignment angle between each others. Furthermore, the cubic system mineral inclusions captured in diamonds from the same mine show nearly the same angle orientation to their host diamonds. However, the monoclinic (chrome-diopside) and orthorhombic (olivine) inclusions have various orientations between inclusions and diamond hosts.

Corresponding to the rotation angles in Chapter 5, the other method for elucidating structural relationship of inclusions within diamonds was studied basing on special twin laws. Using a special direction vector of inclusions as the rotation axis, the twinning matrices were exhibited from the diamonds and their inclusion components orientation matrices and the degrees of rotations were calculated. Most of the individual diamonds which contain more than one crystal of chrome-pyrope inclusions showed the

rotation angles with small misalignments from  $0.0^\circ$  up to  $2.6^\circ$ . Excluding the sample DHV12.3, which contained six crystals of chrome-pyrope inclusions, which showed the deviation from the average value of the twinning rotation angle up to  $14.4^\circ$ . The chromite inclusions captured in diamonds showed the deviation from the average value of twinning rotation angles with small misalignments up to  $0.4^\circ$ . The chrome-diopside and olivine inclusions in diamonds showed the deviation from the average value of rotation up to  $15.4^\circ$  and  $6.4^\circ$  for chrome-diopside and olivine, respectively.

The results provide the distinct orientation relationships of the diamonds and their inclusions and prove that the chrome-pyrope and chromite inclusions showing the similar orientation to diamond hosts, have grown together in the individual diamonds. For improved statistical reliability more analyses of crystal structural relations have to be carried out.

The chemical compositions of mineral inclusions were obtained from nine diamond samples, which were polished along  $\{110\}$  or  $\{111\}$  faces. The exposed inclusions are three chrome-pyrope inclusions from Koffiefontein, Finsch and Venetia mines (two from three coexisting with enstatite), one chromite from Udachnaya (Siberia/Russia), three chrome-diopside from Koffiefontein, Koingnaas and Udachnaya (Siberia/Russia) and two olivine inclusions from De Beers Pool and Koingnaas. On the basis of chemical composition, mineral inclusions in diamonds in this study can usually be assigned to peridotite suite.

Chrome-pyrope inclusions are dominated by harzburgitic paragenesis (clinopyroxene absent) due to their calcium and chromium contents. The sinusoidal REE<sub>N</sub> patterns for chrome-pyrope inclusions represent the interrupted stages in the equilibration process of chrome-pyrope inclusions.

Since the two enstatite inclusions occur as coexisting mineral pairs with chrome-pyrope in DHK6.2 and DHF10.2, they are assigned also to the harzburgitic paragenesis, being confirmed by the Mg# of enstatite, which fall in Mg# range of peridotitic orthopyroxene inclusions. The enstatite inclusion in diamond DHK6.2 has Mg# of 94.20 and DHF10.2 has Mg# of 94.56.

The chromite inclusion in DHU3.1 is belonging to peridotitic paragenesis, due to the Cr# of 85.6 – 86.0 and Mg# of 62.6 – 63.6, which fits to the predicted values given by Stachel and Harris (2008) who states that within the diamond stability field only spinels with Cr# of at least about 80 will be stable in cratonic peridotite.

On the basis of the chemical composition and their emerald-green colour, chrome-diopside inclusions can usually be assigned to the peridotite (lherzolitic - clinopyroxene bearing) paragenesis. DHU1.1 contain 0.9 – 1.2 wt% Cr<sub>2</sub>O<sub>3</sub> with Mg# 81.7 – 93.5, DHK7 has 1.4 – 1.5 wt% Cr<sub>2</sub>O<sub>3</sub> with Mg# 84.8 – 84.9 and DHK14 contain 1.9 – 2.0 wt% Cr<sub>2</sub>O<sub>3</sub> with Mg# 90.7 – 94.8 comparable to typical peridotitic clinopyroxenes, which contain Cr<sub>2</sub>O<sub>3</sub> between 0.6 and 2.4 wt% with high Mg#.

Olivine is one of the most typical inclusions in peridotitic diamonds, which are generally high in forsterite content (Fo). The olivine inclusions in DHD8.2 and DHK13 have 94.6 mol% Fo and 92.1 mol% Fo, respectively.

The diamond samples in this study mostly contain chrome-pyrope without chrome-diopside or chrome-diopside without chrome-pyrope in individual diamonds. As a result of harzburgitic paragenesis, when the temperature is raised, the clinopyroxene are depleted. Except the diamonds from Koingnaas (alluvial deposit), which contain chrome-diopside show coexisting (non-touching) chrome-pyropes. Corresponding to the forsterite content (Fo) of olivine, inclusion in diamond DHK13 from Koingnaas fall in the lherzolitic suite with olivine (Fo 90.1 to 93.6) as reported by Stachel and Harris (2008).

The genetically interpretation on the base of geothermobarometry proved by inclusions was investigated by the partitioning of Fe and Mg between touching inclusions (chrome-pyrope + enstatite) in individual diamonds. Average temperatures and pressures are estimated for 1087 (±15) °C, 5.2 (±0.1) GPa for diamond DHK6.2 from Koffiefontein mine and 1041 (±5) °C, 5.0 (±0.1) GPa for diamond DHF10.2 from Finsch mine, respectively. However, the estimated temperatures and pressures from this study are similar to the temperature and pressures range of diamonds from Koffiefontein and Finsch mines in previous works. According to the cubo-octahedral morphology of chrome-pyrope + enstatite inclusions, the estimated temperatures and

---

pressures which fall in the diamond stability field at depth below 150 km under the continental region, the inclusions are presumed to have formed simultaneously within the crystallization process of their diamond hosts.

## 8. REFERENCES

- Abduriyim, A. and Kitawaki, H., 2006. Applications of Laser Ablation-Inductively Coupled Plasma-Mass Spectrometry (LA-ICP-MS) to Gemology. *Gems & Gemology*. 42: 98-118.
- Allen, B. P. and Evans, T., 1981. Aggregation of nitrogen in diamond, including platelet formation. *Proceedings of the Royal Society of London, Series A: Mathematical and Physical Sciences*. 375: 93-104.
- Appleyard, C. M., Viljoen (Fanus), K. S. and Dobbe, R., 2004. A study of eclogitic diamonds and their inclusions from the Finsch kimberlite pipe, South Africa. *8<sup>th</sup> International Kimberlite Conference, Extended Abstract, Canada*.
- Banas, A., Stachel, T., Shimizu, N., Phillips, D., Viljoen (Fanus), K. S. and Harris, J. W., 2008. Ancient metasomatism recorded by ultra-depleted garnet inclusions in diamonds from De Beers Pool, South Africa. *9<sup>th</sup> International Kimberlite Conference, Extended Abstract, Frankfurt, Germany*.
- Barron, L. M., Mernagh, T. P. and Barron, B. J., 2008. Using strain birefringence in diamond to estimate the remnant pressure on an inclusion. *Australian Journal of Earth Sciences*. 55: 159-165.
- Berman R., 1965. *Physical Properties of Diamond*. Oxford: Clarendon Press. 443pp.
- Berman, R., Hudson, P.R. and Martinez, M., 1975. Nitrogen in diamond: evidence from thermal conductivity. *Journal of Physics C: Solid State Physics*. 8: L430-4.
- Boppart, H., van Straaten, J. and Silvera, I. F., 1985. Raman spectra of diamond at high pressures. *Physical Review B*. 32: 1423-1425.
- Boyd, F. R. and Finnerty, A. A., 1980. Conditions of origin of natural diamonds of Peridotite affinity. *Journal of Geophysical Research*. 85: 6911-6918.

- Boyd, F. R., Gurney, J. J. and Richardson, S. H., 1985. Evidence for a 150-200-km thick Archaean lithosphere from diamond inclusion thermobarometry. *Nature*, 315: 387-389.
- Boyd, F. R., Gurney, J. J., 1986. Diamonds and the African lithosphere. *Science*, 232: 472-477.
- Brozel, M. R., Evans, T. and Stephenson, R. F., 1978. Partial dissociation of nitrogen aggregates in diamond by high temperature – high pressure treatments. *Proceedings of the Royal Society of London, Series A: Mathematical and Physical Sciences*, 361: 109-127.
- Bruton, E., 1970. *Diamonds*. London: N.A.G. Press Ltd. 372pp.
- Bulanova, G. P., 1995. The formation of diamond. *Journal of Geochemical Exploration*, 53: 1-23.
- Bundy, F. P., Bassett, W. A., Weathers, M. S., Hemley, R. J., Mao, H. K. and Goncharov, A. F., 1996. The pressure-temperature phase and transformation diagram for carbon; updated through 1994. *Carbon*, 34: 141-153.
- Censier, C. and Tourenq J., 1995. Crystal forms and surface textures of alluvial diamonds from the Western Region of the Central African Republic. *Mineralium Deposita*, 30: 314-322.
- Collins, A. T., 1982. Colour centres in diamond. *Journal of Gemmology*, 18: 37-75.
- Davies, G., 1976. The A nitrogen aggregate in diamond - its symmetry and possible structure. *Journal of Physics C: Solid State Physics*, 9: L537-L542.
- Davies, R. M., Griffin, W. L., O'Reilly, S. Y. and Doyle, B. J., 2004. Mineral inclusions and geochemical characteristics of microdiamonds from the DO27, A154, A21, A418, DO18, DD17 and Ranch Lake kimberlites at Lac de Gras, Slave Craton, Canada. *Lithos*, 77: 39-55.
- Deer, W. A., Howie, R. A. and Zussman, J., 1966. *An Introduction to the Rock Forming Minerals*. UK. Richard Clay (The Chaucer Press) Ltd. 528pp.

- Deer, W. A., Howie, R. A. and Zussman, J., 1992. *An Introduction to the Rock Forming Minerals*. 2<sup>nd</sup> edition. Longman Scientific & Technical, UK. 696pp.
- Deines, P., Gurney, J. J. and Harris, J. W., 1984. Associated chemical and carbon isotopic composition variations in diamonds from Finsch and Premier kimberlite, South Africa. *Geochimica et Cosmochimica Acta*. 48: 325-342.
- Deines, P., Viljoen, F. and Harris, J. W., 2001. Implications of the carbon isotope and mineral inclusion record for the formation of diamonds in the mantle underlying a mobile belt: Venetia, South Africa. *Geochimica et Cosmochimica Acta*. 65: 813-838.
- Eppler, W. F., 1961. Inclusions in diamond. *The Journal of Gemmology*. 8: 1-13.
- Evans, T. and Qi, Z., 1982. The kinetics of the aggregation of nitrogen atoms in diamond. *Proceedings of the Royal Society of London. Series A, Mathematical and Physical Sciences*. 381: 159-178.
- Gornova, M. A., Polozov, A. G., Ignat'ev, A. V. and Velivetskaya, T.A., 2007. Peridotite nodules from the Udachnaya kimberlite pipe: 'nonmantle' oxygen isotope ratios in garnets. *Doklady Earth Sciences*. 415: 777-781.
- Griffin, W. L., Gurney, J. J. and Ryan, C. G., 1992. Variations in trapping temperatures and trace elements in peridotite-suite inclusions from African diamonds: evidence for two inclusion suites, and implications for lithosphere stratigraphy. *Contributions to Mineralogy and Petrology*. 110: 1-15.
- Grimsditch, M. H., Anastassakis, E. and Cardona, M., 1978. Effect of uniaxial stress on the zone-center optical phonon of diamond. *Physical Review B*. 18: 901-904.
- Gurney, J. J. and Switzer, G. S., 1973. The discovery of garnets closely related to diamonds in the Finsch pipe, South Africa. *Contributions to Mineralogy and Petrology*. 39: 103-116.
- Gurney, J. J. and Zweistra, P., 1995. The interpretation of the major element compositions of mantle minerals in diamond exploration. *Journal of Geochemical Exploration*. 53: 293-309.



- Haggerty, S. E., 1999. A diamond trilogy: Superplumes, supercontinents and supernovae. *Science*. 285: 851-860.
- Hanfland, M., Syassen, K., Fahy, S., Louie, S. G. and Cohen, M. L., 1985. Pressure dependence of the first-order Raman mode in diamond. *Physical Review B*. 31: 6896-6899.
- Harley, S. L. and Green, D. H., 1982. Garnet-orthopyroxene bprpmetry for granulites and peridotites. *Nature*. 300: 697-701.
- Harley, S. L., 1984. An experimental study of the partitioning of Fe and Mg between garnet and orthopyroxene. *Contributions to Mineralogy and Petrology*. 86: 359-373.
- Harris, J. W., Hawthorne, J. B., Oosterveld, M. M. and Wehmeyer, E., 1973. A classification scheme for diamond and a comparative study of South African diamond characteristics. *Physics and Chemistry of the Earth*. vol.9. A. Wheaton & Co., Exeter, Great Britain, 940p.
- Harris, J. W. and Gurney, J. J., 1979. Inclusions in diamond. *The properties of diamond*. J. E. Field. London, Academic press Inc. (London) Ltd.: 555-591.
- Harris, J. W., 1987. Recent physical, chemical and isotopic research of diamond. In: Nixon, P.H. (Ed.), *Mantle Xenoliths*. John Wiley & Sons Ltd., New York: 477-500.
- Harris, J. W., 1993. The geology of diamond: time and depth profiles from inclusions. *Diamond and Related Materials*. 2: 75-79.
- Harte, B., Gurney, J. J. and Harris, J. W., 1980. The formation of peridotitic suite inclusions in diamonds. *Contributions to Mineralogy and Petrology*. 72: 181-190.
- Hervig, R. L., Smith, J. V., Steele, I. M., Gurney, J. J., Meyer, H. O. A. and Harris, J. W., 1980. Diamonds: Minor elements in silicate inclusions: Pressure-temperature implications. *Journal of Geophysical Research*. 85: 6919-6929.

- Hoal, K. E. O, Hoal, B. G., Erlank, A.J. and Shimizu, N., 1994. Metasomatism of the mantle lithosphere recorded by rare earth elements in garnets. *Earth and Planetary Science Letters*. 126: 303-313.
- Howell, D., Jones, A., Dobson, D., Wood, I., Nasdala, L. and Harris, J., 2008. Quantifying strain birefringence haloes around inclusions in diamond. 9<sup>th</sup> *International Kimberlite Conference*, Extended Abstract, Frankfurt, Germany.
- Izraeli, E. S., Harris, J. W. and Navon, O., 1999. Raman barometry of diamond formation. *Earth and Planetary Science Letters*. 173: 351-360.
- Izraeli, E. S., Harris, J. W. and Navon, O., 2004. Fluid and mineral inclusions in cloudy diamonds from Koffiefontein, South Africa. *Geochimica et Cosmochimica Acta*. 68: 2561-2575.
- Kaiser, W. and Bond, W. L., 1959. Nitrogen, a major impurity in Common type I diamond. *Physical Review*. 115(4): 857-863.
- Kamenetsky, V. S., Kamenetsky, M. B., Sobolev, A. V., Golovin, A. V., Demouchy, S., Faure, K., Sharygin, V. V. and Kuzmin, D. V., 2007. Olivine in the Udachnaya-East Kimberlite (Yakutia, Russia): Types, compositions and origins. *Journal of Petrology*. 00: 1-17.
- Keller, P., 1990 *Gemstones and Their Origins*. Van Nostrand Reinhold, New York, 144 p.
- King, J. M., Shigley, J. E., Gelb, T. H., Guhin, S. S., Hall, M. and Wang, W., 2005. Characterization and grading of natural-colour yellow diamonds. *Gems & Gemology*. 41: 88-115.
- Kirkley, M. B., Gurney, J. J. and Levinson, A. A., 1991. Age, origin and emplacement of diamonds: Scientific advances in the last decade. *Gems & Gemology*. 27: 2-25.
- Kirkley, M. B., 1998. The origin of diamonds: Earth processes. *The Nature of Diamonds*. George E. Harlow. Cambridge University Press, USA: 48-71.

- Klein, C. and Hurlbut, C. S. Jr., 1993. *Manual of mineralogy*. 21<sup>st</sup> ed after Dana, J. D., John Wiley & Sons, Inc., Canada, 681 p.
- Kunz, M., Gillet, P., Fiquet, G., Sautter, V., Graafsma, H., Conrad, P. and Harris, J., 2002. Combined in situ X-ray diffraction and Raman spectroscopy on majoritic garnet inclusions in diamonds. *Earth and Planetary Science Letters*. 198: 485-493.
- Lang, A. R., 1979. Internal structure. *The properties of diamond*. J. E. Field. London, Academic press Inc. (London) Ltd.: 425-469.
- Lax, M. and Burstein, E., 1955. Infrared lattice absorption in ionic and homopolar crystals. *Physical Review*. 97: 39-52.
- Mainwood A., 1994. Nitrogen and nitrogen-vacancy complexes and their formation in diamond. *Physical Review B*. 49(12): 7934-7940.
- Marshall, T. R. and Baxter-Brown, R., 1995. Basic principles of alluvial diamond exploration. *Journal of Geochemical Exploration*. 53: 277-292.
- Matthes, S. 1987. *Mineralogie*, Springer-Verlag Berlin, Germany, 444 p.
- McDonough, W. F. and Sun, S.-s., 1995. The composition of the Earth. *Chemical Geology*. 120: 223-253.
- Meyer, H. O. A., 1968. Chrome pyrope: An inclusion in natural diamond. *Science*. 160: 1446-1447.
- Meyer, H. O. A. and Boyd, F. R., 1972. Composition and origin of crystalline inclusions in natural diamonds. *Geochimica et Cosmochimica Acta*. 36: 1255-1273.
- Meyer, H. O. A. and Tsai H.-M., 1976. Mineral inclusions in diamond: temperature and pressure of equilibration. *Science*. 191(4229): 849-851.
- Meyer, H. O. A., 1985. Genesis of diamond: a mantle saga. *American Mineralogist*. 70: 344-355.

- Meyer, H. O. A., 1987. *Inclusions in diamond*. In: Nixon, P.H. (Ed.), *Mantle Xenoliths*. John Wiley & Sons Ltd., New York, pp. 501-522.
- Mitchell, R. S. and Giardini, A. A., 1977. Some mineral inclusions from African and Brazillian diamonds: their nature and significance. *American Mineralogist*. 62: 756-762.
- Mitchell, R. S., 1989. Aspects of the petrology of kimberlites and lamproites: some definitions and distinctions. *International Kimberlite Conference 4<sup>th</sup>*, 7-45.
- Nasdala, L., Brenker, F. E., Glöckner, J., Hofmeister, W., Gasparik, T., Harris, J. W., Stachel, T. and Reese, I., 2003. Spectroscopic 2D-tomography: Residual pressure and strain around mineral inclusions in diamonds. *European Journal of Mineralogy*. 15: 931-935.
- Nasdala, L., Hofmeister, W., Harris, J. W. and Glöckner, J., 2005. Growth zoning and strain patterns inside diamond crystals as revealed by Raman maps. *American Mineralogist*. 90: 745-748.
- Nugent, K. W. and Prawer, S., 1998. Confocal Raman strain mapping of isolated single CVD diamond crystals. *Diamond and Related Materials*. 7: 215-221.
- Patel, A. R and Ramanathan, S., 1962. Etch pits on diamond surfaces. *Philosophical Magazine*. 7: 1305-1314.
- Pearson, D. G., Shirey, S. B., Harris, J. W. and Carlson, R. W., 1998. Sulphide inclusions in diamonds from the Koffiefontein kimberlite, S Africa: constraints on diamond ages and mantle Re-Os systematics. *Earth and Planetary Science Letters*. 160: 311-326.
- Phillips, D., Harris, J. W., Viljoen, K. S., 2004. Mineral chemistry and thermobarometry of inclusions from De Beers Pool diamonds, Kimberley, South Africa. *Lithos*. 77: 155-179.
- Prinz, M., Merson, D. V., Hlava, P. F. and Keil, K., 1975. Inclusions in diamonds: Garnet lherzolite and eclogite assemblages. *Physics and Chemistry of the Earth*. 9: 798-815.

- Richardson, S. H., Gurney, J. J., Erlank, A. J. and Harris, J. W., 1984. Origin of diamonds in old enriched mantle. *Nature*. 310: 198-202.
- Richardson, S. H., 1986. Latter-day origin of diamonds of eclogitic paragenesis. *Nature*. 322: 623-626.
- Richardson, S. H., Erlank, A. J., Harris, J. W. and Hart, S. R., 1990. Eclogitic diamonds of Proterozoic age from Cretaceous kimberlites. *Nature*. 346: 54-56.
- Rickard, R. S., Harris, J. W., Gurney, J. J. and Cardoso, P., 1989. Mineral inclusions in diamonds from Koffiefontein Mine. *International Kimberlite Conference 4<sup>th</sup>*, 1054-1062.
- Shee, S. R., Gurney, J. J. and Robinson, D. N., 1982. Two diamond-bearing peridotite xenoliths from the Finsch kimberlite, South Africa. *Contributions to Mineralogy and Petrology*. 81: 79-87.
- Shimizu, N. and Richardson, S. H., 1987. Trace element abundance patterns of garnet inclusions in peridotite-suite diamonds. *Geochimica et Cosmochimica Acta*. 51: 755-758.
- Shirey, S. B., Harris, J. W., Richardson, S. H., Fouch, M., James, D. E., Cartigny, P., Denies, P. and Viljoen, F., 2003. Regional patterns in the paragenesis and age of inclusions in diamond, diamond composition, and the lithospheric seismic structure of Southern Africa. *Lithos*. 71: 243-258.
- Smith, C. B., 1983. Pb, Sr and Nd isotopic evidence for sources of southern African Cretaceous kimberlites. *Nature*. 304: 51-54.
- Smyth, J. R. and Bish, D. L., 1988. *Crystal Structures and Cation Sites of the Rock-Forming Minerals*. Biddles Limited, Guildford, Surrey, UK. 332pp.
- Sobolev, N. V., Lavrent'ev, Yu. G., Pokhilenko, N. P. and Usova, L. V., 1973. Chrome-rich garnets from the kimberlites of Yakutia and their parageneses. *Contributions to Mineralogy and Petrology*. 40: 39-52.

- Sobolev, N. V., Kaminsky, F. V., Griffin, W. L., Yefimova, E. S., Win, T. T., Ryan, C. G. and Botkunov, A.I., 1997. Mineral inclusions in diamonds from the Sputnik kimberlite pipe, Yakutia. *Lithos.* 39: 135-157.
- Sobolev, N. V., Fursenko, B. A., Gorzainov, S. V., Shu, J., Hemlez, R. J., Mao, H-K. and Bozd, F. R., 2000. Fossilized high pressure from the Earth's deep interior: The coesite-in-diamond barometer. *Proceedings of the National Academy of Sciences of the United States of America.* 97(22): 11875-11879.
- Sobolev, N. V., Logvinova, A. M., Zedgenizev, D. A., Seryotkin, Y. V., Yefimova, E. S., Floss, C. and Taylor, L. A., 2004. Mineral inclusions in microdiamonds and macrodiamonds from kimberlites of Yakutia: a comparative study. *Lithos.* 77: 225-242.
- Sobolev, N. V., Logvinova, A. M., Zedgenizov, D. A., Pokhilenko, N. P., Kuzmin, D. V. and Sobolev, A. V., 2008. Olivine inclusions in Siberian diamonds: high-precision approach to minor elements. *European Journal of Mineralogy.* 20: 305-315.
- Stachel, T. and Harris, J. W., 1997a. Syngenetic inclusions in diamond from the Birim field (Ghana) – a deep peridotitic profile with a history of depletion and re-enrichment. *Contributions to Mineralogy and Petrology.* 127: 336-352.
- Stachel, T. and Harris, J. W., 1997b. Diamond precipitation and mantle metasomatism – evidence from the trace element chemistry of silicate inclusions in diamonds from Akwatia, Ghana. *Contributions to Mineralogy and Petrology.* 129: 143-154.
- Stachel, T., Viljoen, K. S., Brey, G. and Harris, J. W., 1998. Metasomatic process in lherzolitic and harzburgitic domains of diamondiferous lithospheric mantle: REE in garnets from xenoliths and inclusions in diamonds. *Earth and Planetary Science Letters.* 159: 1-12.
- Stachel, T., Brey, G. P., Harris, J. W., 2000. Kankan diamonds (Guinea) I: from the lithosphere down to the transition zone. *Contributions to Mineralogy and Petrology.* 140: 1-15.

- Stachel, T., 2003. Peridotitic and eclogitic diamond sources and the origin of cratonic roots. 7 p.
- Stachel, T., Aulbach, S., Brey, G. P., Harris, J. W., Leost, I., Tappert, R. and Viljoen (Fanus), K. S., 2004. The trace element composition of silicate inclusions in diamonds: a review. *Lithos*. 77: 1-19.
- Stachel, T., Brey, G. P. and Harris, J. W., 2005. Inclusions in sublithospheric diamonds: Glimpses of deep earth. *Elements*. 1: 73-78.
- Stachel, T., 2007. 'Diamond' *The Geology of gem deposits*. Mineralogical Association of Canada, Short Course Series 37: 1-22.
- Stachel, T. and Harris, J. W., 2008. The origin of cratonic diamonds – Constraints from mineral inclusions. *Ore Geology Reviews*. 34: 5-32.
- Stuart, S.-A., Praver, S. and Weiser, P. S., 1993. Variation of the Raman diamond line shape with crystallographic orientation of isolated chemical-vapour-deposited diamond crystals. *Diamond and Related Materials*. 2: 753-757.
- Sutherland, G. B. B. M. and Willis, H. A., 1945. Some new peculiarities in the infra-red spectrum of diamond. *Transactions of the Faraday Society*. 41: 289-292.
- Sutherland, F.R.S., G. B. B. M., Blackwell, D. E. and Simeral, W. G., 1954. The problem of the two types of diamond. *Nature*. 13: 901-904.
- Taylor, L. A., Anand, M., Promprated, P., 2003. Diamonds and their inclusions: are the criteria for syngeneses valid?. *8<sup>th</sup> International Kimberlite Conference*, Extended Abstract, Victoria, Canada.
- Varma, C. K. R., 1967. Etch Pits and Trigons on diamond. *Philosophical Magazine*. 16: 611-620.
- Viljoen, K. S., 2002. An infrared investigation of inclusion-bearing diamonds from the Venetia kimberlite, Northern Province, South Africa: implications for diamonds from craton-margin setting. *Contributions to Mineralogy and Petrology*. 144: 98-108.

- Viljoen, K. S. (Fanus), Dobbe, R., Smit, B., Thomassot, E. and Cartigny, P., 2004. Petrology and geochemistry of a diamondiferous lherzolite from the Premier diamond mine, South Africa. *Lithos*. 77: 539-552.
- Vlasov, I. I., Ralchenko, V. G., Obraztsova, E. D., Smolin, A. A. and Konov, V. I., 1997. Stress mapping of chemical-vapor-deposited diamond film surface by micro-Raman spectroscopy. *Applied Physics Letters*. 71: 1789-1791.
- Walker, J., 1979. Optical absorption and luminescence in diamond. *Report on Progress in Physics*. 42: 1606-1659.
- Webster, R., 1994. *Gems: their sources, descriptions and identification*. 5<sup>th</sup> ed. Revised by Read, P. G., Butterworth-Heinemann Ltd, Oxford, 1026 p.
- Weikusat, C., 2005. *Spektroskopische Charakterisierung von Diamant*. Diplomarbeit, Institut für Geowissenschaften / Mineralogie, Johannes Gutenberg-Universität Mainz, 56 p.
- Wilks E. and Wilks J., 1991. *Properties and applications of diamond*. Oxford: Butterworth-Heinemann Ltd. 525 p.
- Zaitsev A. M., 2001. *Optical Properties of Diamond: a data handbook*. Berlin: Springer. 502pp.
- Zhao, Y. X. and Spain, I. L., 1989. X-ray diffraction data for graphite to 20 GPa. *Physical Review B*. 40: 993-997.

**Web sources:**

- [http://www.allaboutgemstones.com/diamond\\_mines\\_russia.html](http://www.allaboutgemstones.com/diamond_mines_russia.html)
- [http://www.coastofdiamonds.co.za/getting\\_around/diamondGeology.pdf](http://www.coastofdiamonds.co.za/getting_around/diamondGeology.pdf)
- <http://www.healingcrystal.com>
- <http://www.mindat.org>
- <http://skywalker.cochise.edu>
- <http://www.wolframalpha.com>



## APPENDIX

### Appendix 1

#### Calculation of an angle between diamond and inclusion

##### DHU2.1 (chrome-pyrope inclusion)

The crystal orientation matrices of diamond (nd) and inclusion (ni) are shown below:

nd1	[-0.900876498,	-0.385324864,	0.199865669]
nd2	[-0.382042416,	0.500645711,	-0.776786627]
nd3	[0.201918986,	-0.776031358,	-0.597498163]
ni1	[-0.801111842,	-0.568061294,	-0.188483907]
ni2	[-0.189386356,	0.538815675,	-0.820859596]
ni3	[0.567798156,	-0.621926803,	-0.539270160]

The angle between [111] direction of diamond and [111] direction of chrome-pyrope inclusion can be calculated by vector  $\vec{d}$  and vector  $\vec{i}$  as follows:

$$\alpha^\circ = \arcsin \left( \frac{\vec{d} \cdot \vec{i}}{|\vec{d}| \cdot |\vec{i}|} \right) \cdot 180/\pi$$

Where  $\vec{d} \cdot \vec{i} = d_x \cdot i_x + d_y \cdot i_y + d_z \cdot i_z$

$$|\vec{d}| = \sqrt{(d_x^2 + d_y^2 + d_z^2)}$$

$d_x, d_y, d_z$  are the components of vector  $\vec{d}$  in x, y and z direction.

$$\begin{aligned} \vec{d}_{[111]} &= [nd1_x + nd2_x + nd3_x, nd1_y + nd2_y + nd3_y, nd1_z + nd2_z + nd3_z] \\ &= [-1.08099993, -0.66071051, -1.17441912] \end{aligned}$$

$$\begin{aligned} \vec{i}_{[111]} &= [ni1_x + ni2_x + ni3_x, ni1_y + ni2_y + ni3_y, ni1_z + ni2_z + ni3_z] \\ &= [-0.42270004, -0.65117242, -1.54861366] \end{aligned}$$

$$\vec{d} \cdot \vec{i} = 2.70589668$$

$$|\vec{d}| \cdot |\vec{i}| = 1.72752988 \times 1.73231208 = 2.99262088$$

$$\alpha \text{ (radian)} = \arcsin \left( \frac{\vec{d} \cdot \vec{i}}{|\vec{d}| \cdot |\vec{i}|} \right) = 0.4413$$

$$\alpha^\circ = \alpha \text{ (radian)} \cdot 180/\pi = 25.28$$

## Appendix 2

### Calculation of the rotation angle between diamond and inclusion

#### DHU2.2 (chrome-pyrope inclusion)

The crystal orientation matrices of diamond (nd) and inclusion (ni) are shown below:

nd1	[0.861069753,	-0.118626171,	-0.494455976]
nd2	[0.425451169,	0.695200848,	0.579385092]
nd3	[0.275452245,	-0.704429217,	0.654144891]
ni1	[0.942674356,	-0.012230478,	-0.333489840]
ni2	[0.050091098,	0.995198895,	0.084083536]
ni3	[0.336549650,	-0.096379227,	0.936720544]

To normalized vectors by divide the vectors by length.

$$\text{nd1} = \frac{\mathbf{d1}}{|\mathbf{d1}|} \quad \text{where } |\mathbf{d1}| = \sqrt{(d1_x)^2 + d1_y^2 + d1_z^2}$$

Put vectors in to matrices:

$$\text{ND} = \begin{bmatrix} 0.86 & 0.42 & 0.27 \\ -0.11 & 0.69 & -0.70 \\ -0.49 & 0.57 & 0.65 \end{bmatrix} \quad \text{NI} = \begin{bmatrix} 0.94 & 0.05 & 0.33 \\ -0.01 & 0.99 & -0.09 \\ -0.33 & 0.08 & 0.93 \end{bmatrix}$$

where ND: matrix of diamond and NI: matrix of inclusion

Calculate twin law matrix:

$$\text{M} = \text{ND} \cdot \text{NI}^{-1} = \begin{bmatrix} 0.92 & 0.38 & 0 \\ -0.31 & 0.76 & -0.57 \\ -0.22 & 0.52 & 0.83 \end{bmatrix}$$

Calculate eigenvalues and eigenvector ([www.wolframalpha.com](http://www.wolframalpha.com))

eigenvalues are: 1.00133, 0.75+0.65i, 0.75-0.65i

eigenvector corresponding to eigenvalues is  $\mathbf{V} = [-0.83, -0.17, 0.52]$

rotation vector in diamond:  $\mathbf{V}_d = \text{ND}^T \cdot \mathbf{V} = [-0.95, -0.17, 0.52]$

where  $\text{ND}^T$ : diamond transpose matrix

rotation angle is 40.73°

## Appendix 3

### Chrome-pyrope analyses

	DHV12.3					DHK6.2				DHF10.2			
	1	2	3	4	5	1	2	3	4	1	2	3	4
SiO <sub>2</sub>	42.24	42.87	42.41	42.56	42.69	42.33	42.30	42.30	42.17	42.53	42.46	42.80	42.81
TiO <sub>2</sub>	0.26	0.20	0.23	0.21	0.25	0.09	0.09	0.12	0.07	0.02	0.02	0	0
Al <sub>2</sub> O <sub>3</sub>	20.77	21.03	21.13	20.80	20.71	18.58	18.60	18.74	18.70	19.37	19.28	19.30	19.38
Cr <sub>2</sub> O <sub>3</sub>	3.83	3.76	3.77	3.74	3.66	7.49	7.51	7.31	7.32	6.68	6.75	6.63	6.63
FeO	5.89	5.93	5.92	5.82	6.07	5.58	5.59	5.59	5.37	5.60	5.61	5.80	5.68
MgO	22.61	23.03	22.82	22.68	22.86	23.78	24.04	23.78	23.85	24.38	24.36	24.84	24.62
CaO	3.72	3.65	3.65	3.63	3.74	2.28	2.20	2.34	2.33	1.40	1.44	1.36	1.40
MnO	0.24	0.31	0.26	0.26	0.26	0.21	0.26	0.21	0.24	0.30	0.34	0.26	0.27
NiO	0.00	0.00	0.04	0.02	0.00	0.01	0.00	0.01	0.03	0.04	0.02	0.00	0.00
Na <sub>2</sub> O	0.04	0.01	0.05	0.05	0.07	0.04	0.04	0.03	0.02	0.02	0.00	0.00	0.00
K <sub>2</sub> O	0.02	0.01	0.01	0.02	0.01	0.02	0.02	0.02	0.02	0.00	0.00	0.01	0.02
<b>Total</b>	<b>99.62</b>	<b>100.80</b>	<b>100.29</b>	<b>99.79</b>	<b>100.32</b>	<b>100.41</b>	<b>100.65</b>	<b>100.45</b>	<b>100.12</b>	<b>100.34</b>	<b>100.28</b>	<b>101.00</b>	<b>100.81</b>
Numbers of ions on the basis of 24(O)													
Si	5.998	6.011	5.981	6.026	6.021	6.000	5.984	5.991	5.989	6.001	5.998	6.002	6.010
Ti	0.027	0.022	0.024	0.023	0.026	0.010	0.009	0.013	0.008	0.003	0.002	0.000	0.000
Al	3.476	3.476	3.512	3.471	3.443	3.104	3.101	3.128	3.130	3.221	3.210	3.190	3.207
Cr	0.430	0.417	0.420	0.419	0.408	0.839	0.840	0.819	0.822	0.745	0.754	0.735	0.736
Fe <sup>2+</sup>	0.700	0.696	0.698	0.689	0.716	0.661	0.661	0.662	0.638	0.661	0.663	0.680	0.667
Mg	4.786	4.814	4.797	4.786	4.806	5.025	5.069	5.021	5.049	5.128	5.130	5.192	5.153
Ca	0.566	0.548	0.552	0.551	0.565	0.346	0.333	0.355	0.354	0.212	0.218	0.205	0.211
Mn	0.029	0.037	0.031	0.031	0.032	0.025	0.031	0.026	0.029	0.035	0.041	0.031	0.032
Ni	0.000	0.000	0.004	0.002	0.000	0.001	0.000	0.002	0.004	0.004	0.002	0.000	0.000
Na	0.010	0.002	0.014	0.015	0.020	0.010	0.010	0.009	0.004	0.007	0.000	0.000	0.000
K	0.004	0.002	0.001	0.004	0.002	0.003	0.004	0.003	0.003	0.000	0.000	0.002	0.003
Mol per cent end-members													
Prp	78.71	78.98	78.92	79.02	78.54	82.95	83.17	82.80	83.17	84.96	84.78	85.00	85.00
Alm	11.50	11.41	11.49	11.38	11.70	10.92	10.85	10.92	10.51	10.95	10.95	11.14	11.00
Sps	0.48	0.61	0.51	0.51	0.52	0.41	0.51	0.42	0.48	0.58	0.66	0.51	0.53

Prp: Pyrope; Alm: Almandine and Sps: Spessartine

Ideal formula  $(\text{Mg,Fe}^{2+},\text{Mn,Ca})_3(\text{Al,Fe}^{3+},\text{Cr})_2(\text{Si,Al})_3\text{O}_{12}$

End members:  $\text{Mg}_3\text{Al}_2$  pyrope;  $\text{Fe}^{2+}_3\text{Al}_2$  almandine and  $\text{Mn}_3\text{Al}_2$  spessartine

End-member percentages

Pyrope  $\text{Mg} \times 100 / (\text{Mg} + \text{Fe} + \text{Mn} + \text{Ca})$   
 $4.786 \times 100 / (4.786 + 0.700 + 0.029 + 0.566) = 78.71\%$

Almandine  $\text{Fe} \times 100 / (\text{Mg} + \text{Fe} + \text{Mn} + \text{Ca})$   
 $0.700 \times 100 / (4.786 + 0.700 + 0.029 + 0.566) = 11.50\%$

Spessartine  $\text{Mn} \times 100 / (\text{Mg} + \text{Fe} + \text{Mn} + \text{Ca})$   
 $0.029 \times 100 / (4.786 + 0.700 + 0.029 + 0.566) = 0.48\%$

## Appendix 4

### Chromite analyses

	1a	2a	3a	4a	5a	1b	2b	3b	4b	5b
<b>SiO<sub>2</sub></b>	0.14	0.17	0.19	0.14	0.11	0.12	0.14	0.19	0.14	0.16
<b>TiO<sub>2</sub></b>	0.12	0.19	0.15	0.16	0.20	0.16	0.20	0.13	0.17	0.11
<b>Al<sub>2</sub>O<sub>3</sub></b>	7.11	7.18	7.19	7.24	7.17	7.08	7.06	7.15	7.03	7.13
<b>Cr<sub>2</sub>O<sub>3</sub></b>	63.99	64.35	64.50	64.43	64.57	64.25	64.51	64.50	64.40	64.56
<b>FeO</b>	14.71	14.53	14.48	14.49	14.36	14.47	14.77	14.61	14.61	14.72
<b>MgO</b>	13.82	14.24	13.99	13.81	14.22	13.87	14.11	14.15	14.30	14.39
<b>CaO</b>	0.01	0.01	0.00	0.00	0.00	0.01	0.00	0.01	0.02	0.01
<b>MnO</b>	0.38	0.31	0.28	0.28	0.30	0.24	0.31	0.30	0.27	0.32
<b>NiO</b>	0.15	0.06	0.12	0.11	0.17	0.07	0.03	0.06	0.09	0.10
<b>Na<sub>2</sub>O</b>	0.02	0.04	0.00	0.01	0.00	0.00	0.00	0.00	0.00	0.04
<b>K<sub>2</sub>O</b>	0	0.01	0.00	0.01	0.01	0.00	0.00	0.00	0.00	0.00
<b>Total</b>	100.45	101.09	100.90	100.68	101.11	100.27	101.13	101.10	101.03	101.54
Numbers of ions on the basis of O (32)										
<b>Si</b>	0.01	0.02	0.00	0.01	0.00	0.00	0.00	0.00	0.00	0.02
<b>Ti</b>	0.04	0.04	0.05	0.04	0.03	0.03	0.04	0.05	0.04	0.04
<b>Al</b>	0.00	0.00	0.00	0.00	0.00	0.00	0.00	0.00	0.00	0.00
<b>Cr</b>	0.02	0.04	0.03	0.03	0.04	0.03	0.04	0.03	0.03	0.02
<b>Fe<sup>2+</sup></b>	3.22	3.15	3.15	3.16	3.11	3.17	3.21	3.17	3.17	3.18
<b>Mg</b>	2.19	2.19	2.20	2.22	2.19	2.18	2.16	2.19	2.15	2.17
<b>Ca</b>	5.39	5.51	5.42	5.37	5.50	5.41	5.46	5.47	5.54	5.54
<b>Mn</b>	0.00	0.00	0.00	0.00	0.00	0.00	0.00	0.00	0.00	0.00
<b>Ni</b>	13.24	13.20	13.26	13.28	13.24	13.30	13.24	13.23	13.23	13.19
<b>Na</b>	0.08	0.07	0.06	0.06	0.07	0.05	0.07	0.07	0.06	0.07
<b>K</b>	0.03	0.01	0.03	0.02	0.04	0.01	0.01	0.01	0.02	0.02
Atomic percentages										
<b>Cr#</b>	85.79	85.74	85.75	85.65	85.80	85.89	85.97	85.82	86.00	85.86
<b>Mg#</b>	62.61	63.59	63.26	62.95	63.83	63.08	63.00	63.32	63.57	63.54

$$\text{Cr\#} = 100\text{Cr}/(\text{Cr} + \text{Al})$$

$$\text{Mg\#} = 100 \text{Mg}/(\text{Mg} + \text{Fe}^{2+})$$

## Appendix 5

### Chrome-diopside analyses

	DHK7					DHK14				DHU1.1			
	1	2	3	4	5	1	2	3	4	1	2	3	4
SiO <sub>2</sub>	55.31	55.29	55.04	55.04	55.75	55.53	50.09	51.03	56.15	55.29	51.17	54.19	54.33
TiO <sub>2</sub>	0.39	0.40	0.32	0.39	0.33	0.00	0.05	0.00	0.00	0.03	0.00	0.01	0.04
Al <sub>2</sub> O <sub>3</sub>	5.12	5.11	5.24	5.20	4.74	1.02	1.10	0.96	1.11	0.63	0.61	0.61	0.58
Cr <sub>2</sub> O <sub>3</sub>	1.46	1.56	1.50	1.44	1.46	2.00	1.97	2.03	1.98	1.08	1.26	1.16	1.07
FeO	4.79	4.79	4.92	4.72	4.87	1.70	2.74	1.70	1.84	2.16	6.38	3.99	3.96
MgO	15.33	15.52	15.25	15.28	15.58	18.32	15.59	16.51	19.13	18.46	16.48	17.92	17.93
CaO	12.82	12.82	13.01	12.92	12.73	20.54	20.08	20.41	20.21	21.91	20.50	21.41	21.32
MnO	0.08	0.12	0.12	0.15	0.10	0.08	0.11	0.10	0.08	0.11	0.18	0.13	0.09
NiO	0.09	0.06	0.14	0.09	0.10	0.05	0.09	0.04	0.00	0.05	0.05	0.03	0.04
Na <sub>2</sub> O	3.49	3.46	3.58	3.45	3.07	0.64	0.81	0.68	0.57	0.73	0.61	0.60	0.63
K <sub>2</sub> O	0.18	0.18	0.17	0.18	0.20	1.07	1.11	1.14	0.99	0.11	0.13	0.12	0.12
<b>Total</b>	99.06	99.31	99.29	98.86	98.93	100.95	93.74	94.60	102.06	100.56	97.37	100.17	100.11
Numbers of ions on the basis of 6(O)													
Si	1.996	1.992	1.987	1.992	2.011	1.991	1.961	1.968	1.987	1.987	1.947	1.975	1.979
Ti	0.011	0.011	0.009	0.010	0.010	0.000	0.001	0.000	0.000	0.001	0.000	0.001	0.001
Al	0.218	0.217	0.223	0.222	0.202	0.043	0.050	0.043	0.046	0.027	0.027	0.026	0.025
Cr	0.042	0.044	0.043	0.041	0.042	0.057	0.061	0.062	0.055	0.031	0.038	0.033	0.031
Fe <sup>2+</sup>	0.144	0.144	0.148	0.143	0.147	0.051	0.090	0.055	0.043	0.065	0.203	0.122	0.121
Mg	0.825	0.833	0.821	0.824	0.838	0.979	0.910	0.949	1.009	0.990	0.935	0.974	0.974
Ca	0.496	0.495	0.503	0.501	0.492	0.790	0.842	0.843	0.766	0.845	0.836	0.836	0.832
Mn	0.002	0.004	0.004	0.005	0.003	0.002	0.003	0.003	0.002	0.003	0.006	0.004	0.003
Ni	0.003	0.002	0.004	0.002	0.003	0.001	0.003	0.001	0.000	0.001	0.002	0.001	0.001
Na	0.244	0.242	0.251	0.252	0.215	0.044	0.061	0.051	0.039	0.051	0.045	0.042	0.044
K	0.008	0.008	0.008	0.008	0.009	0.049	0.056	0.056	0.045	0.005	0.006	0.006	0.006
Atomic percentages													
Mg	56.29	56.59	55.73	56.14	56.73	53.82	49.40	51.38	55.15	52.12	47.36	50.41	50.54
ΣFe	0.15	0.15	0.15	0.15	0.15	0.05	0.09	0.06	0.06	0.07	0.21	0.12	0.12
Ca	33.84	33.60	33.18	34.12	33.32	43.38	45.73	75.65	41.88	44.46	42.35	43.29	43.20
Mg#	84.86	84.93	84.34	84.82	84.82	94.82	90.71	94.22	94.66	93.53	81.74	88.56	88.74

$$\Sigma\text{Fe} = \text{Fe}^{2+} + \text{Mn}$$

$$\text{Mg\#} = 100 \text{ Mg}/(\text{Mg} + \text{Fe}^{2+} + \text{Mn})$$

## Appendix 6

### Olivine analyses

	DHD8.2					DHK13				
	1	2	3	4	5	1	2	3	4	5
<b>SiO<sub>2</sub></b>	41.64	41.50	40.84	41.35	41.61	41.11	40.62	40.80	40.55	40.04
<b>TiO<sub>2</sub></b>	0.00	0.00	0.00	0.04	0.00	0.02	0.02	0.03	0.00	0.00
<b>Al<sub>2</sub>O<sub>3</sub></b>	0.01	0.02	0.00	0.00	0.01	0.02	0.02	0.01	0.04	0.05
<b>Cr<sub>2</sub>O<sub>3</sub></b>	0.02	0.06	0.08	0.05	0.06	0.06	0.13	0.05	0.05	0.08
<b>FeO</b>	5.43	5.33	5.46	5.35	5.35	7.66	7.70	7.65	7.68	7.59
<b>MgO</b>	52.96	53.28	52.47	52.89	53.54	51.36	50.69	50.97	50.86	49.62
<b>CaO</b>	0.03	0.02	0.05	0.02	0.03	0.05	0.02	0.04	0.05	0.08
<b>MnO</b>	0.04	0.09	0.06	0.03	0.03	0.12	0.10	0.08	0.11	0.07
<b>NiO</b>	0.39	0.31	0.35	0.36	0.34	0.41	0.34	0.41	0.40	0.36
<b>Na<sub>2</sub>O</b>	0.02	0.01	0.01	0.03	0.02	0.04	0.04	0.00	0.01	0.04
<b>K<sub>2</sub>O</b>	0.02	0.02	0.01	0.03	0.01	0.00	0.02	0.00	0.00	0.01
<b>Total</b>	100.56	100.64	99.33	100.15	101.00	100.85	99.70	100.04	99.75	97.94
Numbers of ions on the basis of 4(O)										
<b>Si</b>	0.996	0.992	0.990	0.993	0.991	0.992	0.991	0.992	0.989	0.994
<b>Ti</b>	0.000	0.000	0.000	0.001	0.000	0.000	0.000	0.001	0.000	0.000
<b>Al</b>	0.000	0.000	0.000	0.000	0.000	0.000	0.000	0.000	0.001	0.002
<b>Cr</b>	0.000	0.001	0.001	0.001	0.001	0.001	0.002	0.001	0.001	0.001
<b>Fe<sup>2+</sup></b>	0.109	0.106	0.111	0.107	0.106	0.154	0.157	0.156	0.157	0.158
<b>Mg</b>	1.888	1.898	1.896	1.894	1.901	1.846	1.844	1.847	1.850	1.837
<b>Ca</b>	0.001	0.000	0.001	0.000	0.001	0.001	0.001	0.001	0.001	0.002
<b>Mn</b>	0.001	0.002	0.001	0.001	0.000	0.002	0.002	0.002	0.002	0.002
<b>Ni</b>	0.007	0.006	0.007	0.007	0.006	0.008	0.007	0.008	0.008	0.007
<b>Na</b>	0.001	0.000	0.001	0.001	0.001	0.002	0.002	0.000	0.000	0.002
<b>K</b>	0.000	0.000	0.000	0.001	0.000	0.000	0.001	0.000	0.000	0.000
End-member percentages										
<b>Fo</b>	94.52	94.60	94.42	94.60	94.66	92.17	92.05	92.16	92.09	92.02
<b>Fa</b>	5.48	5.40	5.58	5.40	5.34	7.83	7.95	7.84	7.91	7.98

Fo: Forsterite and Fa: Fayalite

End-member percentages

$$\text{Fo} = \text{Mg} \times 100 / (\text{Mg} + \text{Fe} + \text{Mn}) = 1.888 \times 100 / (1.888 + 0.109 + 0.001) = 94.52\%$$

